IN-47 -CR
46299
119P.

Analysis of the Inflow and Air-Sea Interactions in Hurricane Frederic (1979)

Final Report
NASA Grant NAG 5-398

by

John Kaplan
William M. Frank
The Pennsylvania State University
Department of Meteorology
503 Walker Building
University Park, PA 16802

December 1986

ABSTRACT

The contents of this technical report are taken from the M.S. thesis of the lead author, Mr. John Kaplan, published in 1986 by the Department of Meteorology, The Pennsylvania State University.

An unusually large amount of aircraft, rawinsonde, satellite, ship and buoy data from hurricane Frederic (1979) are composited over a 40 hr period. These are combined with Frank's (1984) analysis of Frederic's core and Powell's (1982) surface wind analysis to analyze Frederic's three-dimensional low-level structure between the storm center and a radius of 10 deg. latitude. The analysis is improved significantly by determining the levels at which low-level cloud motion winds (CMW's) are in the best agreement with verification wind data and then adjusting the winds to uniform analysis levels. In the past, it has been assumed that all low-level CMW's tracked in a tropical cyclone environment approximate the wind near cloud base. However, in this study it is observed that low-level CMW's are representative of levels between 300 and 5000 m. It is demonstrated that assigning all low-level CMW's to an assumed analysis level of 560 m rather than to their correct levels results in substantial errors in the wind fields.

Due to the unusually good low-level wind resolution afforded by this data set, it is possible to obtain kinematically derived fields of vorticity, divergence and vertical velocity. These analyses are observed to be internally consistent and should prove useful for future analysis. Analysis of Frederic's surface to 560 m angular momentum budget beyond 2 deg. radius indicates that surface drag coefficients

increase slightly with increasing radius and decreasing wind speed. While these estimates contradict earlier studies, they are believed to be superior to previous estimates derived from budgets since the current study represents the first attempt to estimate surface drag coefficients outside a tropical cyclone's core using observed winds from a single storm. Estimates of storm rainfall obtained by performing a moisture budget between the surface and the top of the inflow layer show that most storm rainfall falls inside about 4 deg. radius and that substantial underestimation of storm rainfall occurs when all low-level CMW's are assigned to 560 m.

Chapter 1

INTRODUCTION

Tropical cyclones are potentially the most destructive of all meteorological phenomena and are capable of producing billions of dollars in damages and claiming numerous lives. During 1985, 8 tropical cyclones made landfall in the United States claiming 30 lives and producing property damage in excess of $4 billion. This made the 1985 tropical cyclone season the costliest in United States history. The record damage in 1985 reflects both the unusually large number of tropical cyclone landfalls in the United States and the rapid population increase which has taken place along the East and Gulf coasts of the United States during the last several decades. In 1980 the population along coastal counties between Brownsville, Texas, and Eastport, Maine, was about 40 million; the population along the same stretch of coastline in 1940 was just over 20 million. Fortunately, despite the increase in population along the East and Gulf coastlines, better warning systems have resulted in a decrease in the number of lives lost in the United States due to tropical cyclones during this same period. Nevertheless, it remains possible that substantial loss of life could occur if a major tropical cyclone were to strike a densely populated portion of either the East or Gulf coast of the United States.

In response to the obvious need to better understand these dangerous storms, numerous observational studies of tropical cyclone

structure have been performed. Observational studies of the core (radius $\lesssim$ 150 km) of a tropical cyclone have been especially plentiful, since research aircraft normally obtain large quantities of data inside roughly 100-150 km. Riehl and Malkus (1961), Laseur and Hawkins (1963), Hawkins and Imbembo (1976), Frank (1984) and many others have performed detailed studies of the core of a single storm, while Shea and Gray (1973) and Gray and Shea (1973) performed composite studies of a tropical cyclone's core using data from many storms. Observational studies of the tropical cyclone structure beyond about 150 km have been performed less frequently due to limited data availability. Since the quantity of data available outside the core for a single storm is normally insufficient to obtain accurate analyses of the outer storm structure, Frank (1977a,b,c), McBride (1981a,b), Nunez and Gray (1977), Holland (1983a,b) and others composited rawinsonde data from many storms to analyze the large-scale storm structure. While the above studies were instrumental in documenting the mean tropical cyclone structure, none had sufficient data both inside and outside the core to obtain a detailed multiple-scale analysis of a single tropical cyclone, especially at low-levels where wind resolution has been quite poor.

In this thesis, an unusually dense data set comprised of aircraft, rawinsonde, satellite, ship and buoy data is used to study hurricane Frederic's mean multiple-scale low-level wind structure and to perform budgets of momentum and moisture. To improve the quality and

resolution of the low-level wind analysis used in this study, a considerable effort is made to determine the levels to which low-level cloud motion winds (CMW's) should be assigned and then adjusting the CMW's to the 560 and 1600 m analysis levels. Although it has been quite common for researchers (i.e., Hasler and Morris, 1986, Rodgers and Gentry, 1983 and others) to assign all low-level CMW's to a single assumed analysis level of roughly 950 mb, it is believed that assigning CMW's to their correct levels and then adjusting them to the 560 and 1600 m analysis levels will yield a more realistic low-level wind analysis.

Angular momentum budgets are performed for the surface to 560 m and 560 to 1600 m layers to investigate sinks of momentum and drag coefficients outward of 2 deg. radius. Due to inadequate low-level wind resolution, previous studies of a tropical cyclone's angular momentum budget (i.e., Holland, 1983a, McBride, 1981b, Frank, 1977b and others) have provided only composite analyses outside the core. Consequently the angular momentum budget presented here should prove to be quite informative. The surface to 560 m angular momentum budget is employed to obtain estimates of the frictional dissipation at the sea surface and thus C_D. The estimates of C_D obtained in this thesis are thought to be an improvement over past estimates since they represent the first attempt to compute C_D outside the core using observed surface winds and the winds from a single storm.

A moisture budget is performed between the surface and the top of the inflow layer to obtain estimates of storm rainfall. These are used to determine the rainfall errors which result when all low-level CMW's

are assigned to a single assumed analysis level rather than to the correct levels.

Following the introduction, a description of the data set and analysis procedure is given in Chapter 2. Included in Chapter 2 is a detailed description of the techniques used to assign heights to the low-level CMW's and to adjust these winds to the 560 and 1600 m analysis levels. In Chapter 3, analyses of the storm's winds structure are presented at the surface, 560 and 1600 m. Angular momentum budgets for the surface to 560 m and 560 to 1600 m layers are presented in Chapter 4. In Chapter 5, estimates of storm rainfall obtained by performing a moisture budget between the surface and the top of the inflow layer are presented. A summary of the results is given in Chapter 6.

Chapter 2

DATA AND ANALYSIS

2.1 Storm History

After regaining hurricane intensity over the western end of Cuba at about 1200 GMT 10 September 1979, hurricane Frederic moved northwest then north-northwestward through the Gulf of Mexico before crossing Dauphin Island at about 0300 GMT and the coastline near the Mississippi-Alabama border at approximately 0400 GMT 13 September. Frederic's central pressure decreased slowly during this period from 980 mb at 1200 GMT on 10 September to 945 mb at 0400 GMT on 13 September. Despite deepening 35 mb during the aforementioned time period, Frederic's maximum sustained flight-level winds remained fairly constant. Maximum sustained flight-level winds increased by 10 ms^{-1}, from 48 ms^{-1} to 58 ms^{-1}, during the interval between 1600 GMT 11 September to 1600 GMT 12 September, and no significant change in flight-level winds occurred between 1600 GMT 12 September and storm landfall at about 0400 GMT 13 September. Frederic's storm track, including minimum sea-level pressures, is depicted in Fig. 2.1.

Frederic's day and one-half journey through the eastern portion of the United States caused $2.3 billion in damage and resulted in the loss of 5 lives. At the time, the damage estimate of $2.3 billion made Frederic the costliest hurricane in United States history. Much of the damage was incurred by residents living along the Gulf of Mexico coast between Pascagoula, Mississippi, and Mobile, Alabama, where tides

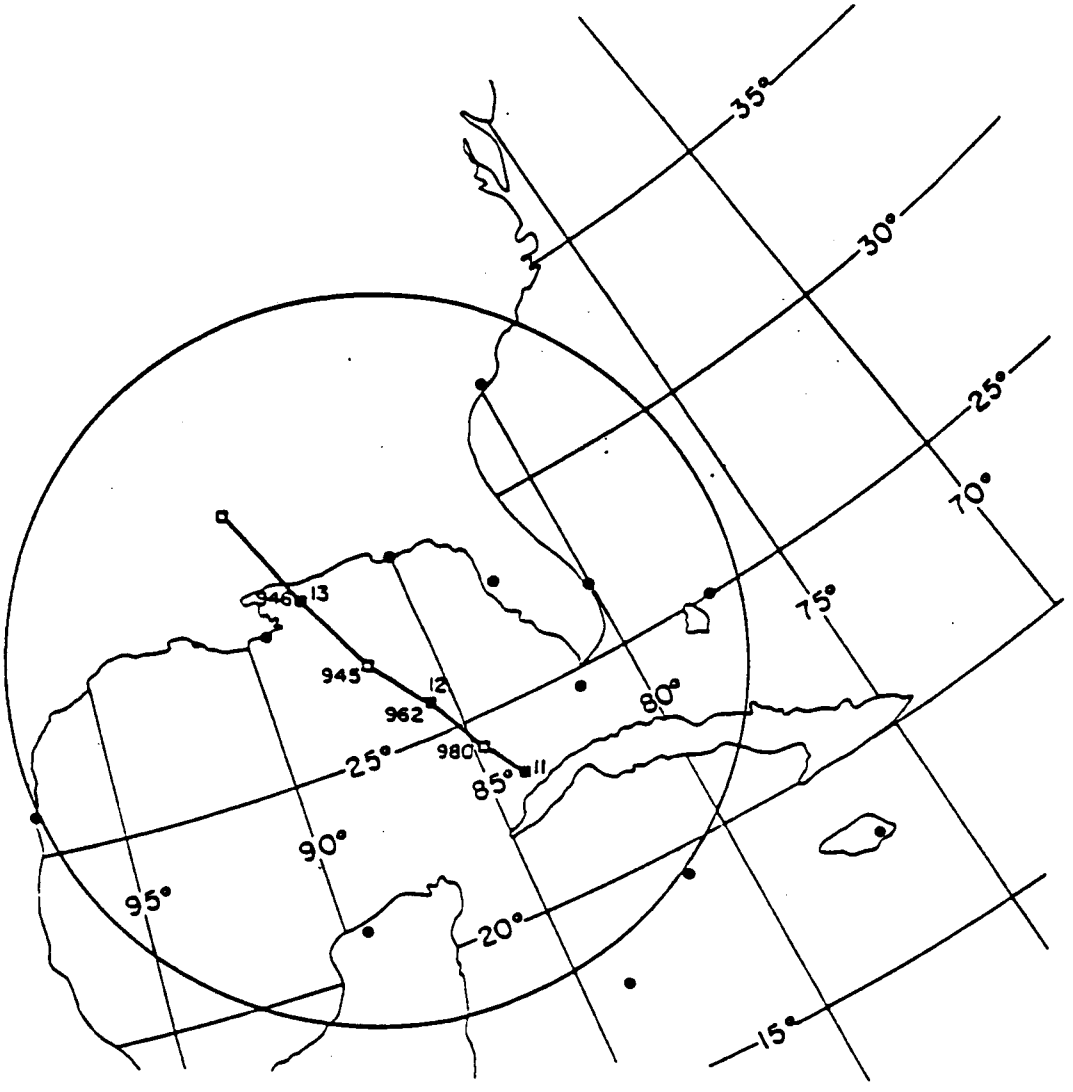

Figure 2.1 Hurricane Frederic's positions and central pressures (mb) at 12 hr intervals between 0000 GMT 11 September and 1200 GMT 13 September. Filled-in circles denote rawinsonde locations. The large circle illustrates the areal coverage of the compositing grid for the mean composite storm position.

2.4-3.7 m or more above normal and 20-30 cm of rain were observed. Additional information concerning Frederic's history can be found in Hebert (1980).

2.2 Data

2.2.1 Aircraft Data

Approximately 175 aircraft wind observations obtained between 1500 GMT 11 September and 0400 GMT 13 September are employed to resolve Frederic's wind structure inside 250 km. It is important to note that each of the aforementioned aircraft observations reflects values which have been averaged in both time and space. Inside 140 km, wind data are obtained from Frank's (1984) over-water aircraft composite analysis of Frederic's core, while wind data between 140 km and 250 km are obtained from aircraft data supplied by Mark Powell and David Jorgenson of the Hurricane Research Division (HRD) of the Atlantic Oceanographic and Meteorological Laboratory.

Frank composited aircraft data collected between the storm center and 140 km onto a cylindrical grid comprised of 120 grid spaces 10 km in radial and 45 deg. in azimuthal extent. All 1 sec. aircraft observations which fell within a given grid space were averaged and the resultant mean value assigned to the center of that grid space. Frank used this compositing technique at 560 and 1600 m to obtain the time and space averaged aircraft observations employed here at each respective level.

Between 140 km and 250 km, the majority of aircraft observations employed in this thesis are supplied by Powell. Powell obtained

aircraft data between 1600 GMT 11 September and 1800 GMT 12 September from a total of 4 research flights. He obtained the time-averaged wind observations used here by averaging a series of 30 consecutive 1 sec. aircraft wind measurements. Most of the time-averaged wind measurements used are near 560 m or 1600 m; however, observations ranging from 300 m to 2000 m are employed.

Additional wind observations from between 140 km and 250 km are obtained from aircraft data collected between 1130 GMT 11 September and 0200 GMT 13 September and supplied by D. Jorgenson. These data are examined for flight-leg segments at radii between 140 and 250 km which contain at least 30 1-sec. observations. To guard against using non-representative aircraft data, flight-leg segments are checked for substantial fluctuations in aircraft heading and altitude. As suggested by Frank (personal communication, 1984), a flight-leg segment is not used if the aircraft heading changes by more than 1 deg. per second between any 2 observations. Moreover, flight-leg segments exhibiting radar altitude changes of more than 200 m are not used. Flight-leg segments which satisfy the above criteria are averaged over a period of 30 sec., and the resultant mean wind values are assigned to the time-averaged aircraft location and radar altitude.

For each aircraft observation employed, radial (V_r) and tangential (V_t) wind components and inflow angle (α) are computed.

2.2.2 Surface Data

The availability of a large number of surface wind observations provides reasonably good surface wind coverage out to a radius of

1000 km. Approximately 325 over-water surface wind observations are obtained between 1200 GMT 11 September and 0400 GMT 13 September from ships of opportunity, NOAA buoys, research aircraft and satellite data. The surface wind data distribution is depicted in Fig. 2.2.

Inside a radius of 150 km, surface wind observations are obtained from Frank's (1984) over-water composite analysis of Frederic's core. Frank obtained surface wind values by adjusting 560 m composite aircraft winds to the surface based upon vertical wind shear relationships developed by Powell (1982). The resultant surface analysis affords good wind data resolution over the entire core domain.

Outside approximately 150 km, most surface wind observations are obtained from ships of opportunity and NOAA buoys. The majority of ship and buoy data are supplied by Powell. Additional ship and buoy data are obtained from the National Center for Atmospheric Research (NCAR).

In large data void regions, a limited number of surface wind values are estimated to enhance surface wind resolution. The procedure used to estimate surface winds here is essentially the same one Frank (1984) used to estimate surface winds inside Frederic's core. The only difference is that surface winds are estimated using satellite data instead of aircraft data. A description of the procedure used to estimate surface winds is given below.

In areas clearly devoid of surface wind data, satellite winds which had been adjusted previously to 560 m (see Section 2.33) are reduced to the surface using correction factors derived by Powell

Figure 2.2 Surface wind data (ms^{-1}) for the 40 hr composite period between 1200 GMT 11 September and 0400 GMT 13 September. Open symbols denote data from 11 September (1200 GMT 11 to 0000 GMT 12 September) and filled-in symbols indicate data from 12 September (0000 GMT 12 to 0400 GMT 13 September). For the sake of clarity, only a limited number of Frank's (1984) composite aircraft observations employed inside about 1.5 deg. radius are plotted. In certain regions beyond about 1.5 deg. radius, the density of observations preclude plotting wind barbs for every observation, thus only the symbol depicting the data source (i.e., rawinsonde, aircraft, etc.) is plotted for some observations. The circle in the middle of the page denotes the storm center. The large arrow northwest of the storm indicates the mean storm motion for the composite period.

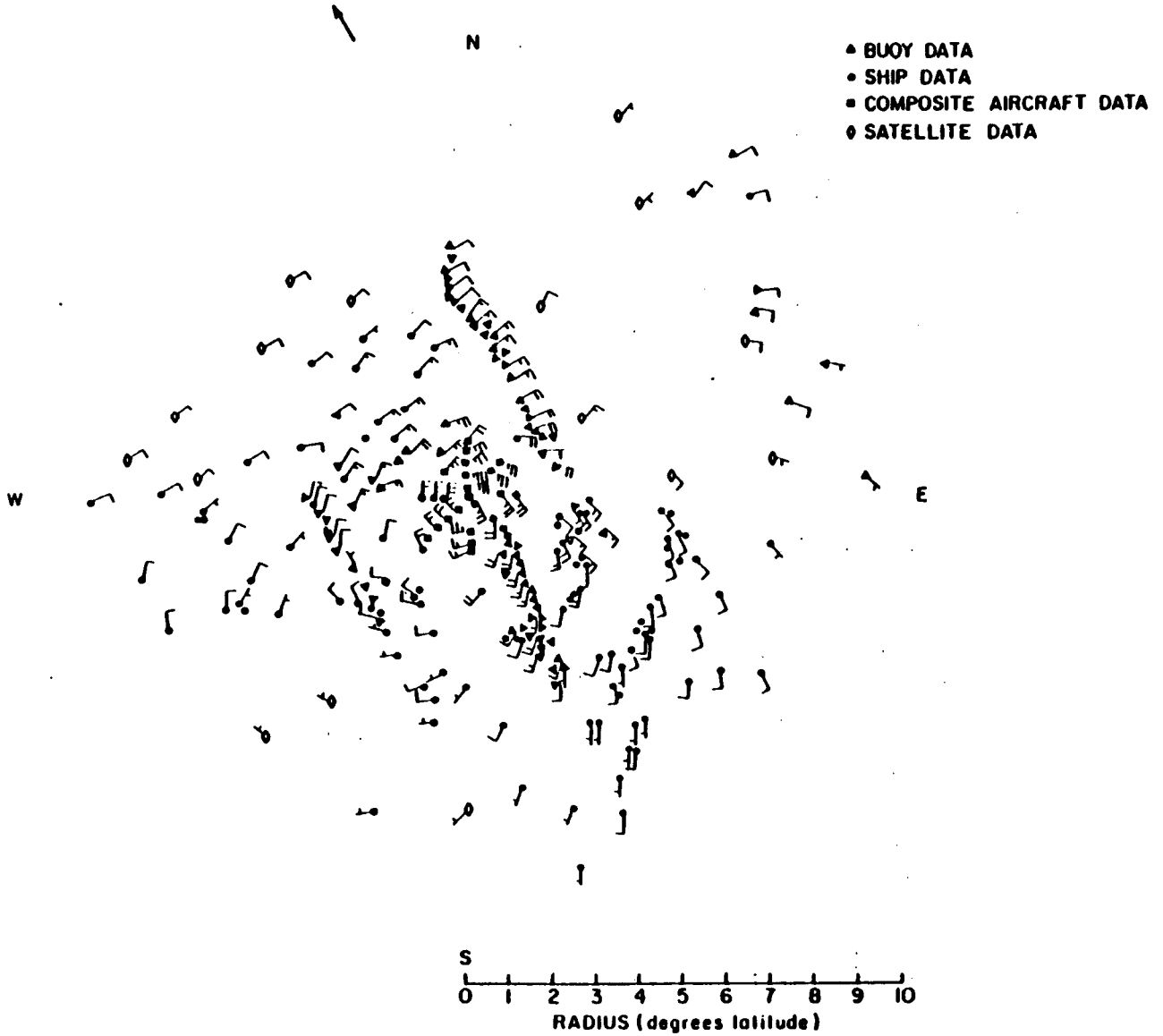
N
W
E
S
▲ BUOY DATA
• SHIP DATA
■ COMPOSITE AIRCRAFT DATA
◊ SATELLITE DATA
0 1 2 3 4 5 6 7 8 9 10
RADIUS (degrees latitude)

(1982). A correction factor of 0.7 is applied to the wind speed if the surface inflow angle beneath the satellite wind is less than 20 deg., while a correction factor of 0.6 is used if the surface inflow angle exceeds 20 deg. Surface inflow angles in data void regions are estimated from analysis of surrounding surface wind data. Surface values of V_r, V_t and α are computed at each observation location using the appropriate raw wind values.

2.2.3 Rawinsonde Data

To augment wind data coverage outside Frederic's core, rawinsonde observations are obtained from 12 coastal launch sites between 1200 GMT 11 September and 0000 GMT 13 September. The locations of rawinsonde launch sites in relation to Frederic's storm track are depicted in Fig. 2.1.

For each rawinsonde launch used, rawinsonde-measured winds at 950, 900, 850, 800, 700, 600 and 500 mb are recorded. Winds which appear to be inconsistent with those at other levels are not used. The heights of all seven pressure levels are estimated from the hypsometric equation using rawinsonde-measured temperature and humidity data. If temperature and humidity data are unavailable at a particular launch site, they are estimated from the nearest available sounding.

Since rawinsonde observations within the lowest 1-2 km may be contaminated by surface friction, winds within the lowest 200 mb are screened carefully. To aid in the screening process, the depth of the mixed-layer (h) is estimated at each rawinsonde launch site whenever possible. Estimates of h are made by determining the level at which the lowest temperature inversion (z) occurs. As discussed by Panofsky

and Dutton (1984), z is a reasonably good estimate of h under most conditions. It is important to note that only observations within the mixed-layer are assumed to be affected significantly by surface friction.

At rawinsonde launch sites where estimates of h are available, rawinsonde-measured winds at pressure levels below h are not used. If no estimate of h is available, rawinsonde-measured winds in the lowest 200 mb are screened subjectively for signs of surface contamination such as anamolously low wind speeds and unrealistic inflow. Observations which exhibit either of these signs are not used.

For each rawinsonde observation used V_r, V_t and α are computed from the raw rawinsonde-measured winds.

2.2.4 Satellite Data

On 11 and 12 September, successive visible GOES-1 satellite images of hurricane Frederic were employed to derive CMW's at radii between approximately 150 km and 1000 km. Cloud motion winds were obtained within the time intervals between roughly 1600-1645 GMT and 1930-2015 GMT on 11 September and 1623-1637 GMT, 1922-1944 GMT and 2200-2230 GMT on 12 September by E. Rodgers of the Laboratory of Atmospheric Sciences, Goddard Space Flight Center, National Aeronautics and Space Administration. Rodgers computed lower-tropospheric CMW's by subjectively tracking clouds using NASA's AOIPS (Atmospheric and Oceanographic Image Processing System) and a computer software package called METPAC (Meteorological and Data Processing Package). AOIPS/METPAC enables the user to select and track a cloud using a

series of consecutive satellite images. A specific point on a cloud, which is visible on all images, is tracked subjectively using an electronic cursor or objectively employing an image correlation mode. The wind velocity of the cloud is computed by dividing the displacement of the cloud in earth relative coordinates by the time between images. A more detailed description of AOIPS and METPAC can be obtained from Billingsley (1976) and Computer Sciences Corporation (1977) respectively.

The approximately 274 low-level CMW's used in this thesis were obtained by tracking convective-scale clouds, with tops between approximately 0 and 5 km, using a series of 3 or 4 successive visible satellite images. The time interval between images tracked was either 7.5 min. or 15 min. and the spatial resolution of all images was 2 km. A summary of the pertinent information regarding the CMW data set used in this thesis is contained in Table 2.1.

Table 2.1 Spatial and temporal resolution employed and number of visible images used when deriving low-level CMW data sets.

Date	Approximate Time (GMT)	Spatial Resolution (km)	Temporal Resolution (min)	Number of Visible Images
11 Sept.	1600-1645	2	15.0	4
11 Sept.	1930-2015	2	15.0	4
12 Sept.	1623-1637	2	7.5	3
12 Sept.	1922-1944	2	7.5	4
12 Sept.	2200-2230	2	15.0	3

Although reasonably good temporal and spatial resolution were employed when deriving CMW's, it is inevitable that wind measurement errors were made during the cloud tracking process. A study by Hasler and Rodgers (1977) suggests that random wind measurement errors of two times the image resolution divided by the total time interval over which clouds were tracked can be expected when tracking clouds in a hurricane environment. Assuming their formulation is correct and applicable to other hurricanes, the mean random wind measurement error (RWME) of the CMW data set is about 2.7 ms^{-1}. The mean error of 2.7 ms^{-1} is obtained by summing up the random wind measurement error computed for each of the 5 times listed in Table 2.1 and dividing by 5.

$$RWME = \frac{1}{5}\,[1.5\ ms^{-1} + 1.5\ ms^{-1} + 4.8\ ms^{-1} + 3.5\ ms^{-1} + 2.2\ ms^{-1}] \approx 2.7\ ms^{-1} \qquad (2.1)$$

While it is not possible to totally eliminate the wind measurement errors made during the cloud tracking process, steps can be taken to improve the quality of the CMW data set. An outline of the technique used to improve the quality of the data set in this thesis is given below.

Each series of visible satellite images used to track CMW's is subjectively checked for large changes in wind speed and direction between images. Cloud motion winds derived from satellite image sets which are thought to contain obvious wind inconsistencies between

images are not used. In addition, all over-land CMW's are eliminated to insure that the CMW's used here do not contain orographically induced wind asymmetries. All remaining CMW's are plotted and compared with neighboring values. CMW's which differ markedly from neighboring values are not used.

2.3 Analysis Procedure

2.3.1 The Cloud Motion Wind Height Determination Problem

In the past, it has been common practice to assign all low-level CMW's obtained in a tropical cyclone environment to cloud base (i.e., 900-950 mb). As justification for making this approximation, researchers such as Hasler and Morris (1986) and Rodgers and Gentry (1983) have cited studies conducted by Hubert and Whitney (1971), Hasler et al. (1977; 1979) and others which indicate that the motion of a cloud can be approximated by the cloud base wind. Hubert and Whitney (1971) compared a total of 612 over-water low-level CMW's to rawinsonde measured winds and concluded that the "deviation minimizing level" -- the level at which rawinsonde measured winds and CMW's were in the best agreement -- was 3000 ft (about 900 mb).

Hasler et al. (1977) used in situ aircraft wind measurements to determine the agreement between the velocity of 40 tropical cumulus clouds -- with bases near 960 mb and tops mainly between 600 and 700 mb -- and the ambient wind at four levels: 150 m, cloud base, mid-cloud and cloud top. The best agreement between the velocity of cumulus clouds, as measured by low-level aircraft, and the ambient wind was found at cloud base. The vector difference between the velocity of

a cumulus cloud and the cloud base wind was found to be 1.3 ms^{-1} for 67% of the 21 cases with track lengths exceeding 1 hr.

In an extension of their previous study, Hasler et al. (1979) compared in situ aircraft measured winds to low-level CMW's obtained over the Northwest Caribbean, Gulf of Mexico, and Northern Atlantic. A total of 42 CMW's were tracked in three different weather regimes -- trade wind, subtropical high and frontal -- and compared to the ambient wind at 150 m, cloud base, mid-cloud and cloud top. The results of their study indicated that in oceanic trade wind and subtropical high regimes, CMW's with average wind speeds of between 5.3 ms^{-1} and 19.0 ms^{-1} agreed best with the wind at cloud base [0.9 $ms^{-1} \leq |\overline{V_{cloud} - V_{CBW}}| \leq 1.7$ ms^{-1} (where the overbar denotes the mean)]. However in frontal regions, CMW's with average wind speeds of 15.7 ms^{-1} were found to be in the best agreement with the mean cloud layer wind [$|\overline{V_{cloud} - V_{MCLW}}| = 2.3$ m^{-1}]. Although these studies were not conducted in a tropical cyclone environment, it has been hypothesized by Hasler and Morris (1986), Rodgers and Gentry (1983) and others that the existence of small vertical wind shear near the center of tropical cyclones suggests that a cloud may move with the wind at cloud base. To date, the only comparisons between verification wind data and CMW's in a tropical cyclone environment have been performed by Rodgers et al. (1979) and Hasler and Morris (1986). While examining the benefits of using short-interval satellite images to derive winds for tropical cyclones, Rodgers et al. (1979) compared low-level CMW's from 3 tropical cyclones to aircraft winds measured 4-6 hr later at elevations between 400 and 960 m. For all 3 CMW data sets, they found

that a mean absolute wind speed difference of 2.5 ms^{-1} existed between aircraft measured winds and CMW's. While their study found fairly good agreement between satellite and aircraft wind speeds, no similar comparison was made between satellite and aircraft wind velocities. In the author's opinion, the failure to account for differences in wind direction make the results of Rodgers et al. inconclusive.

As part of their study on hurricane precipitation and cloud structure, Hasler and Morris (1986) compared CMW's derived from visible stereo imagery of hurricane Frederic (1979) at about 1930 GMT 12 September to nearby rawinsondes. They concluded that the best agreement between CMW's and rawinsonde-measured winds was at about 500 m near water and 1200 m over land. However, these conclusions were made based upon a limited number of comparisons between low-level CMW's and rawinsondes. As will be discussed in Section 2.3.2, these conclusions may not be valid over Frederic's entire domain.

2.3.2 A Technique for Determining Cloud Motion Wind Heights

As noted in Section 2.3.1, a great deal of uncertainty exists concerning the most appropriate level to which CMW's should be assigned in a tropical cyclone environment. In response to the need for further research concerning the height determination problem, a considerable effort is made to determine the levels at which Frederic's low-level CMW's are in the best agreement with verification wind data. As a matter of convenience, the level at which the best agreement between a CMW and verification wind data is observed is hereafter referred to as the Cloud Motion Wind Height (CMWH).

In this section, a technique for ascertaining the CMWH of each low-level satellite-derived wind employed in this thesis is presented. This technique appears to be capable of diagnosing the spatial distribution of low-level CMWH's over the entire storm domain. A detailed description of the technique is presented below.

The technique employed to estimate CMWH's in this thesis is similar to the one used by Hubert and Whitney (1971). CMW's are compared to wind profiles constructed using aircraft, rawinsonde, ship and buoy data to determine the "level of best fit" (LBF) -- an idea first introduced by Hubert and Whitney. Since the LBF is basically the level at which a CMW most closely matches verification winds, it is the level to which CMW's are assigned in this study.

Verification wind profiles are constructed using aircraft, ship, buoy and rawinsonde wind data between about 1200 GMT 11 September and 0400 GMT 13 September. Data obtained between 1200 GMT 11 September and 0000 GMT 12 September are employed to construct wind profiles for 11 September, while data obtained between 0000 GMT 12 September and 0400 GMT 13 September are employed to construct wind profiles for 12 September.

Outside a radius of 250 km, verification wind profiles are constructed between the surface and 500 mb using rawinsonde-measured winds and surface winds estimated from nearby area-averaged surface wind data. Area-averaged surface winds are obtained by subjectively averaging surface wind data wherever clusters of surface observations exist. The centroid of all surface observations is located, and all

observations within a radius of 80 km of the centroid of all points are averaged. The resultant mean surface values are then assigned to the centroid of all points.

The vertical resolution of verification wind profiles outside 250 km varies according to the number of levels of rawinsonde data available at a particular launch site. Although rawinsonde observations are normally available at 950, 900, 850, 800, 700, 600 and 500 mb; data may be unavailable at several of these levels due to the elimination of erroneous wind data.

Inside a radius of about 250 km, wind profiles are constructed between the surface and roughly 2000 m using area-averaged aircraft and surface data. Area-averaged aircraft data are obtained by averaging aircraft observations with altitudes differing by no more than 200 m using the same technique employed to average surface data.

The vertical resolution of each verification wind profile between 150 and 250 km is quite variable due to the sporadic aircraft coverage in the lowest 2000 m. Inside 140 km, Frank's (1984) composite data affords coverage at the surface, 560 m and 1600 m; however, between 150 km and 250 km data are usually available only at the surface and at one additional level.

Upon completion of the verification wind profiles, low-level CMW's are compared to the nearest verification wind profile to determine the LBF. A LBF is assigned to each CMW which lies within 175 km of a verification wind profile for the day the CMW was derived. Inside 250 km, each CMW is assigned a LBF provided a verification wind profile from the day on which the CMW was derived is within 100 km of the CMW. A maximum separation distance of 100 km is used instead of 175 km to

minimize errors incurred when determining the LBF in a region where strong gradients in wind speed and direction are observed.

Each CMW meeting the criteria outlined in the preceding two paragraphs is assigned an LBF. The radial and tangential wind components and inflow angle of each CMW are compared to the nearest verification profile values of V_r, V_t and α to determine the level at which CMW's are in the best agreement with verification wind data. After inspecting verification vertical profiles of V_r, V_t and α, it is found that profiles of V_r and α are somewhat more useful in determining CMWH's than are profiles of V_t. Verification profiles of V_t are often difficult to employ when assigning CMWH's because the magnitude of V_t is often nearly identical at several different levels. Moreover, in many instances, V_t does not change systematically with height. In contrast, verification profiles of V_r and α normally exhibit larger, more systematic variations with height, thus making it easier to employ these profiles when assigning CMWH's. In view of these observations, CMWH's are assigned heights primarily by employing verification profiles of V_r and α. A description of the procedure used to assign CMWH's is given below.

At the nearest vertical profile location, the radial and tangential wind components of a CMW are compared to verification profile values of Vr and α. Based upon these comparisons, the CMW is assigned two heights. The first height assignment is made by determining the level at which the radial wind component of a CMW best fits the verifiction profile of V_r. In a similar manner, a second height assignment is made by determining the level at which the inflow angle of a CMW best fits the verification profile of α.

To determine at which of the two heights the CMW should be assigned, the tangential wind component of a CMW is compared to the verification-derived tangential wind at each level. The CMW is ultimately assigned to the level at which the smallest absolute difference between the tangential wind component of a CMW and the verification-derived tangential wind value is observed. All assigned CMWH's are rounded off to the nearest 100 m. A hypothetical example of the procedure used to assign CMWH's is outlined below.

Given the verification profiles depicted in Fig. 2.3, one could argue that the radial wind component of the CMW best fits the verification profile of V_r at about 1250 m, while the inflow angle of the CMW best fits the verification profile of α at 1750 m. However, since the difference between the tangential wind component of the CMW and the verification-derived tangential wind is smallest at 1750 m, the CMW in this example is assigned to a rounded off height of 1800 m.

While the technique presented here is by no means perfect, the author believes that the heights assigned to CMW's are reasonable and represent a definite improvement over assigning all low-level CMW's to cloud base or to any other single level.

Of the 274 CMW's used in this thesis, a total of 92 are close enough to verification data to be assigned heights by the method outlined above (Fig. 2.4). The procedure used to estimate the heights of the remaining CMW's is described below. Cloud Motion Wind Heights from each of the two analysis days are combined to construct a map of CMWH's believed to be valid for the time interval over which CMW's are derived. Specifically, the analysis is assumed to be valid from about

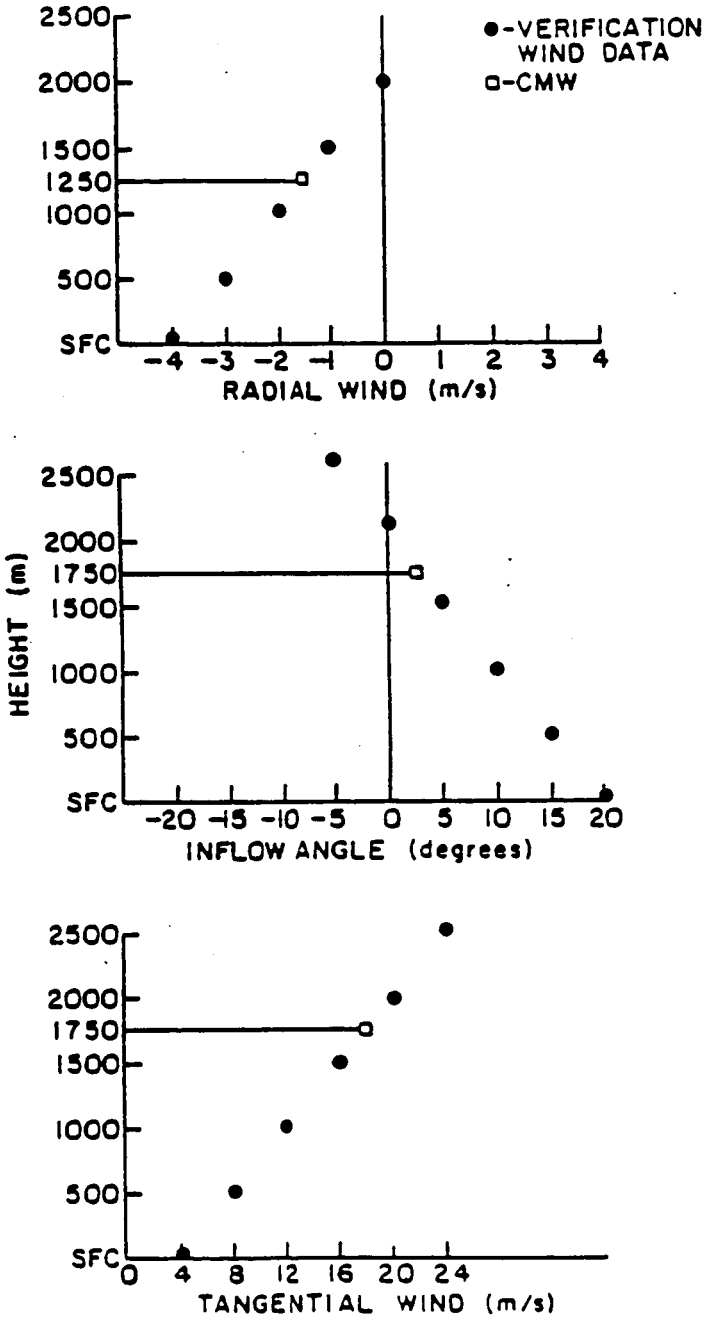

Figure 2.3 A hypothetical example of the technique employed to determine CMWH's. The horizontal line connecting the CMW and the vertical axis on each graph indicates the level of best agreement between the CMW and the verification profiles of the radial and tangential wind and inflow angle.

Figure 2.4 Location and CMWH's (km) of all low-level CMW's assigned heights on either 11 or 12 September using verification wind profiles.

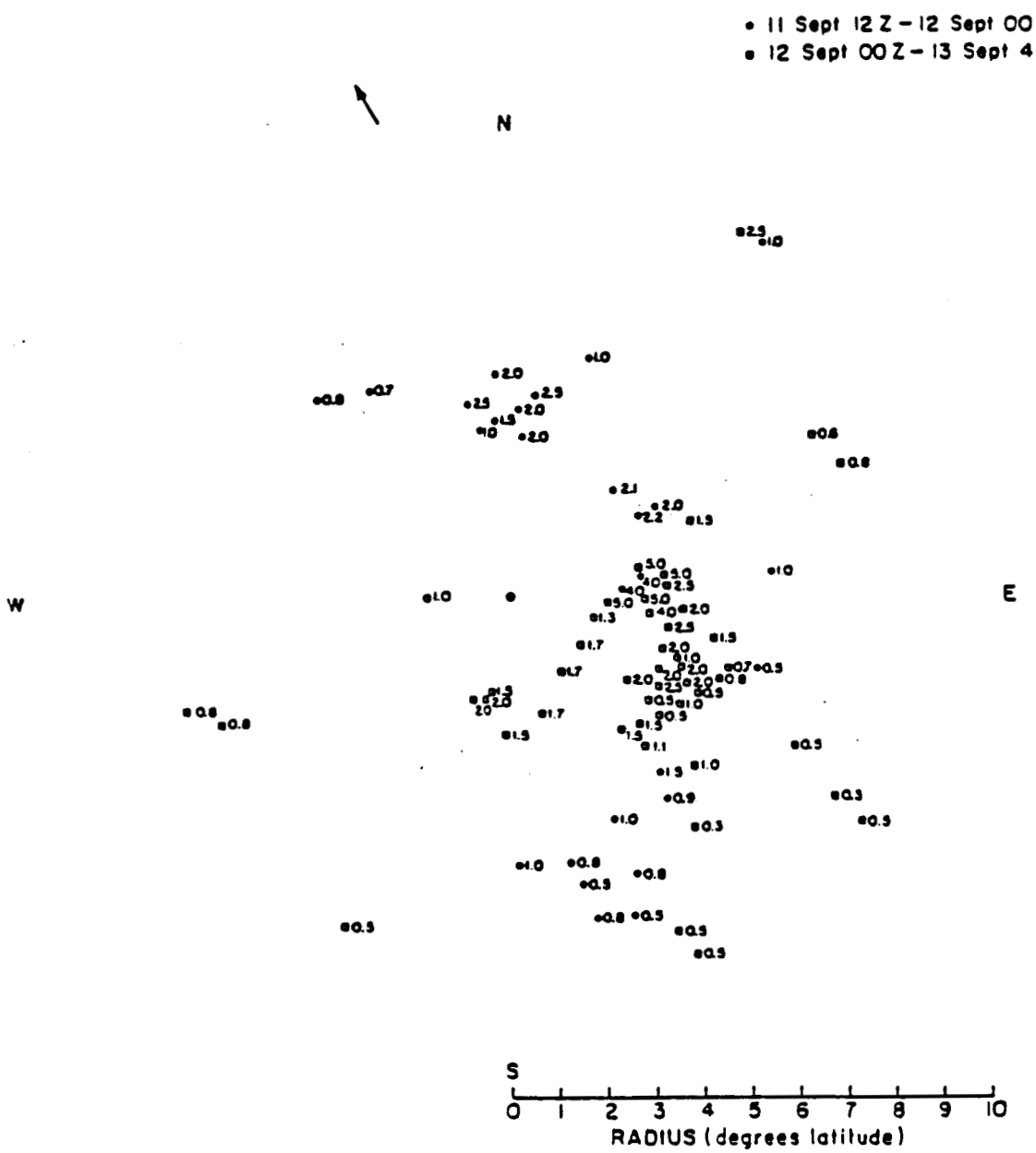
• 11 Sept 12 Z – 12 Sept 00 Z
• 12 Sept 00 Z – 13 Sept 4 Z
N
W
E
S
0 1 2 3 4 5 6 7 8 9 10
RADIUS (degrees latitude)

1600 GMT 11 September to about 2230 GMT 12 September. Since CMWH's seem consistent from 11 to 12 September in areas containing data on both days (Fig. 2.4), the author feels justified in combining CMWH's obtained on 11 and 12 September. The combined set of CMWH's are averaged locally to obtain a smoothed height field and then subjectively analyzed. CMWH's which differ markedly from neighboring height values are not used to obtain the final CMWH analysis depicted in Fig. 2.5.

The resultant map of CMWH's is used to assign heights to the remaining CMW's. Each CMW is assigned a height consistent with its position relative to Frederic's center. Since CMWH's appear to be conservative for the period from 1600 GMT 11 September to 2230 GMT 12 September, assigning CMWH's using the composite height analysis depicted in Fig. 2.5 is reasonable.

Upon inspecting the CMWH analysis shown in Fig. 2.5, it is clear that CMWH's vary systematically over Frederic's domain. Inside about 5 deg. radius, CMWH's generally exceed 1000 m with an area of maximum CMWH's observed about 3 deg. radius east of the storm center. Outside about 5 deg. radius, CMWH's are mainly between 500 and 1000 m with the exception being an area southeast of the storm where CMWH's are less than 500 m.

While the cause of the observed CMWH distribution is uncertain, there are a number of plausible explanations. It is hypothesized that some of the observed CMWH variations are related to variations in the magnitude of the vertical wind shear. Moreover, regional differences in cloud base height and cloud depth also may contribute to the observed CMWH pattern.

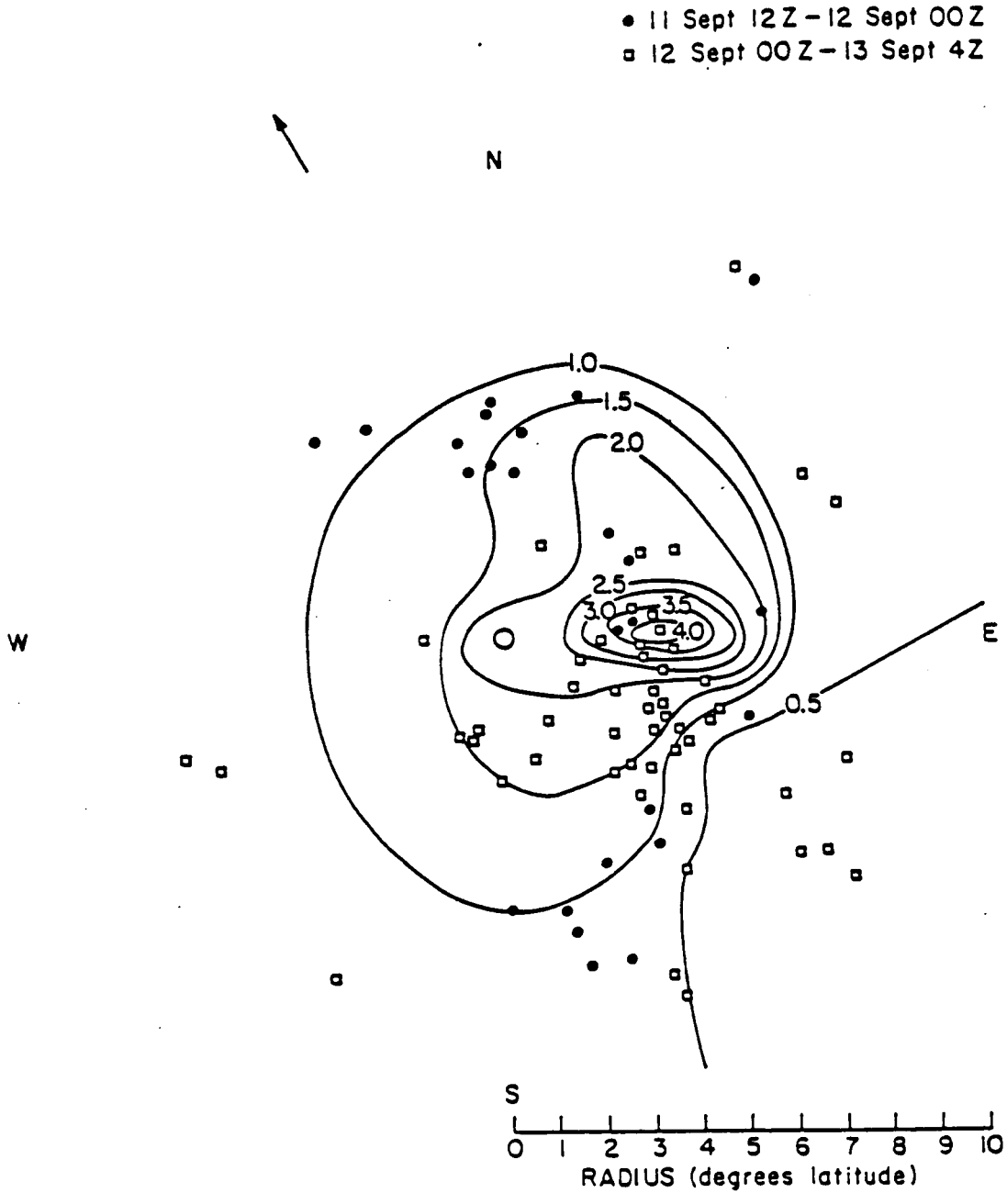

Figure 2.5 Plan view of low-level CMWH's (km). Only the locations of low-level CMW's employed to obtain the final CMWH analysis are shown (see text).

As suggested by Malkus (1949), a cumulus cloud's motion is a function of the cloud base wind and the vertical wind shear. Hence, in a more highly sheared environment one would expect a cumulus cloud to move with the wind at a level other than cloud base. While the evidence is not conclusive, the strength of the vertical wind shear may be partly responsible for the CMWH maximum just east of Frederic's center. The total vertical wind shear measured between the surface and 500 mb in the region of maximum CMWH's is about 2.5×10^{-3} s^{-1}. This is roughly double the vertical wind shear observed in the region of minimum CMWH's southeast of the storm's center. Consequently, it is believed that the region of maximum CMWH's may reflect the tracking of cloud tops which have been sheared off in a region of appreciable wind shear.

Regional differences in the height of cloud base and the depth of a cloud may also contribute to variations in low-level CMWH's. This explanation seems especially applicable southeast of Frederic's center where a wedge of lowered CMWH's coincides with a region of cold water observed by Black (1983). In such a region, one would expect convection to be suppressed thereby leading to shallower clouds and lower CMWH's.

Regardless of which, if either, of these explanations is correct, it seems apparent that low-level cumulus clouds tracked in a tropical cyclone environment do not approximate the wind at one level. Hence, the practice of assigning all low-level CMW's to a constant cloud base height of about 950 mb is believed to be flawed.

2.3.3 Adjustment of Cloud Motion Winds to Analysis Levels

To increase low-level wind resolution CMW's are adjusted to 560 and 1600 m so that they may be combined with aircraft and rawinsonde data at each of the aforementioned levels. As will be shown in Chapters 3 and 4, the availability of integrated wind data sets at 560 and 1600 m as well as a good surface wind analysis provide the wind coverage needed to perform useful analyses.

The radial, tangential and total horizontal wind components of each CMW are adjusted to 560 and 1600 m based upon shears computed at the verification wind profile sites used when assigning low-level CMWH's in Section 2.3.2. Outside 250 km, the availability of rawinsonde-measured wind data between about 950 and 500 mb and a good surface wind analysis make it possible to compute shears in the verification wind components between the following levels: surface and 950 mb (520 m, 33), 950 and 850 mb (1492 m, 21), 850 and 700 mb (3120 m, 36) and 700 and 500 mb (5848 m, 73). The numbers in parenthesis represent the average height and standard deviation of each of the 5 pressure levels.

Inside 250 km, wind data above the surface is obtained solely from research aircraft; hence, it is only possible to compute shears between the surface and 560 m and between 560 and 1600 m.

Shears in V_r, V_t and V computed from verification wind profiles on 11 and 12 September are stratified by layer and wind component. Shears are then plotted relative to Frederic's center and subjectively analyzed to produce analyses of ΔV_r, ΔV_t and ΔV between each of the

five layers outlined above. It is believed that these analyses are representative of the period from 1200 GMT 11 September to 0400 GMT 13 September.

Two approximations are made to facilitate the construction of shear analyses. First, since no significant or systematic change in shear magnitude was observed to have occurred from 11 to 12 September, shears from 11 and 12 September are combined. Moreover, it is assumed that the depth of each of the five layers within which shears are computed is constant over Frederic's entire domain. This assumption seems reasonable since the heights of the five pressure levels do not vary significantly at any verification wind profile site, as evidenced by the small standard deviations in pressure level heights cited previously.

The analyses of ΔV_r, ΔV_t and ΔV are used to adjust CMW's to 560 and 1600 m except in a portion of the SW quadrant where the large distances separating shear values preclude the use of shear analyses. The technique used in that region is discussed later in this section. A hypothetical example of the technique used to adjust the majority of CMW's to each analysis level is given below.

To illustrate the procedure used to adjust CMW's to 560 and 1600 m, consider a CMW assigned a height of 2000 m with a radial wind of -2 ms^{-1}. To adjust the radial wind component of the CMW to both the 560 and 1600 m analysis levels, the shear of the radial wind must be computed between the CMW and each analysis level. Between 2000 and 1600 m, the radial wind shear is computed by employing the analysis of ΔV_r for the layer between 700 and 850 mb discused previously. To illustrate, assume that V_r consistent with the position of the CMW is

about -2×10^{-3} s^{-1} for the layer from 700-850 mb. That shear is then multiplied by the distance between the CMW and the 1600 m analysis level (Δz) to obtain the correction factor (CF) needed to adjust the CMW to 1600 m [$CF = \Delta Vr \cdot \Delta z = -2 \times 10^{-3}$ $s^{-1} \times 400$ m $= -0.8$ m s^{-1}]. This correction factor is then employed to obtain the adjusted CMW radial wind component at 1600 m [$Vr_{1600} = Vr_{2000} + CF = -2.0 + -0.8 = -2.8$ m s^{-1}]. The adjusted radial wind component at 1600 m is then adjusted to 560 m using the same procedure described above with the only difference being that the correction factor is computed using the analysis of ΔV_r for the layer between 850 and 950 mb. The exact same procedure is used to adjust the tangential and total wind components of a CMW to 560 and 1600 m.

As discussed previously, the sparsity of verification wind profiles in a portion of the southwest quadrant precludes the use of the adjustment technique described above. Consequently, a different technique is introduced to adjust the CMW's in this region. For each CMW in this data sparse area, ΔV_r, ΔV_t and ΔV are computed for the layer between the CMW and the surface. The shears are obtained by dividing the difference between the CMW and surface values of V_r, V_t and V by the depth of the layer between the CMW and the surface (i.e., the CMWH). Surface estimates of V_r, V_t and V are obtained using composite surface winds discussed in Chapter 3. The radial, tangential and total wind components of each CMW are adjusted to 560 and 1600 m using the aforementioned shears and the same methods employed to adjust CMW's in other areas of the storm.

All adjusted CMW values are plotted at the appropriate level (i.e., 560 or 1600 m) to check for consistency. Those values which

differ markedly with neighboring values are discarded. The adjusted total CMW's at 560 and 1600 m as well as the aircraft and rawinsonde data at each of these levels are depicted in Figs. 2.6 and 2.7 respectively.

2.4 Composite Procedure

2.4.1 Compositing Philosophy

In this thesis, hurricane Frederic is assumed to be in steady-state between 1200 GMT 11 September and 0400 GMT 13 September. Although Frederic's central pressure dropped from 980 to 945 mb during this period, observations made by Powell (1982) and the author (this study) suggest that the storm's structure remained nearly constant from 1200 GMT 11 September to 0400 GMT 13 September.

Powell's (1982) study of Frederic's core revealed that no appreciable change in storm structure occurred during the period from about 1400 GMT 11 September to 0400 GMT 13 September. As noted in Section 2.1, Powell found that Frederic's maximum sustained flight-level winds increased by only 10 ms^{-1}, from 48 ms^{-1} to 58 ms^{-1}, between 1600 GMT 11 September and 0000 GMT 13 September. Moreover, he found that the radius of maximum winds remained near 35 km from 1400 GMT 11 September to 0200 GMT 13 September.

The author's inspection of winds in the environment surrounding Frederic's core lends support to the steady-state approximation. Specifically, rawinsonde and adjusted CMW velocities do not appear to have changed significantly from 11 to 12 September at either 560 or 1600 m (Figs. 2.6 and 2.7). In addition, as discussed in Section 2.3.3, no significant changes in vertical wind shear occurred from 11 to 12 September.

Figure 2.6 Same as Fig. 2.2, but for wind data at 560 m.

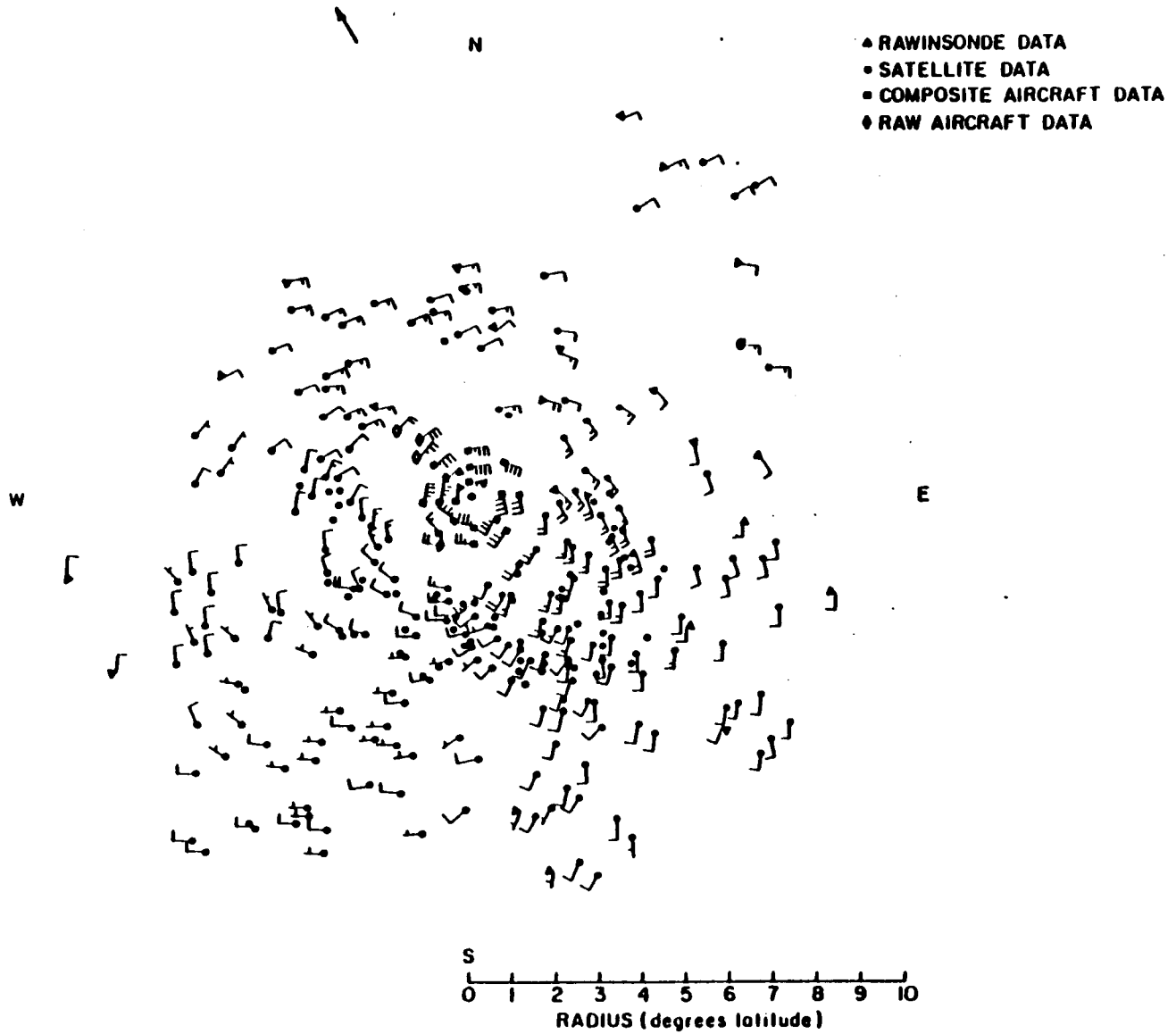
N
W
E
S
▲ RAWINSONDE DATA
• SATELLITE DATA
■ COMPOSITE AIRCRAFT DATA
♦ RAW AIRCRAFT DATA
0 1 2 3 4 5 6 7 8 9 10
RADIUS (degrees latitude)

Figure 2.7 Same as Fig. 2.2, but for wind data at 1600 m.

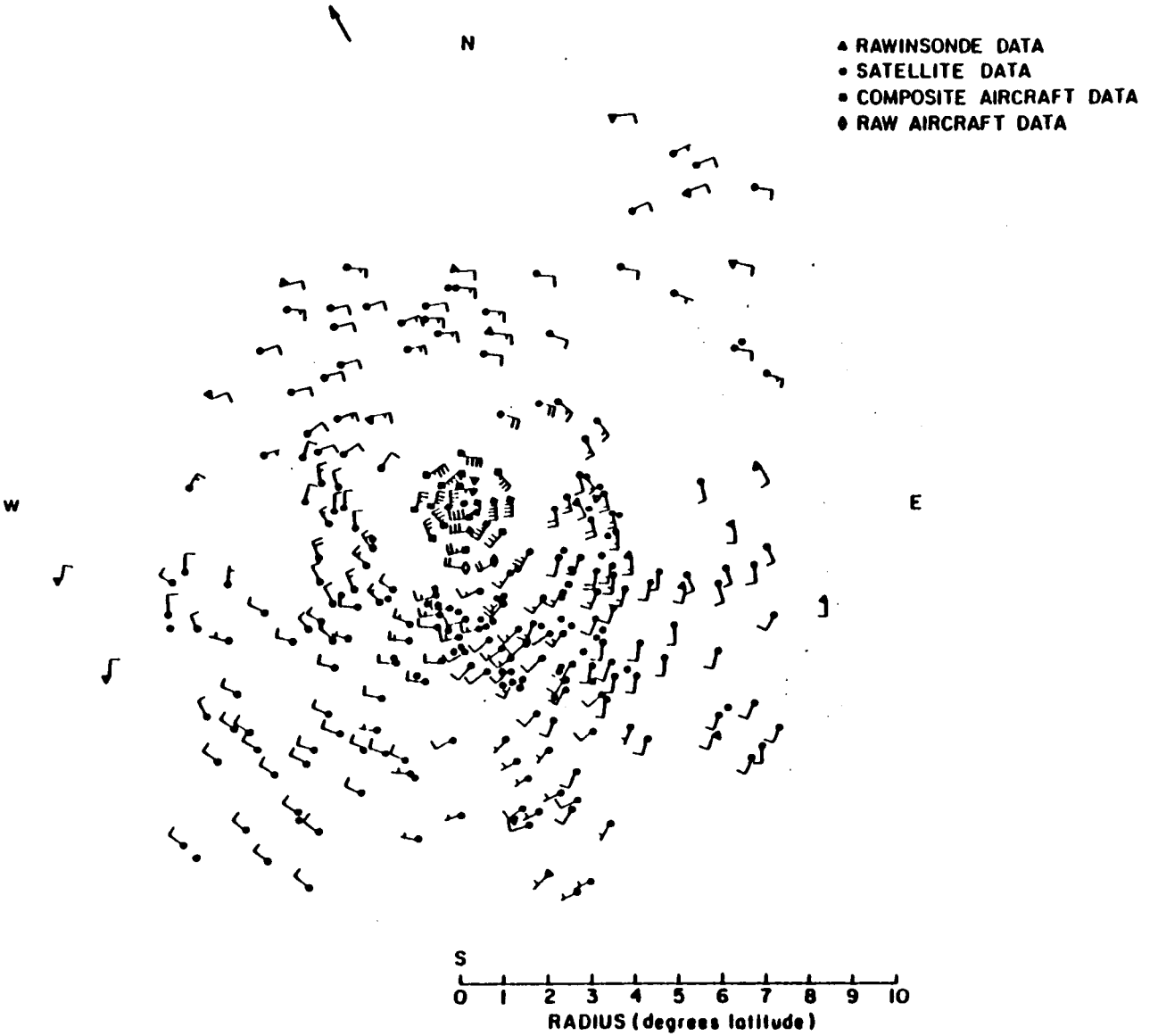
N
W
E
S
▲ RAWINSONDE DATA
• SATELLITE DATA
• COMPOSITE AIRCRAFT DATA
◊ RAW AIRCRAFT DATA
0 1 2 3 4 5 6 7 8 9 10
RADIUS (degrees latitude)

It is believed that the findings of Powell as well as the author's observations justify compositing data collected between 1200 GMT 11 September and 0400 GMT 13 September. While some loss in temporal resolution can be expected to occur when compositing data over a 40 hr period, the benefits of increased data resolution are thought to outweigh any loss in temporal resolution. This is especially true in the northwest and northeast quadrants of the storm, where the removal of overland data has resulted in limited data coverage at 560 and 1600 m on both 11 and 12 September. In these quadrants, compositing data over a 40 hr period is essential to obtaining realistic wind fields.

2.4.2 Compositing Technique

All surface, aircraft, rawinsonde and cloud motion winds collected between 1200 GMT 11 September and 0400 GMT 13 September are composited relative to Frederic's center at the surface, 560 and 1600 m. Frederic's center positions between 1200 GMT and 1600 GMT 11 September are obtained from Jorgenson (personal communication, 1984), while center positions between 1600 GMT 11 September and 0400 GMT 13 September are computed using best fit equations supplied by Powell (personal communication, 1984). Aircraft data composited at 560 and 1600 m deviated by no more than 200 m from each respective composite level. Rawinsonde data composited at 560 and 1600 m are obtained from the 950 and 850 mb presure levels respectively and are within about 100 m of those levels. By definition, adjusted 560 and 1600 m CMW's are assumed to apply to the 560 and 1600 m composite levels.

Composite wind data sets at the surface, 560 and 1600 m are objectively analyzed on the PSU meteorology computer system using a Bergthorssen-Cressman-Doos (BCD) analysis scheme. The BCD analysis scheme is very similar to the Cressman scheme (1959) with the major improvement being the scheme's ability to locate maximum and minimum values in the analyzed field. A more detailed description of the BCD analysis scheme can be found in Glahn, Hollenbaugh and Lowry (1969).

Objectively analyzed winds at the surface, 560 and 1600 m are composited onto a 40 x 30 rectangular grid. A grid spacing of 70 km is used, thus the grid domain is 2730 km long and 2030 km wide. The number and radii of influence of passes employed to objectively analyze composite winds are chosen based upon their ability to fill data void regions while preserving the asymmetries of the original wind field. At the surface, it was determined that passes made at 140, 100 and 70 km were most successful in accomplishing these goals, while passes made at 120, 85 and 65 km were found to be most successful at 560 and 1600 m.

Since it is more appropriate to employ cylindrical coordinates rather than cartesian coordinates when analyzing hurricanes, objectively analyzed winds are composited onto a cylindrical grid (Fig. 2.8). The grid employed here is comprised of 10, 1 deg. radial bands, each of which is divided into 16 sections 22.5 deg. in azimuthal extent (160 grid spaces). All wind data which fall within a given grid space are averaged together, and the resultant mean wind value is assigned to the center of the grid space. This procedure is employed to obtain mean values of V_r, V_t and V for each grid space. Winds are

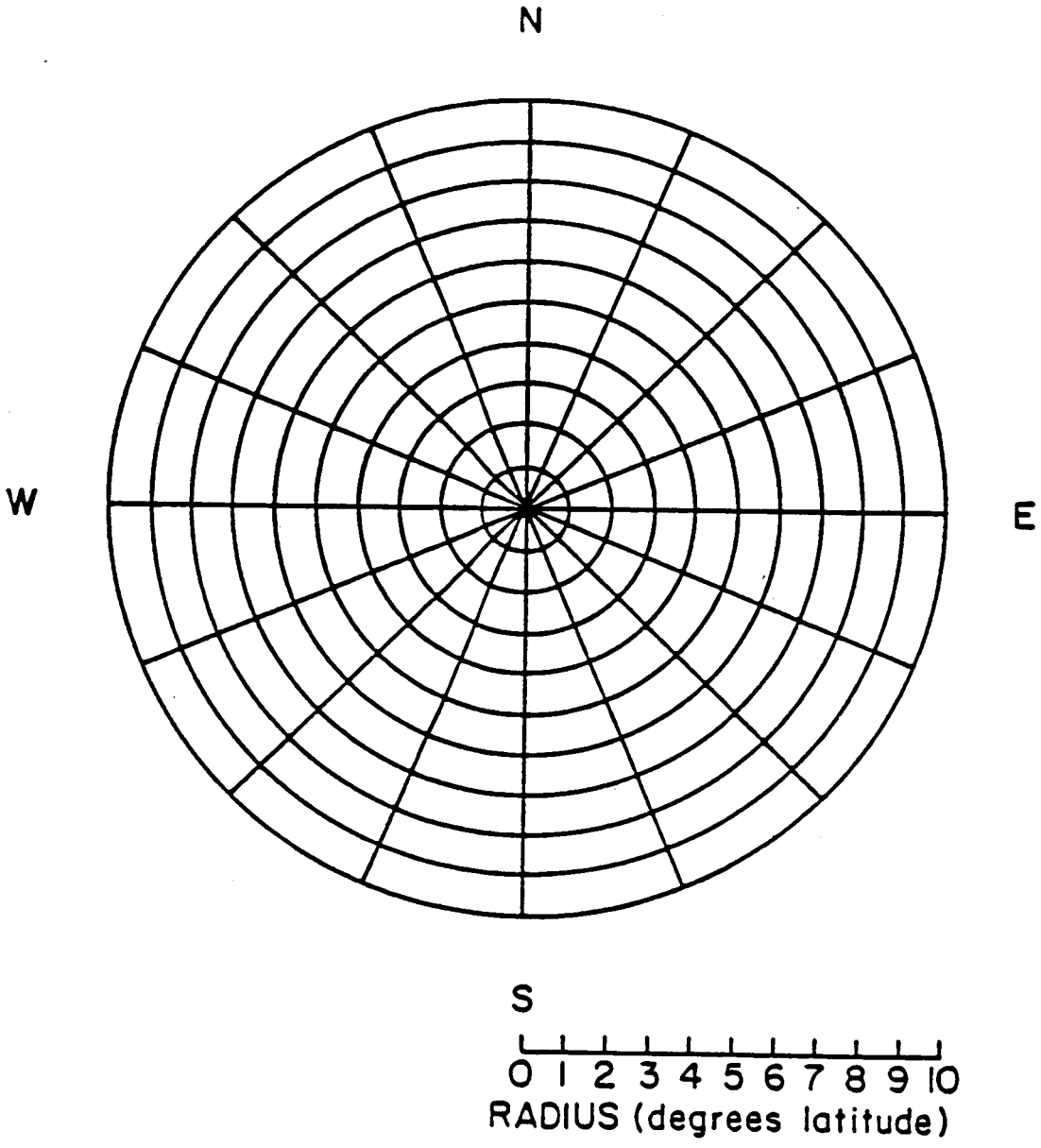

Figure 2.8 Compositing grid. Grid is aligned so that N points north when compositing data in either NAT or MOT coordinates.

composited in both natural (NAT) and motion (MOT) coordinates. To obtain motion winds, the mean storm motion of 5.5 ms^{-1} from 149° is subtracted from all winds. As will be discussed in subsequent chapters, these values are used for all of the analyses performed in this thesis.

Chapter 3

COMPOSITE WINDS

In the past, it has been difficult to perform an accurate multiple-scale analysis of the inflow layer structure of a single tropical cyclone due to the absence of adequate wind coverage over the entire storm domain. Inside about 150 km research aircraft have afforded good horizontal wind coverage of a storm's low-level structure but only limited vertical wind resolution, since aircraft-measured winds have generally been available only at a single level (usually around 900 mb) within the lowest 200 mb. Outside 150 km rawinsonde and satellite winds have been employed to resolve a storm's large scale structure; however, the density, quality and vertical resolution of the wind measurements provided by these sources has generally been insufficient to obtain accurate analyses of a storm's large-scale low-level structure.

The availability of unusually good wind coverage at the surface, 560 and 1600 m make it possible to overcome the aforementioned problems and enable the author to analyze the low-level structure of a single tropical cyclone (Frederic) out to a radius of 10 deg. latitude. In this chapter, composite winds at the surface, 560 and 1600 m are employed to investigate the axisymmetric and asymmetric low-level wind structure of hurricane Frederic. Analyses of Frederic's radial and tangential wind components as well as divergence (Div) and vorticity (ζ) fields are presented at the surface, 560 and 1600 m,

while analyses of the storm's vertical velocity (w) fields are depicted at 560 and 1600 m.

The analysis procedure employed in this thesis is not capable of resolving the detailed storm structure inside a radius of about 1.5 deg.; consequently, the magnitude and location of features within this radius are only approximate ones. A detailed analysis of Frederic's inner 1.5 deg. radius can be found in Frank (1984).

Throughout this chapter, an effort is made to illustrate the differences between the analyzed wind fields of this study and those which result when all CMW's are assigned to a constant height of 560 m rather than to the heights determined in Section 2.3.2. To accomplish this, analyses of V_r, V_t, Div, ζ and w are obtained at 560 and 1600 m using corrected and raw wind data sets and then compared. Both corrected and raw wind data sets are comprised of rawinsonde, aircraft and CMW data; however, only corrected wind data sets are adjusted for the variations in low-level CMWH's shown in Fig. 2.5. In the raw wind data sets, all CMW's are assigned to the 560 m analysis level without adjustment.

3.1 Radial Winds

Plan view analyses of V_r in NAT coordinates at the surface, 560 and 1600 m are presented in Figs. 3.1-3.3. The radial wind fields depicted in these figures appear reasonably consistent between levels, which is encouraging considering that surface winds are obtained largely from different sources than are those at 560 and 1600 m.

Inflow is observed over the majority of the storm's domain at each analysis level. The region of enhanced radial inflow observed

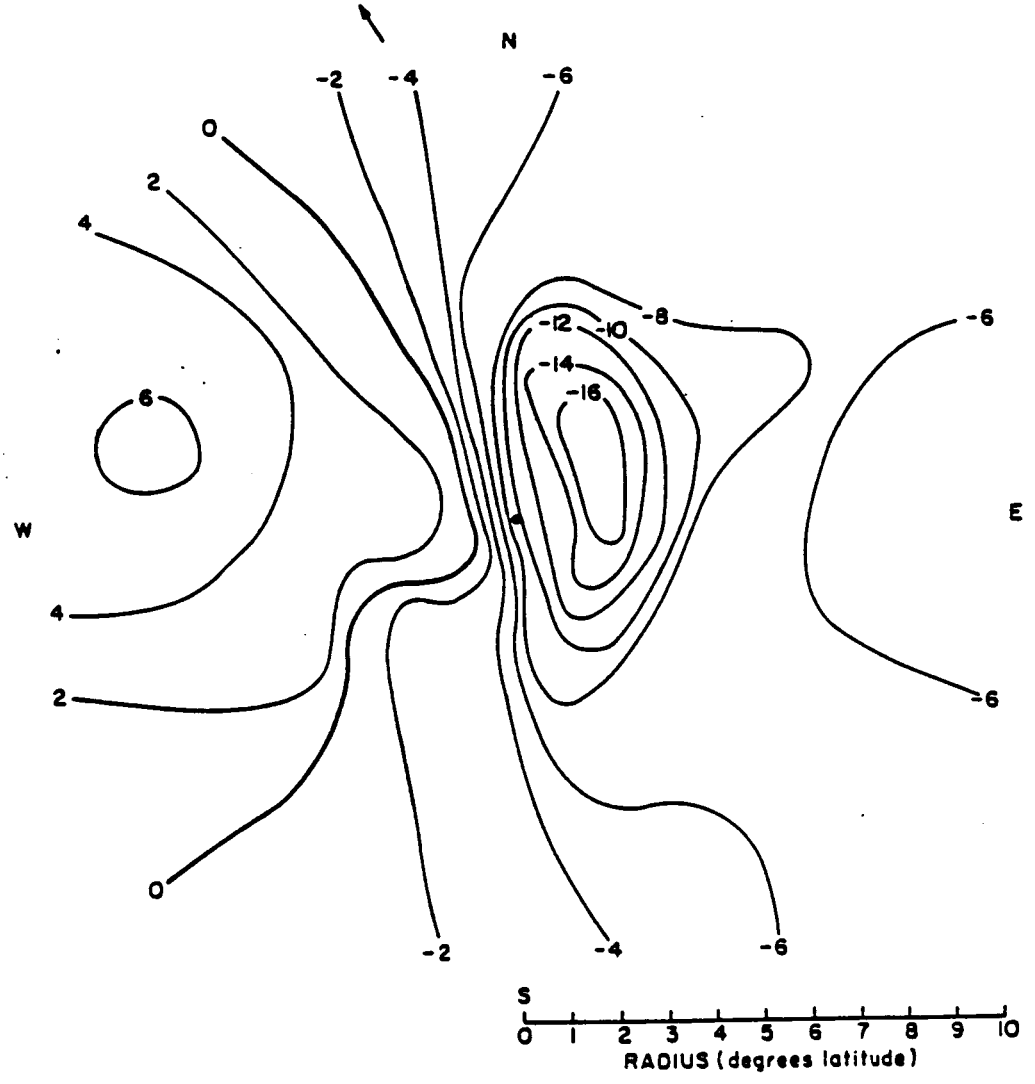

Figure 3.1 Plan view of radial winds (ms^{-1}) at the surface in NAT coordinates.

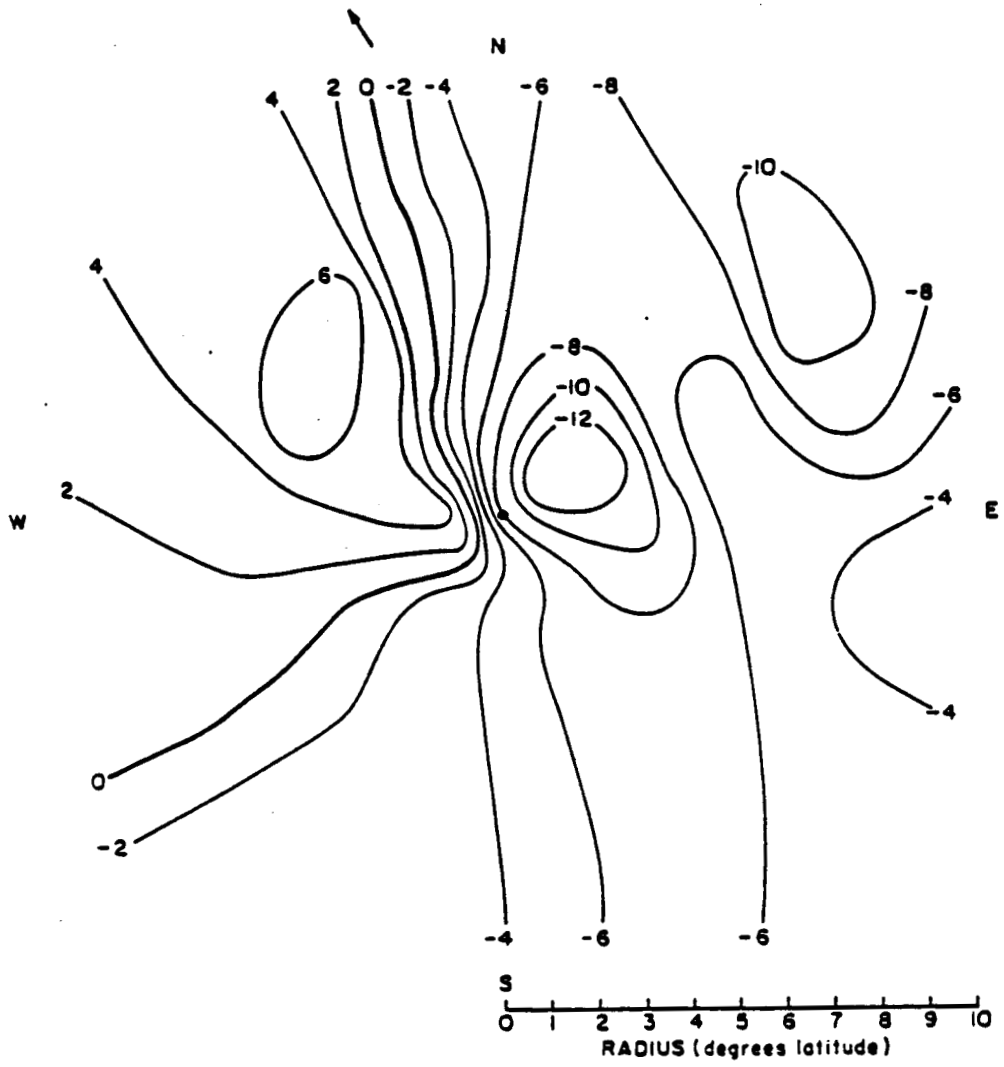

Figure 3.2 Same as Fig. 3.1, but at 560 m.

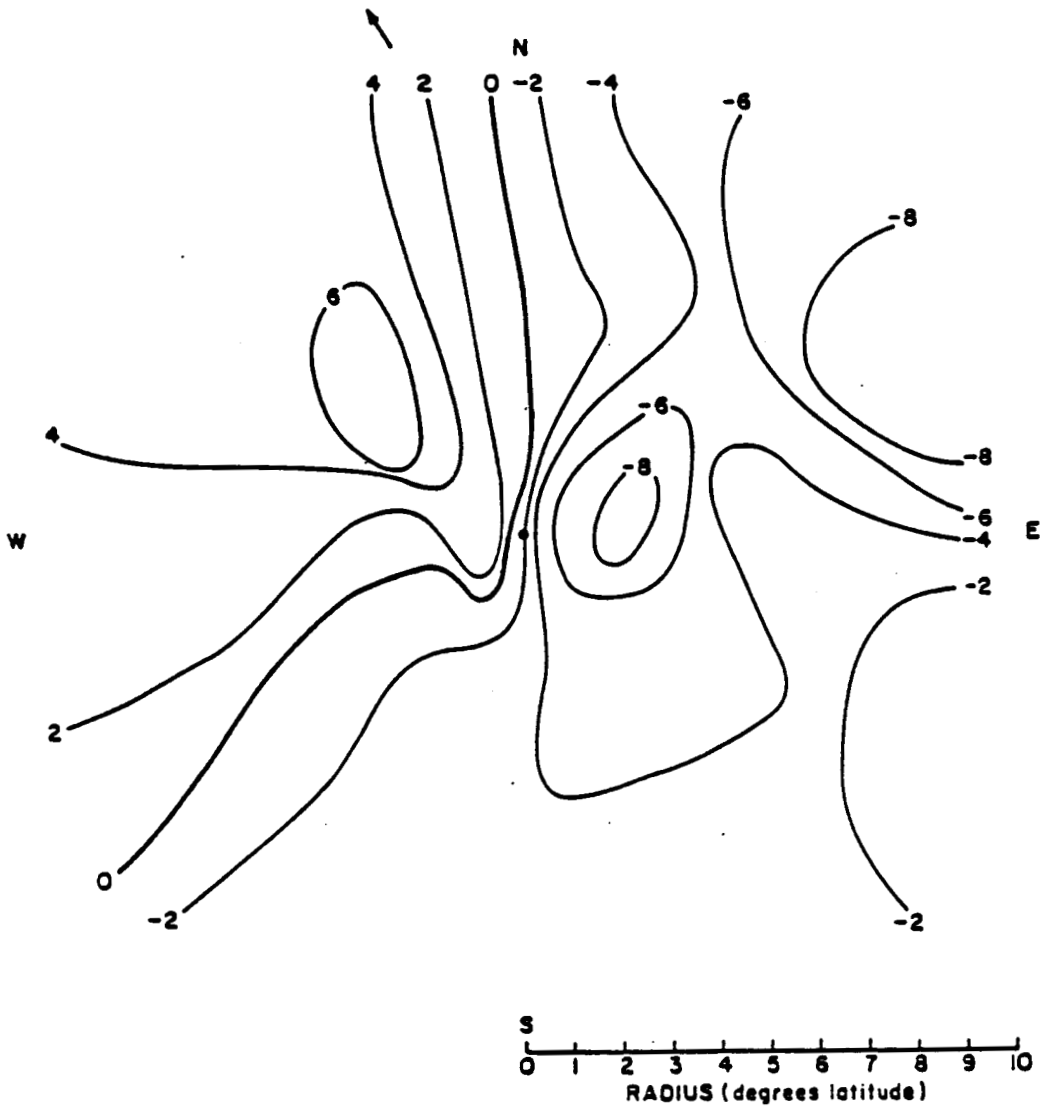

Figure 3.3 Same as Fig. 3.1, but at 1600 m.

southeast of the storm center is consistent with Powell's (1982) surface wind analysis. Powell (1982) suggested that this region of strong inflow may result from decoupling of the boundary layer over Frederic's cold wake. A principal inflow maximum is observed about 2 deg. radius northeast of the storm center at each analysis level with the strongest inflow observed at the surface. The position of the principal inflow maximum is consistent with Frank's (1984) study of Frederic's core. A secondary inflow maximum is observed about 8 deg. radius northeast of Frederic's center at all levels but is most pronounced at 560 m. It is hypothesized that the secondary inflow maximum northeast of the storm center is the result of interaction with a high pressure system ridging down the east coast of the United States.

Outflow is observed over a broad area west of Frederic's center at each analysis level. An outflow maximum is observed at about 5 deg. radius northwest of the storm center at 560 and 1600 m and about 8 deg. radius west of the storm center at the surface.

Plan view analyses of V_r at the surface, 560 and 1600 m in MOT (storm motion subtracted out) coordinates are depicted in Figs. 3.4-3.6. Although the analyses of V_r in MOT coordinates are similar to those in NAT (stationary) coordinates, there are some noteworthy differences. Specifically, radial inflow in MOT coordinates is observed to cover a smaller area than was observed in NAT coordinates. Moreover, while the locations of inflow maxima in MOT coordinates coincide roughly with those in NAT coordinates, the former are somewhat stronger.

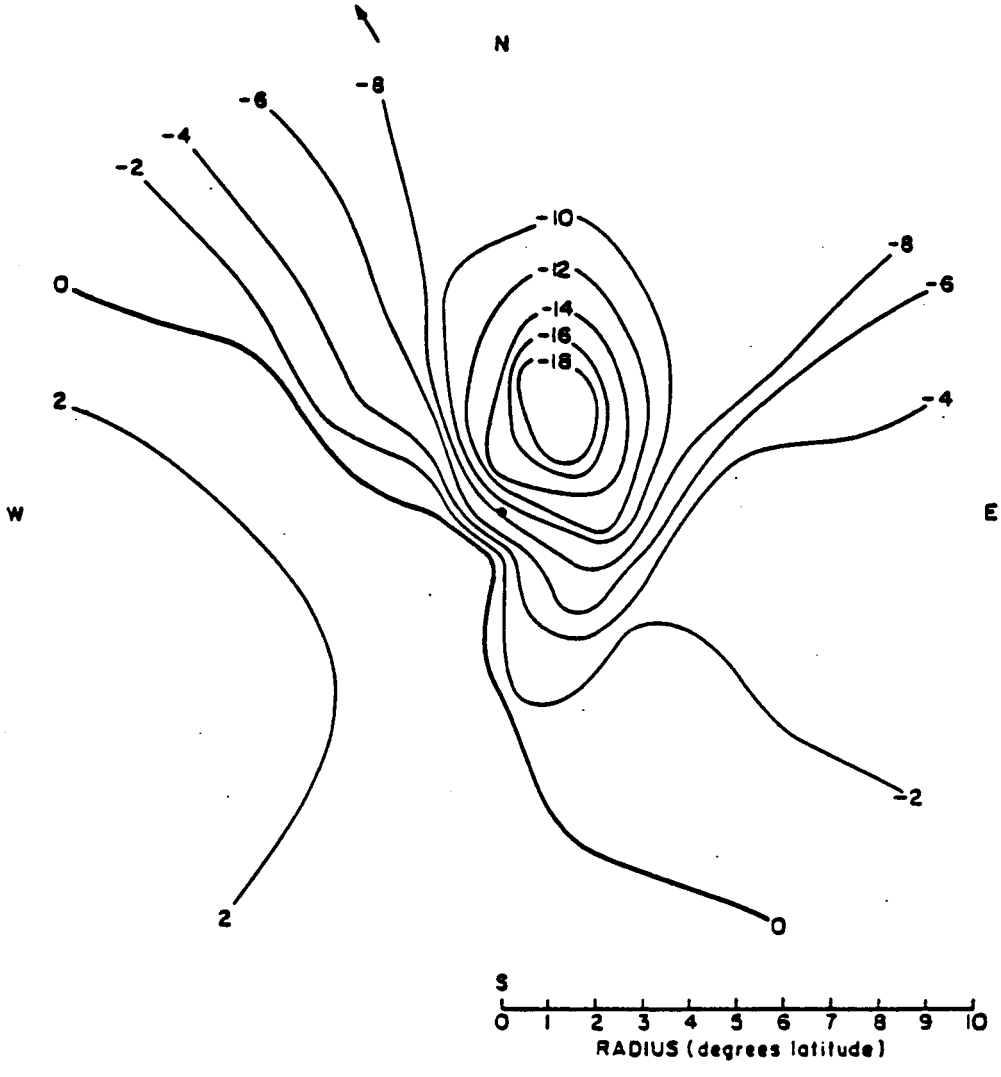

Figure 3.4 Plan view of radial winds (ms^{-1}) at the surface in MOT coordinates.

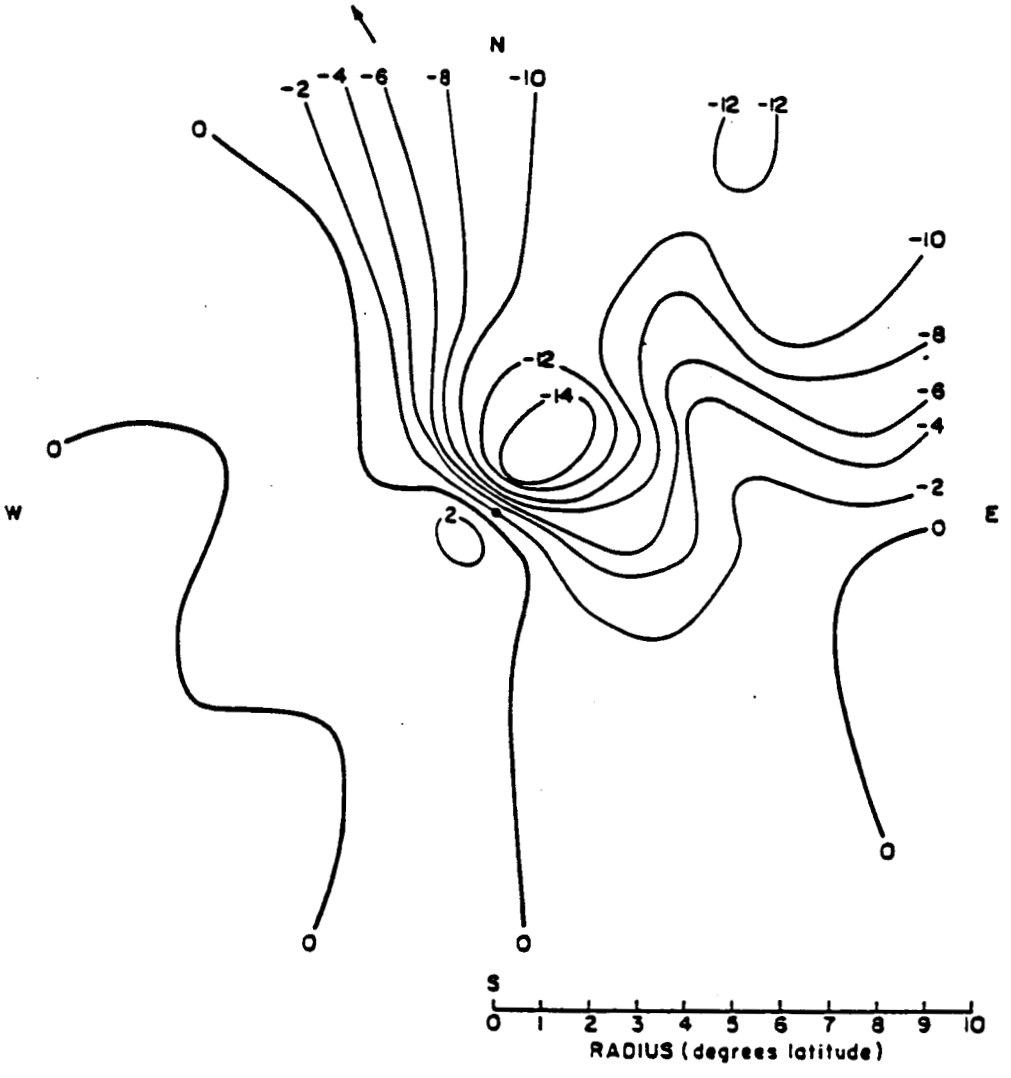

Figure 3.5 Same as Fig. 3.4, but at 560 m.

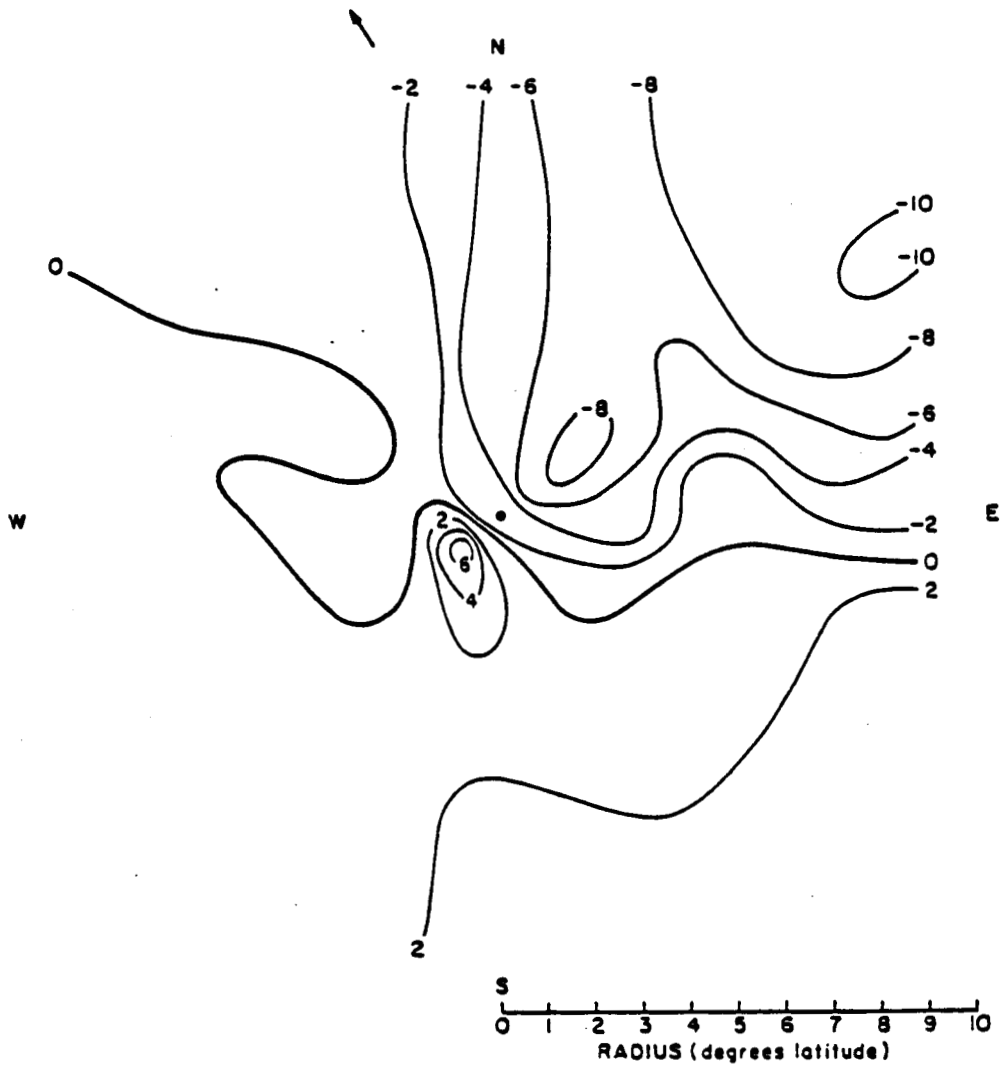

Figure 3.6 Same as Fig. 3.4, but at 1600 m.

The area covered by radial outflow in MOT coordinates is broader than that observed in NAT coordinates at each analysis level. Moreover, outflow maxima observed west of the storm center in NAT coordinates are not visible in MOT coordinates. This is reasonable since subtracting out the mean storm motion of 5.5 ms^{-1} from 149° should result in weaker radial outflow north and west of the storm center in MOT coordinates. It is also worth noting that a well defined outflow maximum is observed southeast of Frederic's center at 1600 m in MOT coordinates, while only weak outflow is observed southeast of Frederic's center in NAT coordinates.

A two-dimensional cross-section of V_r is depicted in Fig. 3.7. Inflow is observed between the surface and 1600 m at all radii between 1 and 10 deg. with maxima observed at approximately 2 and 9 deg. radius. It is noteworthy that maximum radial inflow is found near the surface inside about 6 deg. radius and near 560 m beyond 6 deg. radius. Previous composite studies conducted by Nunez and Gray (1977), Frank (1977a), Holland (1983b) and others indicate that maximum radial inflow occurs near 950 mb at all radii. While it is conceivable that the observed surface inflow maximum is the result of wind asymmetries which are unique to this storm, it is hypothesized that similar surface inflow maxima may have been present in other storms but were not detected because of insufficient over-water surface wind data.

Radial wind anomalies are computed at 560 and 1600 m to determine the differences between radial wind values obtained using corrected and

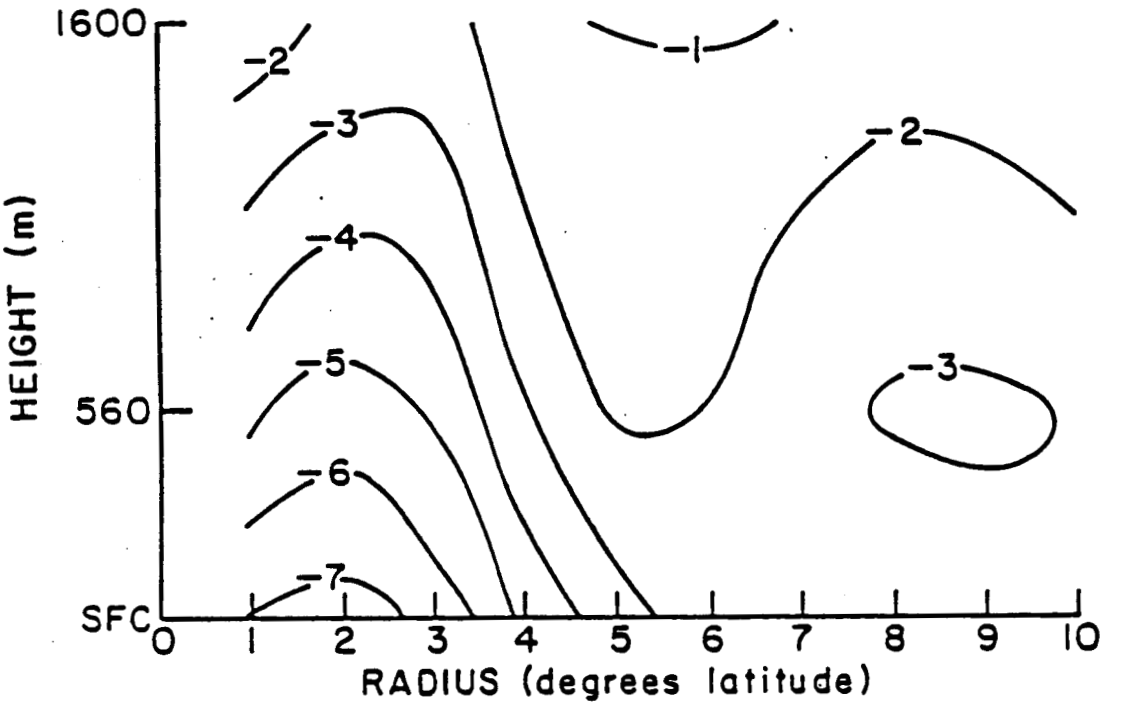

Figure 3.7 Two-dimensional cross-section of radial winds (ms^{-1}).

raw wind sets. The radial wind anomaly ($V_{r_{anomaly}}$) is obtained at each grid point at 560 and 1600 m using the equation:

$$\text{Radial Wind Anomaly} = V_{r_{corrected}} - V_{r_{raw}} \tag{3.1}$$

where $V_{r_{corrected}}$ and $V_{r_{raw}}$ are the grid point radial wind values obtained using corrected and raw wind sets respectively. Plan view analyses of the radial wind anomaly at 560 and 1600 m are presented in Figs. 3.8 and 3.9 respectively. It is important to note that $V_{r_{anomaly}}$ is not analyzed inside 1.5 deg. radius at either 560 or 1600 m because no CMW's were tracked inside that radius; consequently, no differences exist between corrected and raw wind values of V_r.

Examination of Figs. 3.8 and 3.9 indicates that the anomaly patterns are quite similar at both levels, although the radial wind anomalies are somewhat larger at 560 m in some regions. Raw wind sets are observed to underestimate the radial inflow ($V_{r_{anomaly}} < 0$) at 560 and 1600 m over the majority of the storm domain, with the greatest underestimation occurring about 3 deg. radius east of the storm where a radial wind anomaly of less than -6 ms^{-1} is observed at both levels. Overestimation ($V_{r_{anomaly}} > 0$) of the radial inflow by raw wind sets is observed southeast and also west of the storm center. The largest overestimation of radial inflow by raw wind sets is found in a region about 8 deg. radius west of the storm center where $V_{r_{anomaly}}$ exceeds 4 ms^{-1}.

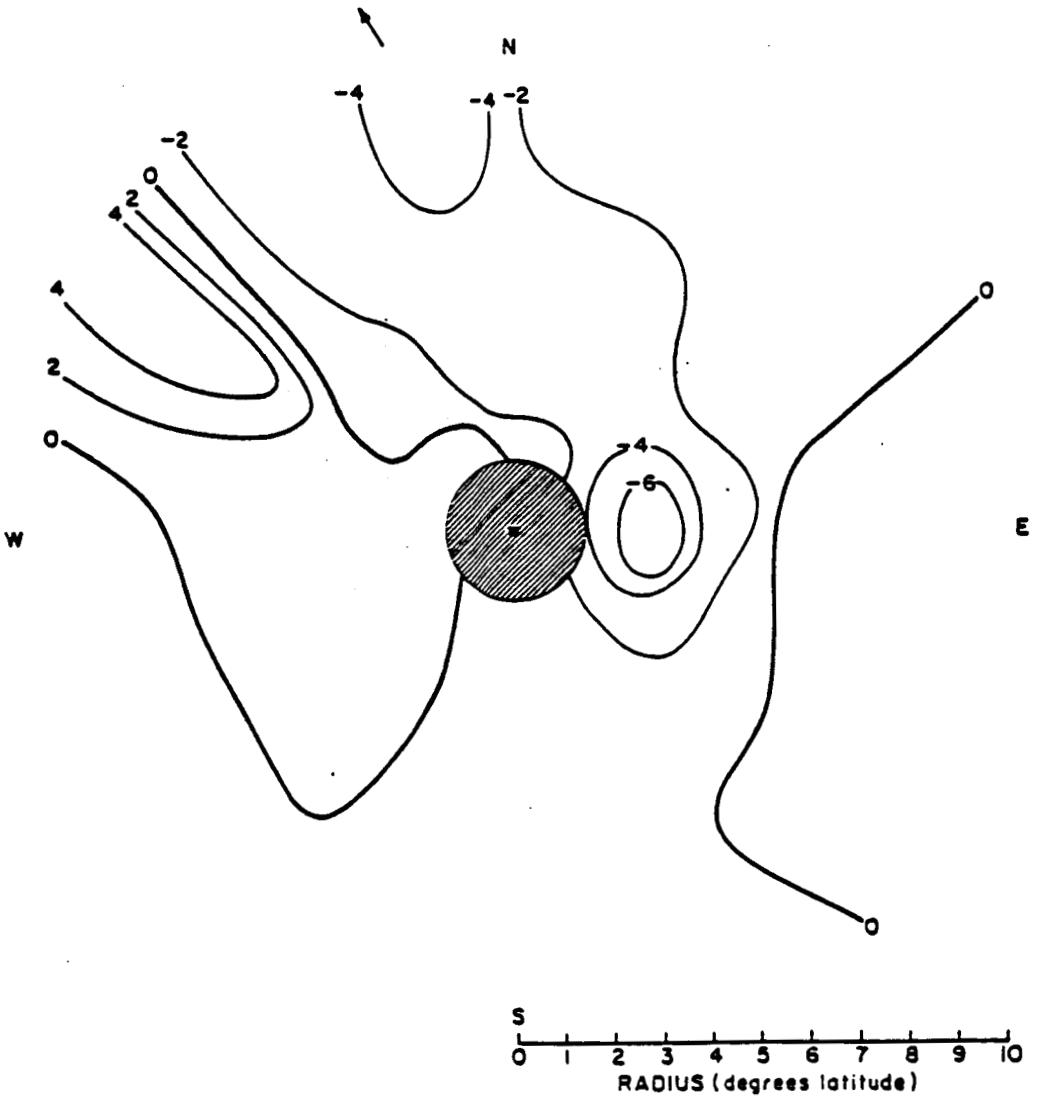

Figure 3.8 Plan view of radial wind anomalies (ms^{-1}) at 560 m.

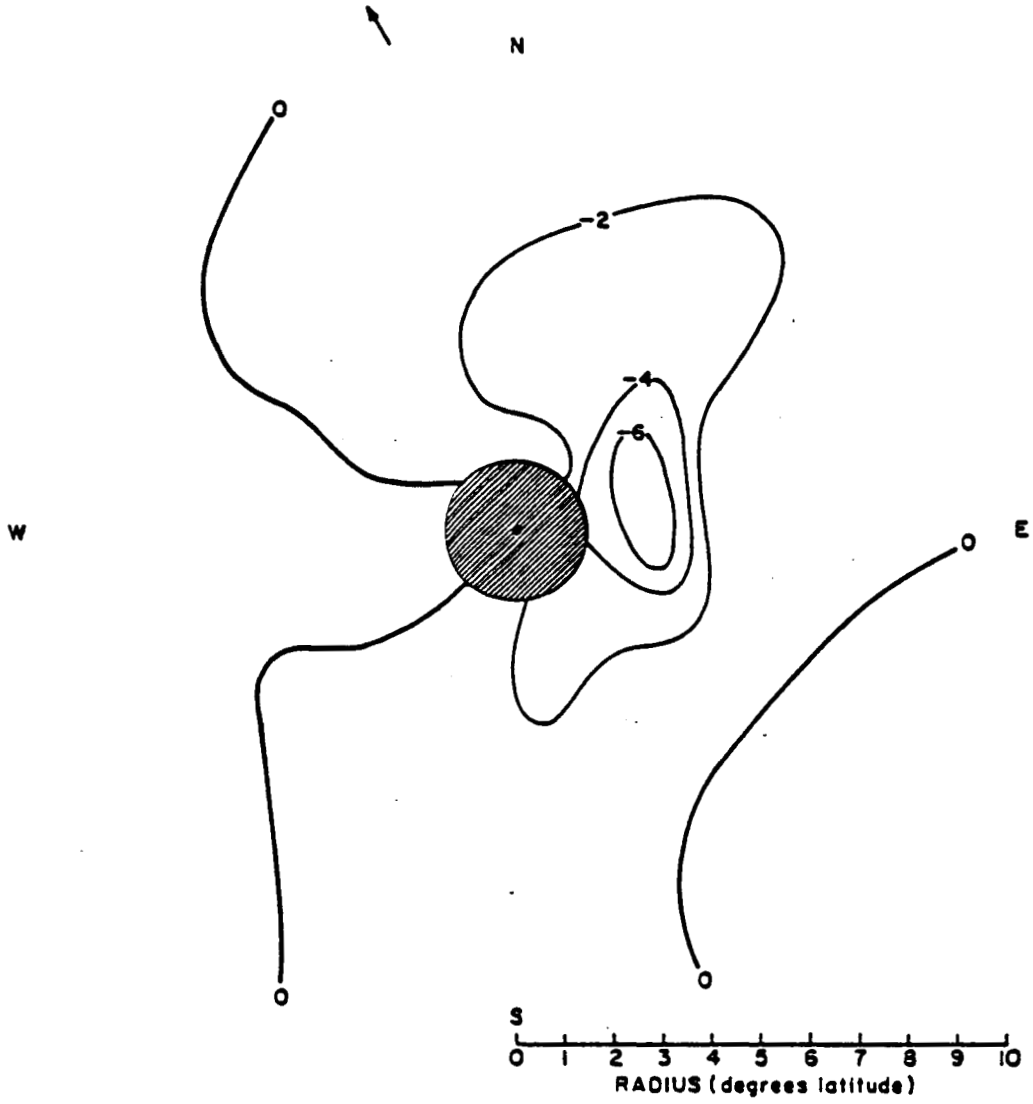

Figure 3.9 Same as Fig. 3.8, but at 1600 m.

For the most part, the radial wind anomaly patterns at 560 and 1600 m are consistent with the CMWH analysis depicted in Fig. 2.5. Raw winds are expected to underestimate the radial winds over much of the storm domain since CMWH's exceed 560 m over the majority of the storm domain and V_r tends to decrease with height. Examination of the radial wind analyses obtained using corrected and raw wind sets indicates that where the latter overestimate the radial winds, they do so because of random errors in the raw radial wind values and not because the CMWH's in those areas are less then 560 m. The exception is southeast of the storm at large radii where analyzed CMWH's are less than 560 m over a broad area. In this region one would expect raw wind sets to overestimate V_r since rawinsonde and surface data indicate V_r is strongest near the surface and decreases with height.

Axisymmetric corrected and raw radial wind values at 560 and 1600 m are shown in Figs. 3.10 and 3.11 respectively. At 1600 m, axisymmetric values of V_r obtained by adjusting 560 m raw winds to 1600 m using a "storm mean" shear corection factor are also shown. The "storm mean" correction factor is calculated based upon the mean 950-850 mb rawinsonde-derived radial wind shear (Chapter 2).

Figures 3.10 and 3.11 indicate that raw wind sets underestimate the radial inflow at all radii > 2 deg. It is important to note that 1 deg. values of V_r obtained using corrected and raw wind sets respectively are equal because no differences between the two data sets exist inside 1.5 deg. radius. The underestimation of radial inflow by raw wind sets generally increases with decreasing radius and is greatest at about 3 deg. radius. It is noteworthy that at 3 and 4 deg.

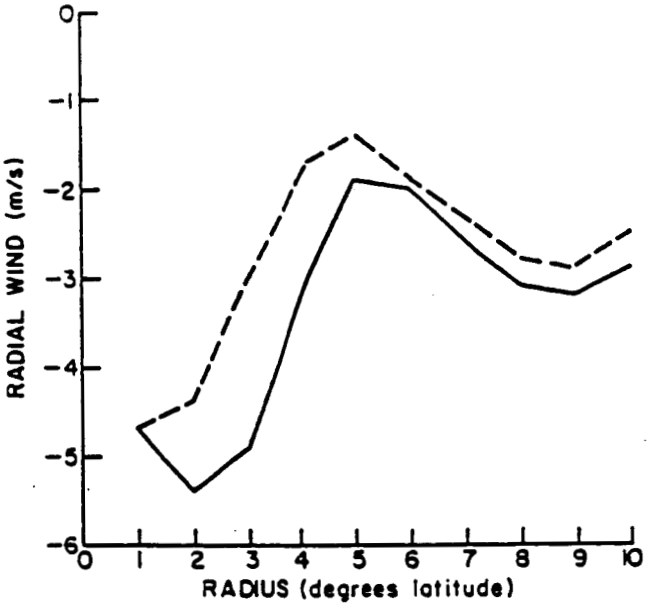

Figure 3.10 Axisymmetric radial winds (ms^{-1}) at 560 m obtained using corrected wind sets (———) and raw wind sets (– – – –).

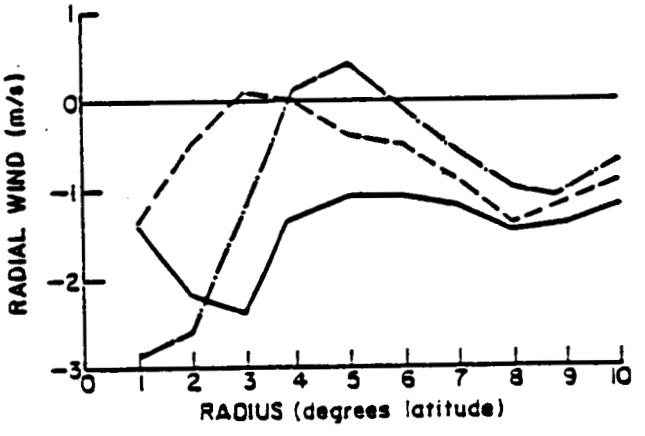

Figure 3.11 Axisymmetric radial winds (ms^{-1}) at 1600 m obtained using corrected wind sets (———), raw wind sets (– – – –) and by applying a storm mean correction factor to the 560 m raw radial wind values (-·-·-·).

radius, raw wind sets suggest that there is weak outflow at 1600 m, while corrected wind sets indicate that inflow exceeds 2 ms^{-1}.

The axisymmetric differences between radial wind values obtained using raw and corrected wind sets are especially important when computing the radial mass flux through the storm. The radial mass flux is computed between the surface and the top of the inflow layer (Z_{top}) using the equation:

$$\text{Radial Mass Flux} = \overline{\rho}\ \overline{V}_r Z_{top} \qquad (3.2)$$

where $\overline{\rho}$ and $\overline{V}_r$ are the layer average density and radial wind between the surface and Z_{top} respectively, and Z_{top} is the height of the top of the inflow layer estimated by determining the level at which $V_r = 0$ by linear extrapolation. Since the quantity of thermodynamic measurements available for this storm is rather limited, the layer average density is estimated using thermodynamic data for the composite typhoon (Frank, 1977a).

Table 3.1 compares the radial mass flux through the storm obtained using corrected and raw wind sets. As shown in the last column of Table 3.1, raw wind sets underestimate the radial mass flux through the storm at all radii between 2 and 10 deg., with substantial underestimation observed inside 7 deg. radius. At 3 and 4 deg. radius, the radial mass flux obtained using corrected wind sets is roughly double that which is obtained using raw wind sets. Beyond 7 deg. radius only minor differences are observed. Considering the crucial role the radial mass flux plays in computing various storm properties,

Table 3.1 Total mass flux through the storm ($\overline{\rho}\ \overline{V}_r Z_{top}$) obtained using corrected wind sets and raw wind sets. Total mass flux per unit area (x 10^3 kg m^{-1} s^{-1}).

Radius (Degrees Latitude)	Corrected Wind Sets	Raw Winds Sets	Corrected Wind Sets/ Raw Wind Sets
1*	-6.7	-6.7	1.0
2	-8.3	-5.9	1.4
3	-8.3	-4.2	2.0
4	-5.3	-2.8	1.9
5	-3.9	-2.4	1.6
6	-3.7	-2.6	1.4
7	-4.3	-3.3	1.3
8	-4.6	-4.5	1.0
9	-4.6	-4.2	1.1
10	-4.0	-3.5	1.1

*NOTE: Total mass flux through the storm obtained using raw and corrected wind sets is identical at 1 deg. radius since no difference exists between raw and corrected wind sets at that radius (see text).

the aforementioned differences in radial mass flux could result in significant errors in many storm computations.

3.2 Tangential Winds

Plan view analyses of V_t in NAT coordinates at the surface, 560 and 1600 m are depicted in Figs. 3.12-3.14. Cyclonic flow is observed at each analysis level over the entire storm domain, and a marked northwest to southeast asymmetry is observed at all levels. This is consistent with the wind asymmetries which Powell (1982) found when analyzing Frederic's total surface winds inside 5 deg. radius. Tangential wind maxima are observed roughly 1 deg. radius north of the storm center at the surface, 560 and 1600 m with the strongest cyclonic winds observed at 1600 m. (Frank's (1984) more detailed analysis of the core showed the radius of maximum of winds to be about 35 km at these levels.)

Plan view analyses of tangential winds in MOT coordinates at the surface, 560 and 1600 m are presented in Figs. 3.15-3.17. Cyclonic flow is visible over the entire storm domain at all levels except at the surface north and east of the storm center, where weak anticyclonic flow is observed. The cyclonic circulation is noticeably stronger west of the storm center at each analysis level. The principal cyclonic jet maximum is located approximately 1 deg. radius west of the storm center at each analysis level and is strongest at 1600 m. A secondary cyclonic jet maximum is observed about 8 deg. radius west of the storm center and is most visible at the surface. The secondary jet maximum is associated with the circulation around a small low pressure system in the western Gulf of Mexico.

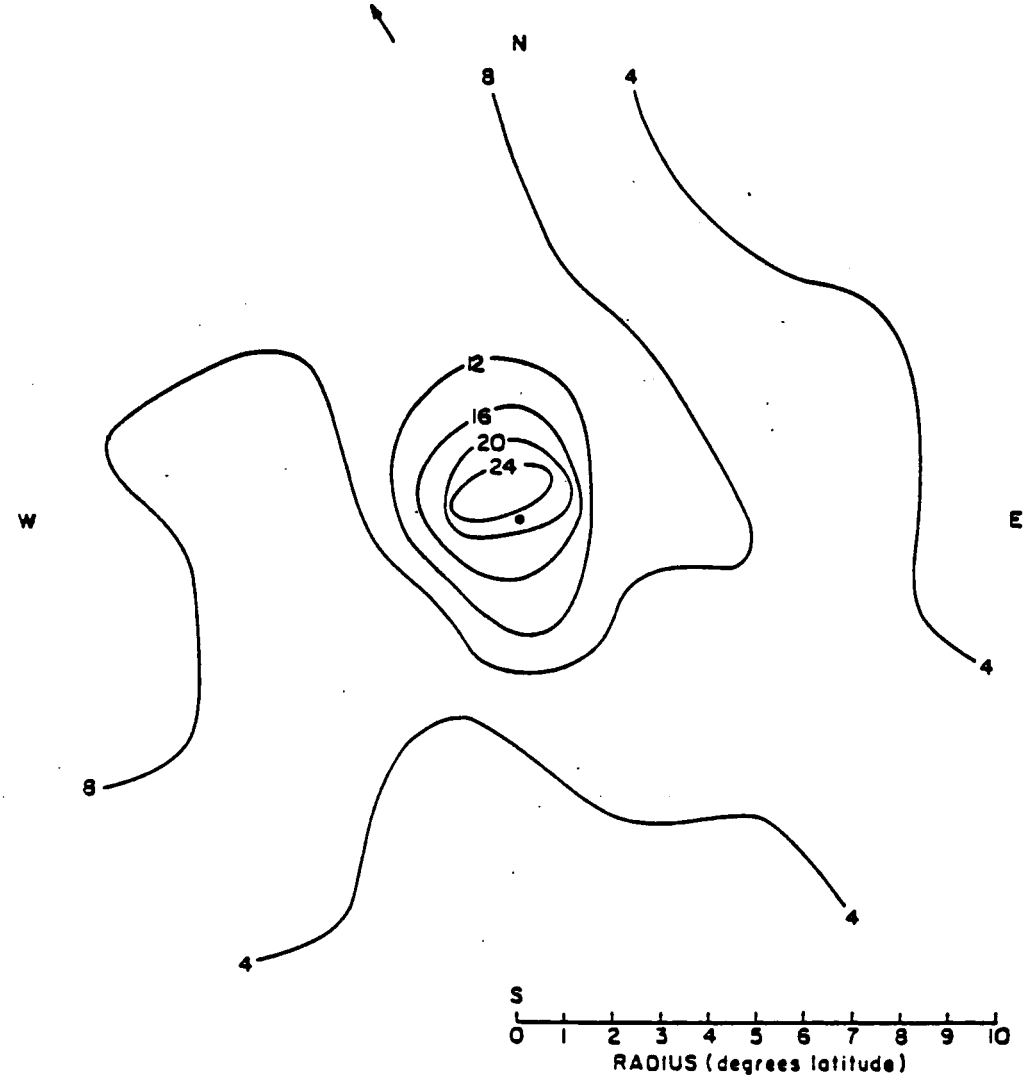

Figure 3.12 Plan view of tangential winds (ms^{-1}) at the surface in NAT coordinates.

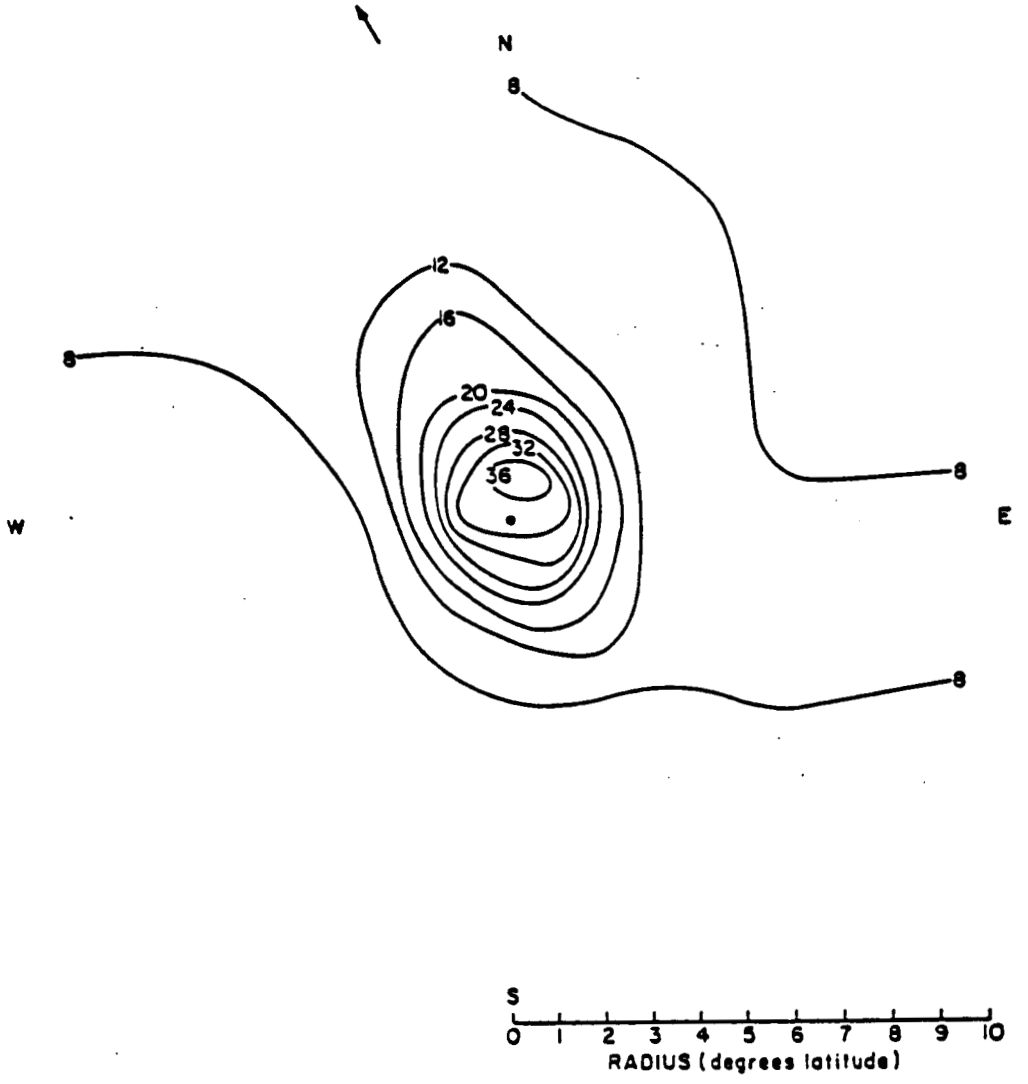

Figure 3.13 Same as Fig. 3.12, but at 560 m.

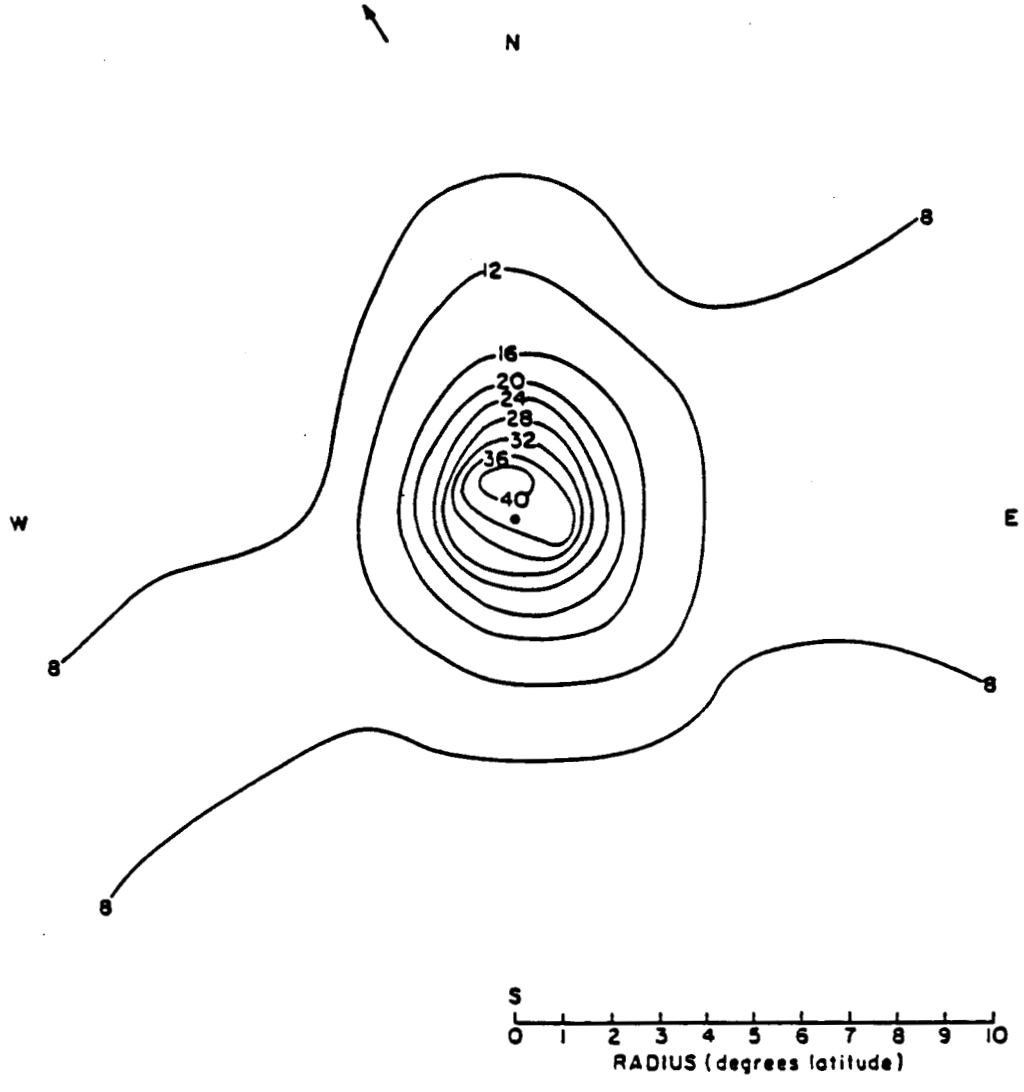

Figure 3.14 Same as Fig. 3.12, but at 1600 m.

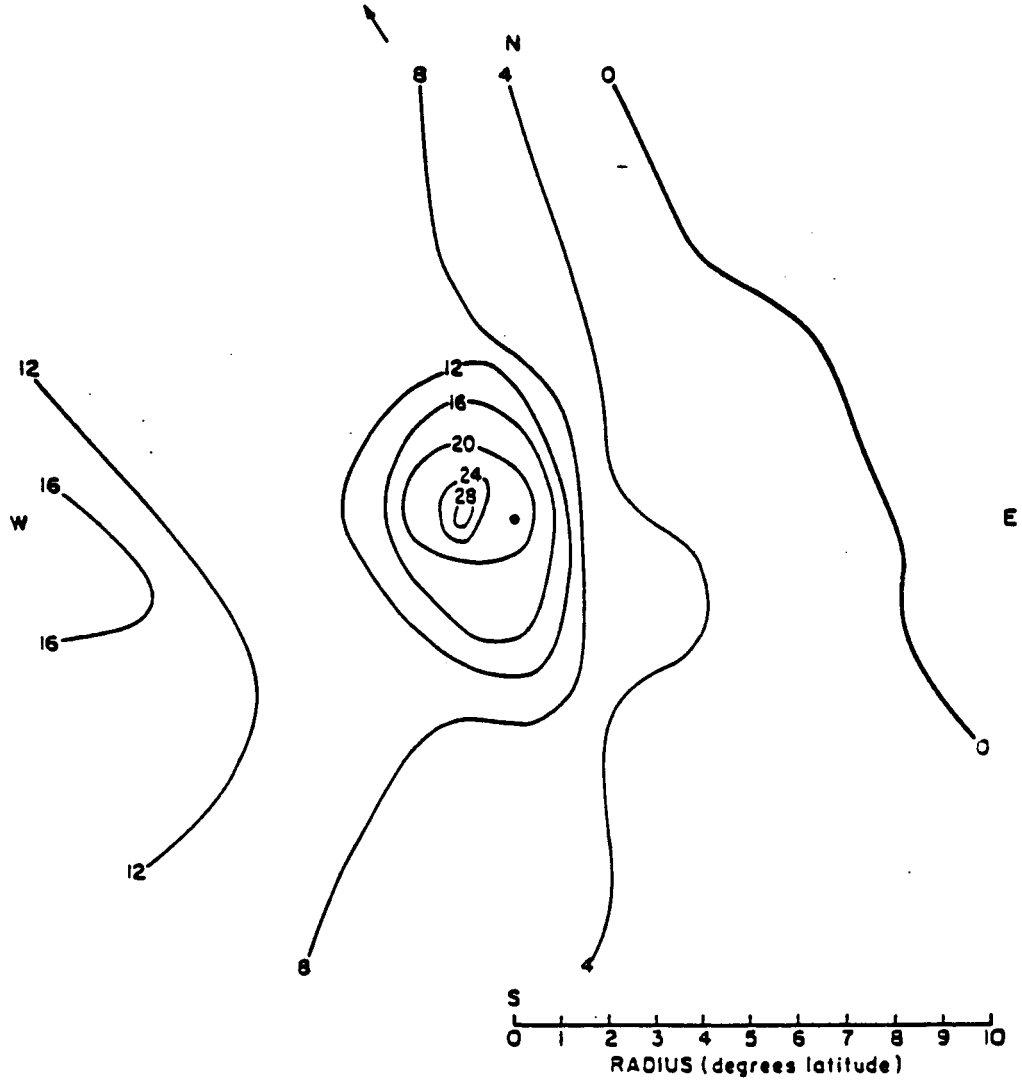

Figure 3.15 Plan view of tangential winds (ms^{-1}) at the surface in MOT coordinates.

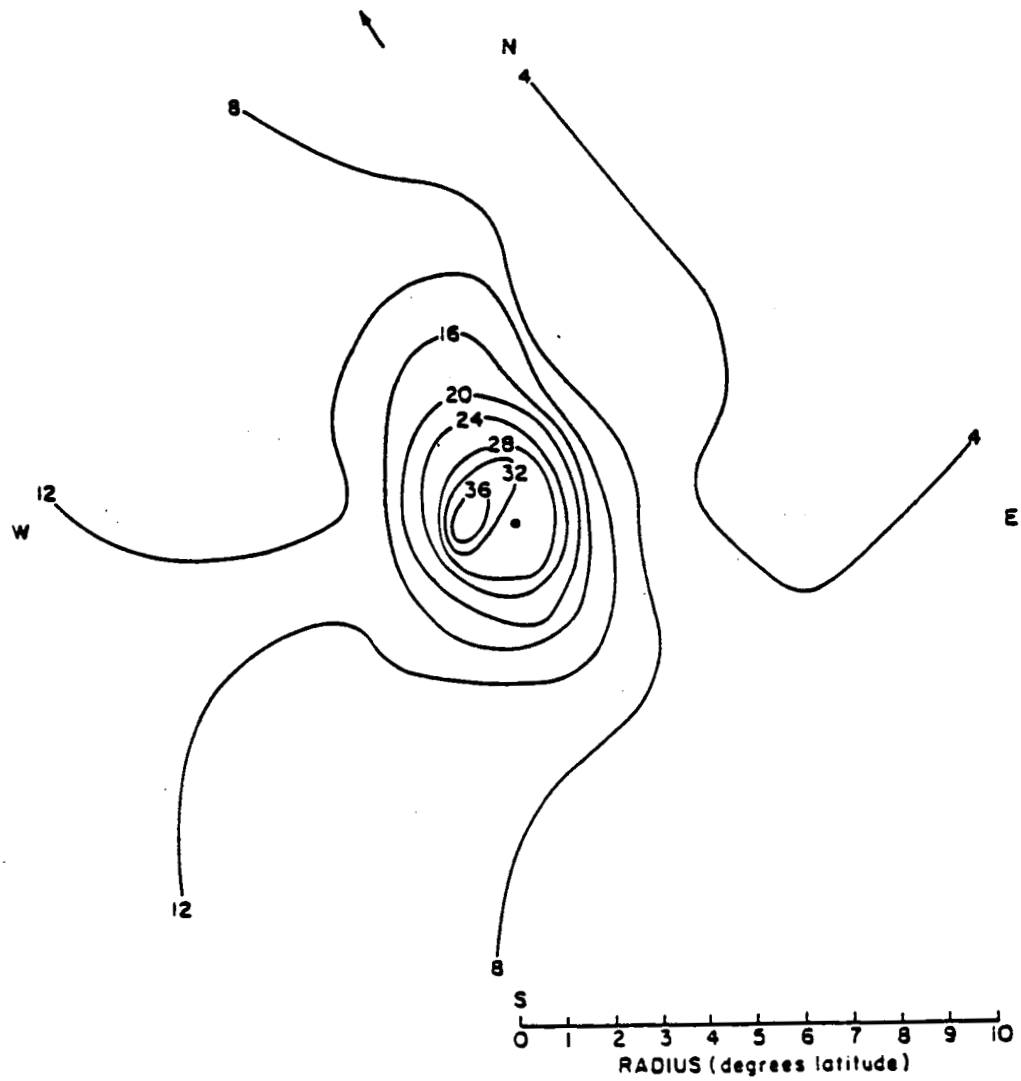

Figure 3.16 Same as Fig. 3.15, but at 560 m .

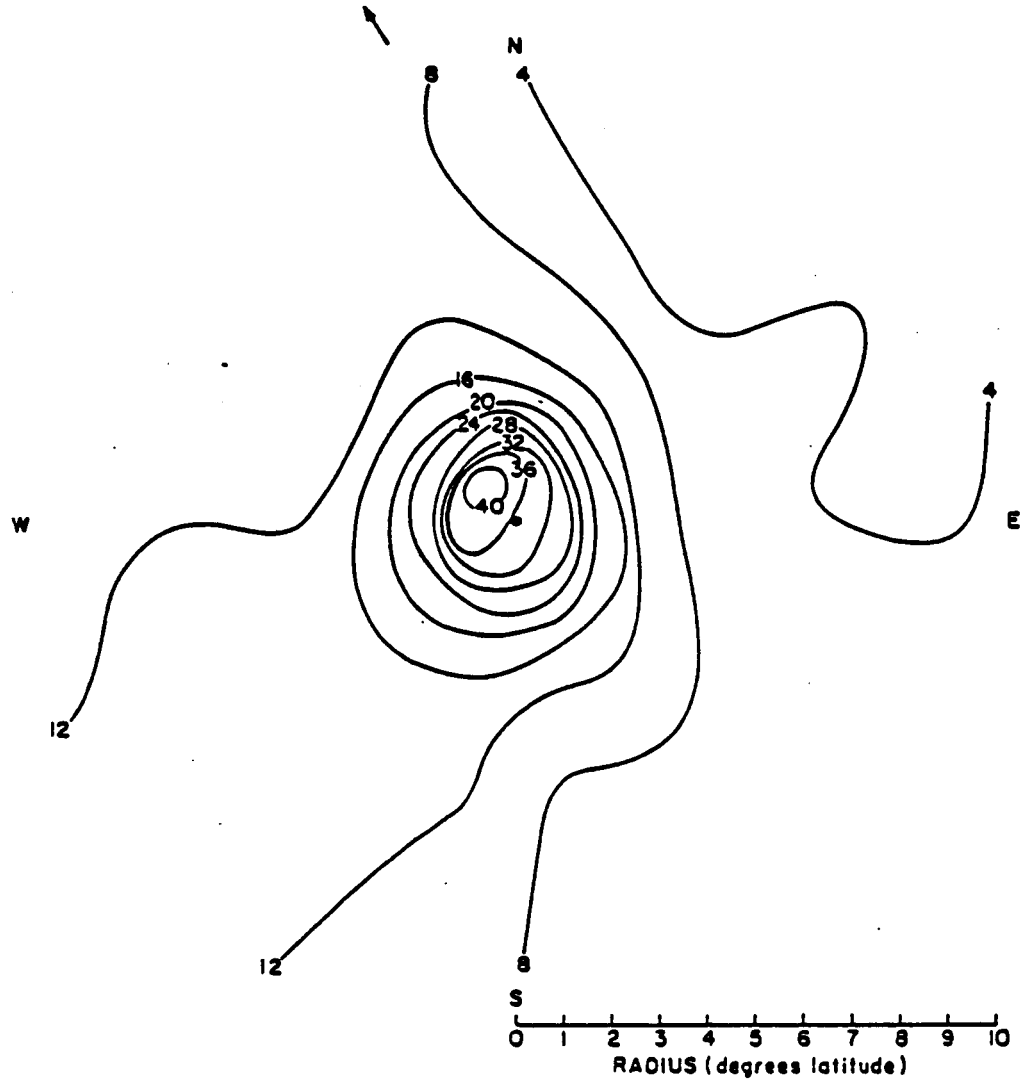

Figure 3.17 Same as Fig. 3.15, but at 1600 m.

A two-dimensional cross-section of V_t is presented in Fig. 3.18. Cyclonic flow is observed at all radii between 1 and 10 deg. with cyclonic winds generally increasing with height from the surface to 1600 m.

To ascertain the difference between corrected and raw values of V_t the tangential wind anomaly ($V_{t_{anomaly}}$) is computed at each grid point at 560 and 1600 m using the equation:

$$\text{Tangential Wind Anomaly} = V_{t_{corrected}} - V_{t_{raw}} \qquad (3.3)$$

where $V_{t_{corrected}}$ and $V_{t_{raw}}$ are the grid point tangential wind values obtained using corrected and raw wind sets respectively. Plan view analyses of the tangential wind anomalies at 560 and 1600 m are depicted in Figs. 3.19 and 3.20 respectively. For reasons discussed in Section 3.1, tangential wind anomalies are not analyzed inside 1.5 deg. radius.

The tangential wind anomaly fields at 560 and 1600 m both indicate that raw winds sets overestimate the tangential wind ($V_{t_{anomaly}} < 0$) over a large portion of the storm domain. The largest overestimation is found about 8 deg. radius northwest of the storm center where $V_{t_{anomaly}}$ is less than -6 ms^{-1} at 560 and 1600 m. Raw wind sets are observed to underestimate V_t at 560 and 1600 m ($V_{t_{anomaly}} > 0$) at radii greater than about 5 deg. radius south and east of the storm center. Raw wind sets also underestimate V_t between roughly 1 and 3 deg. northwest of the storm center at 560 m and within a northeast to

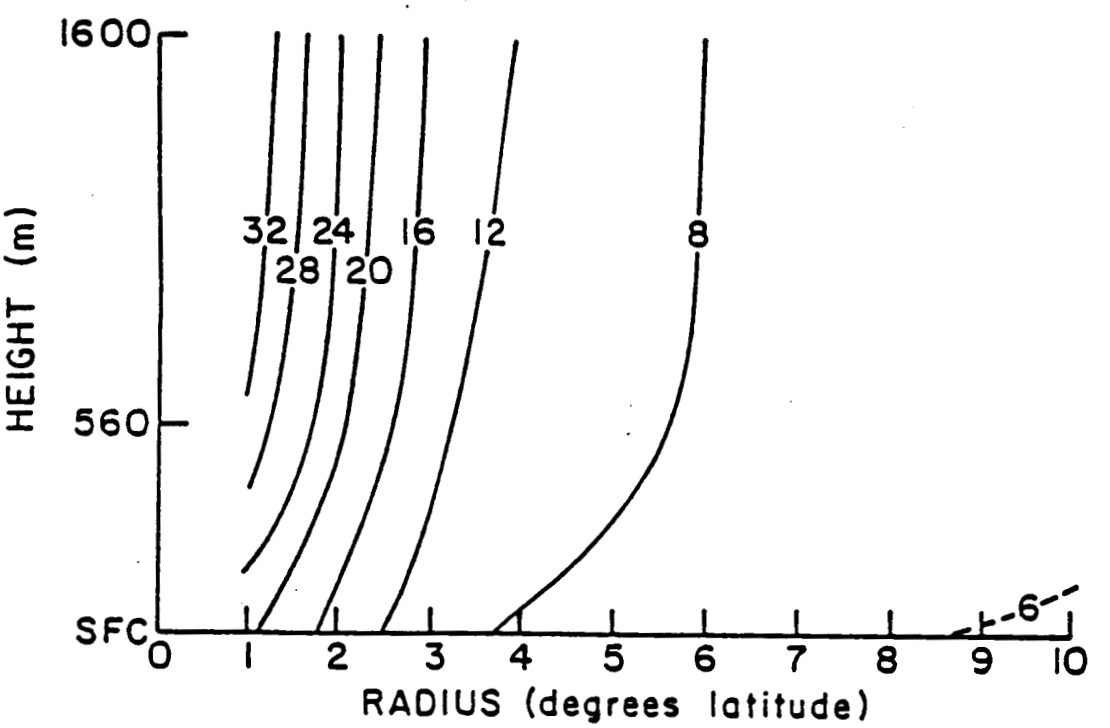

Figure 3.18 Two-dimensional cross-section of tangential winds (ms^{-1}).

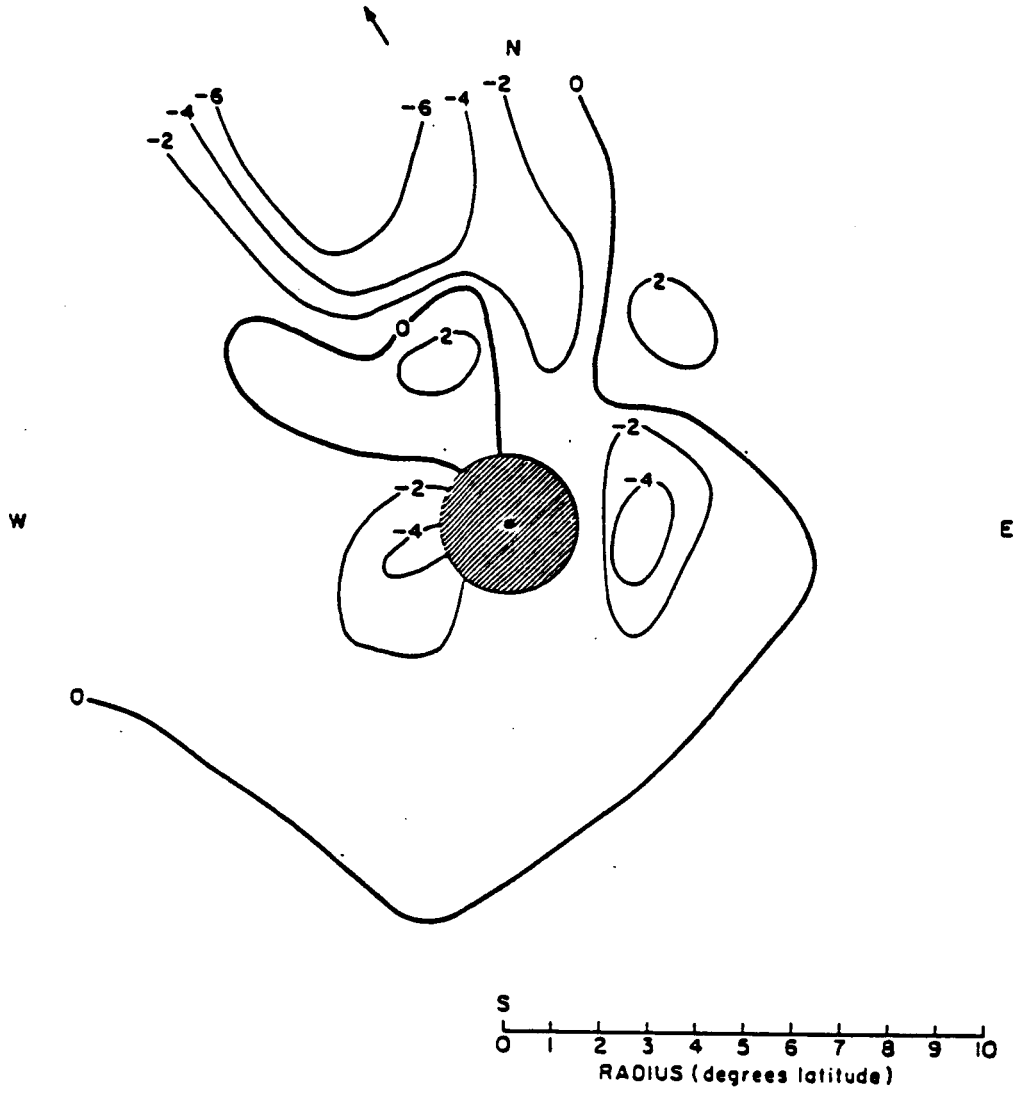

Figure 3.19 Plan view of tangential wind anomalies at 560 m (ms^{-1}).

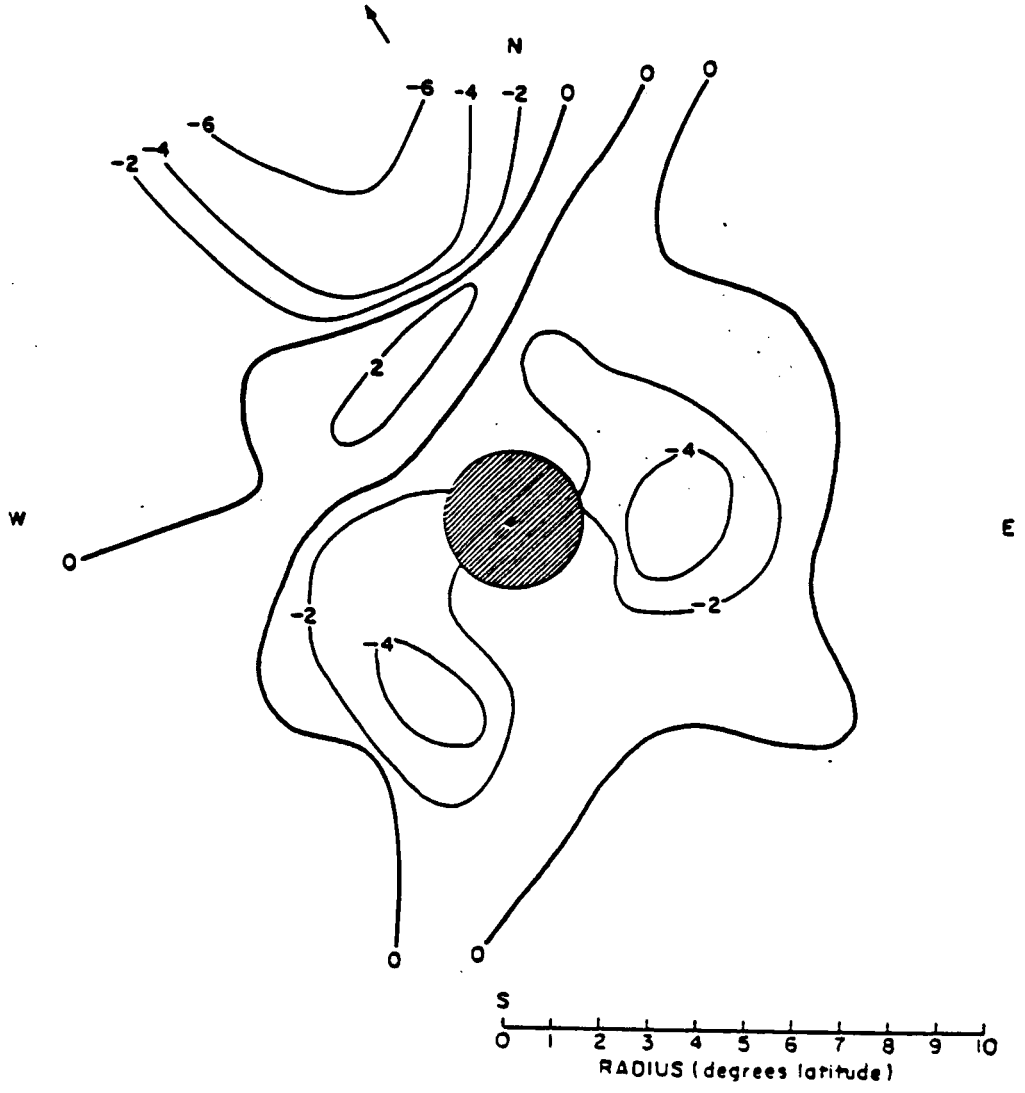

Figure 3.20 Same as Fig. 3.19, but at 1600 m.

southwest oriented band west of the storm center at 1600 m. The most significant underestimation of V_t by raw wind sets at 560 m is observed about 4 deg. radius northwest and 6 deg. radius northeast of the storm center where $V_{t_{anomaly}}$ exceeds 2 ms^{-1}. At 1600 m, the greatest underestimation is observed roughly 4 deg. radius northwest of the storm where $V_{t_{anomaly}}$ exceeds 2 ms^{-1}.

Axisymmetric 560 and 1600 m tangential winds obtained using raw and corrected wind sets are shown in Figs. 3.21 and 3.22 respectively. At 1600 m, axisymmetric values of V_t obtained by adjusting the 560 m raw winds to 1600 m using a "storm mean" shear correction factor are also shown. For reasons noted previously, the 1 deg. radius values of V_t obtained using corrected and raw wind sets are identical.

Figures 3.21 and 3.22 indicate that raw wind sets overestimate V_t at all radii between 2 and 10 deg. However, it is worth noting that raw wind sets overestimate V_t by an average of only 11% at 1600 m and an average of only 6% at 560 m. The relatively small differences observed between corrected and raw wind values of V_t reflect the small tangential wind shear found to exist in the storm's lower levels (see Section 2.3.2).

If these results hold true for other storms, assigning all low-level CMW's to 950 mb may be a reasonable means of obtaining axisymmetric low-tropospheric values of V_t needed for estimating tropical cyclonc intensity using methods described by Weatherford and Gray (1984) and Rodgers and Gentry (1983). However, it is important to note that substantial errors in the asymmetric tangential wind field can occur when all CMW's are assigned to 560 m as Figs. 3.19 and 3.20 indicate.

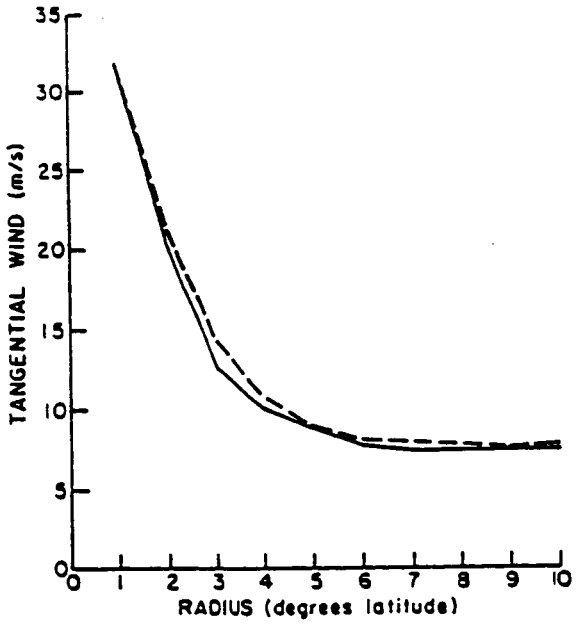

Figure 3.21 Axisymmetric tangential winds (ms^{-1}) at 560 m obtained using corrected wind sets (———) and raw wind sets (– – – –).

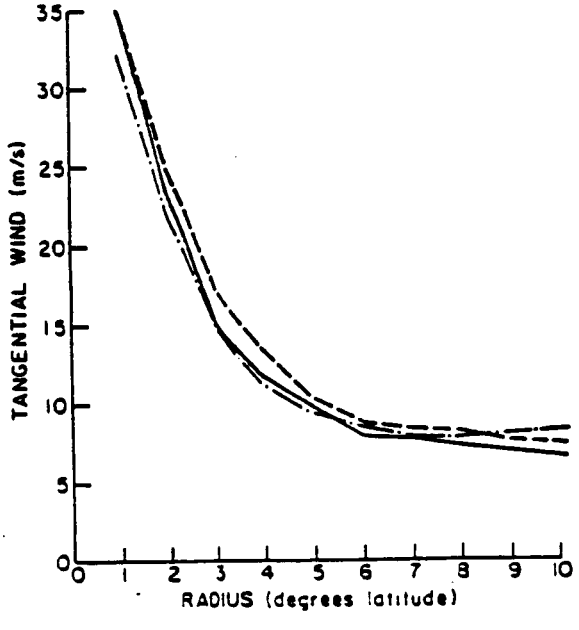

Figure 3.22 Axisymmetric tangential winds at 1600 m obtained using corrected wind sets (———), raw wind sets(– – – – –), and by applying a storm mean shear (–·–·–·) to 560 m raw tangential wind values.

3.3 Divergence

Divergence (DIV) is computed at each grid point at the surface, 560 and 1600 m using the equation:

$$\text{Divergence} = \frac{V_r}{r} + \frac{\partial V_r}{\partial r} + \frac{\partial V_t}{r\partial\theta} \qquad (3.4)$$

where V_r and V_t are the grid point radial and tangential wind values respectively, r is the radial distance from the storm center and $r\partial\theta$ is the azithumal distance between grid points. Plan view analyses of the divergence at the surface, 560 and 1600 m are displayed in Figs. 3.23-3.25.

Convergence is observed over most of the storm domain inside about 2 deg. radius. A principal convergence maximum is observed about 1 deg. radius northeast of the center at each analysis level with the strongest convergence observed at the surface. No organized areas of convergence are observed over the remainder of the storm domain except about 7 deg. radius northeast of the storm center, where a well-defined band of convergence is observed at all analysis levels. It appears that this band of convergence is associated with a stationary front located off the southeast coast of the United States.

Divergence is observed roughly 1 deg. radius northwest of the storm center at the surface, 560 and 1600 m and approximately 1 deg. radius southeast of the storm center at 560 and 1600 m. Well defined albeit small areas of divergence are observed between a radius of about 3 and 6 deg. at each analysis level with the strongest divergence centered roughly 3 deg. radius north of the storm center. The observance of a "moat" region outside the inner core is consistent with

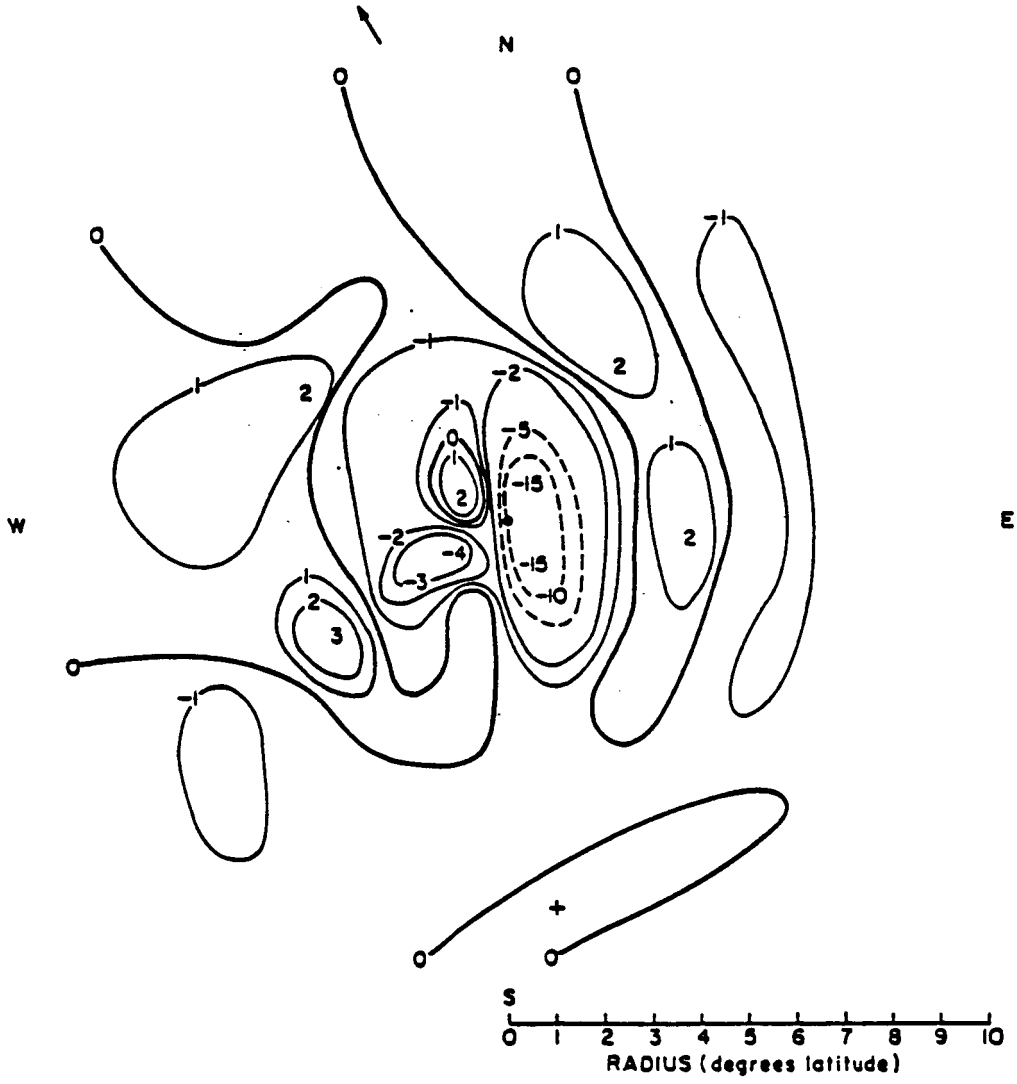

Figure 3.23 Plan view of divergence (x 10^{-5} s^{-1}) at the surface.

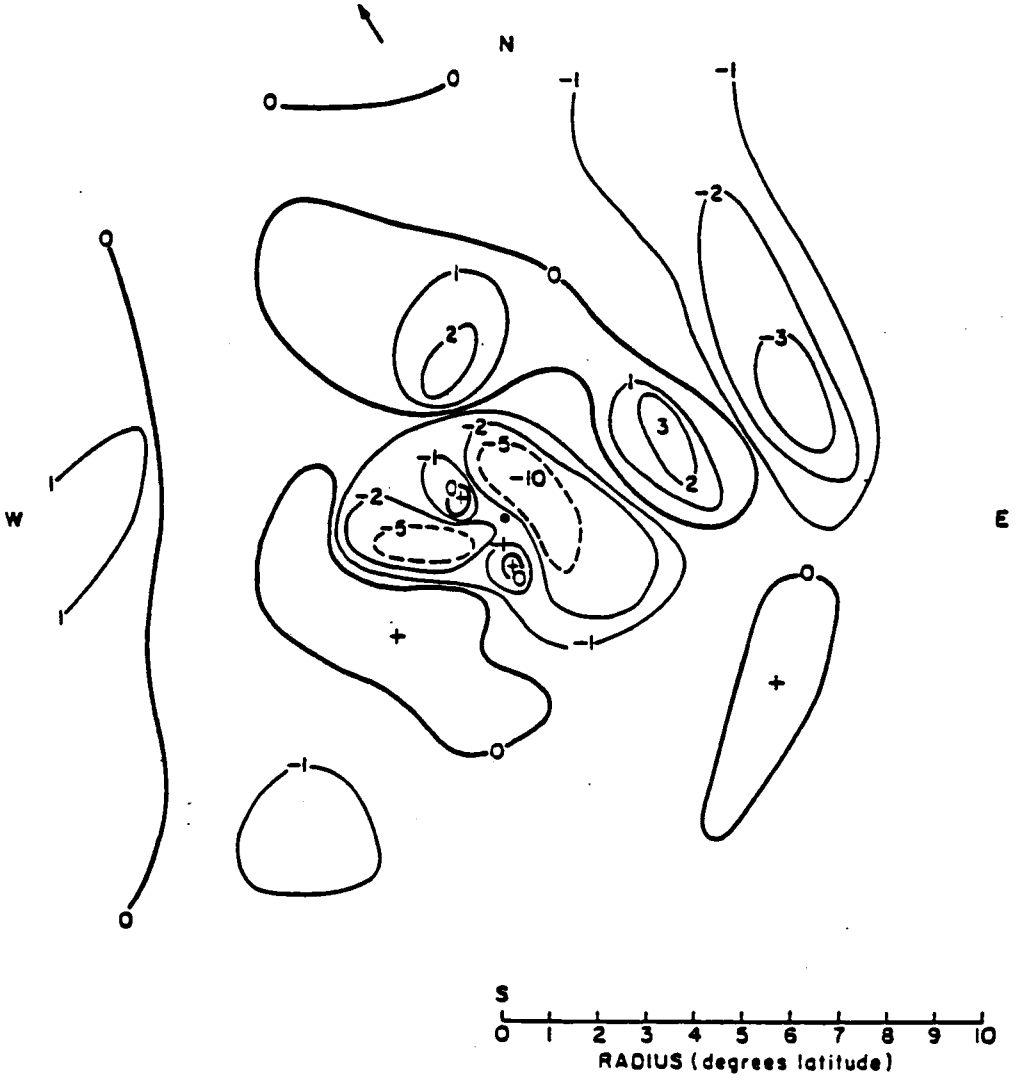

Figure 3.24 Same as Fig. 3.23, but at 560 m.

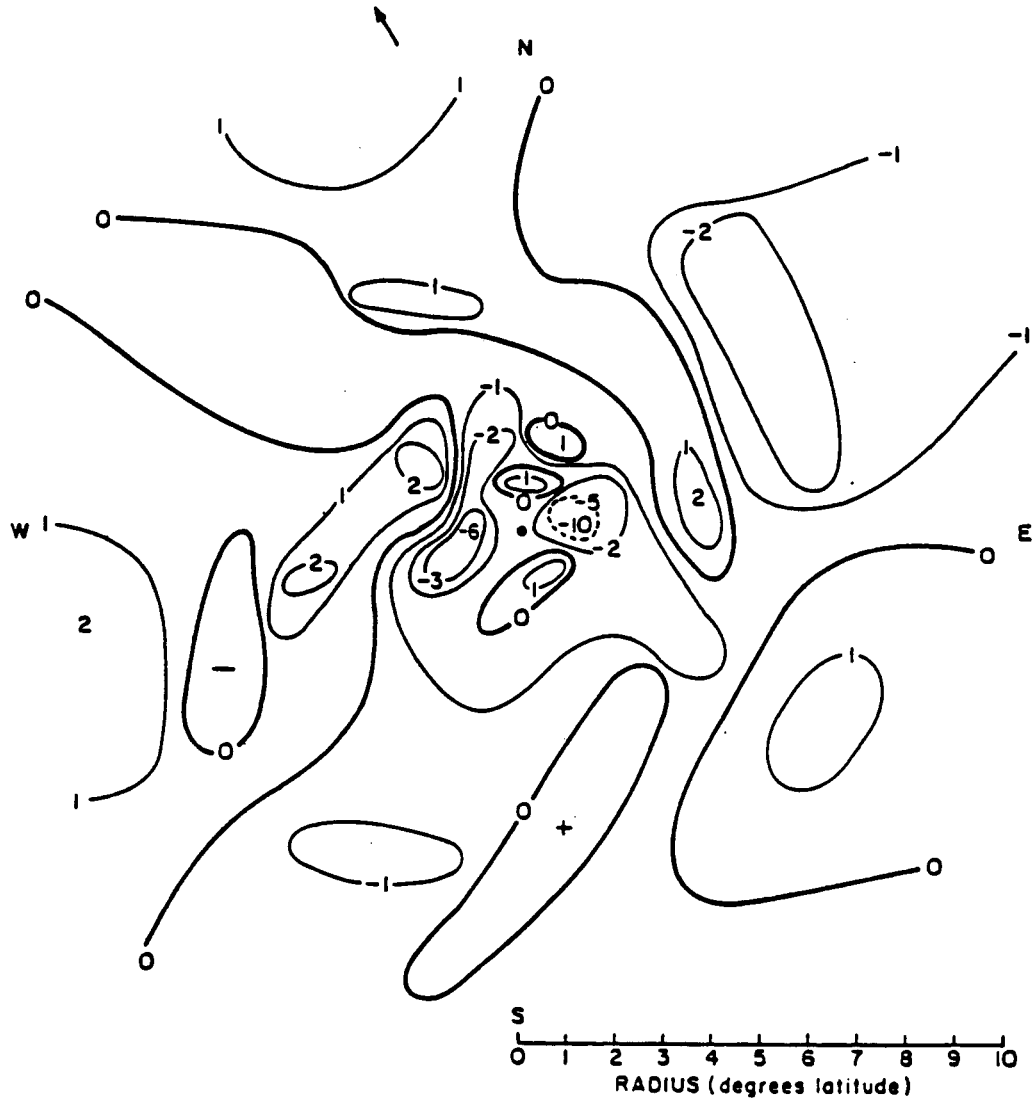

Figure 3.25 Same as Fig. 3.23, but at 1600 m.

Frank's (1977a) tropical cyclone composite study which found that mean divergence existed below 800 mb between 4 and 6 deg. radius. No well-defined divergence maxima are observed beyond a radius of about 6 deg. except about 7 deg. radius west of the storm center, where a fairly broad area of divergence is observed at all levels.

A two-dimensional cross-section of storm divergence is presented in Fig. 3.26. Convergence is observed inside about 3.5 deg. radius and beyond roughly 5.5 deg. radius throughout the lowest 1600 m. A principal convergence maximum is observed near the surface at a radius of about 1 deg., while a secondary convergence maximum is observed near 7 deg. radius at 560 m. Divergence is observed between roughly 3.5 and 5.5 deg. from the surface to 1600 m with maximum divergence observed at about 4 deg. radius near 560 m. As noted previously, the location of this region of mean divergence is in good agreement with Frank's (1977a) study. Although Fig. 3.26 suggests weak divergence exists beyond a radius of about 9.5 deg., this feature may result from inadequate wind resolution near the edge of the composite grid.

Axisymmetric 560 and 1600 m values of divergence computed using corrected and raw wind sets are depicted in Figs. 3.27 and 3.28 respectively. Both figures suggest that raw wind sets underestimate the mean storm convergence inside about 4 deg. radius and the mean storm divergence between about 4 and 6 deg. Beyond 6 deg. radius no substantial differences between raw and corrected values of divergence are observed. These results seem consistent with Figs. 3.10 and 3.11 which show that the 560 and 1600 m differences between corrected and raw values of V_r are generally largest inside 6 deg. radius.

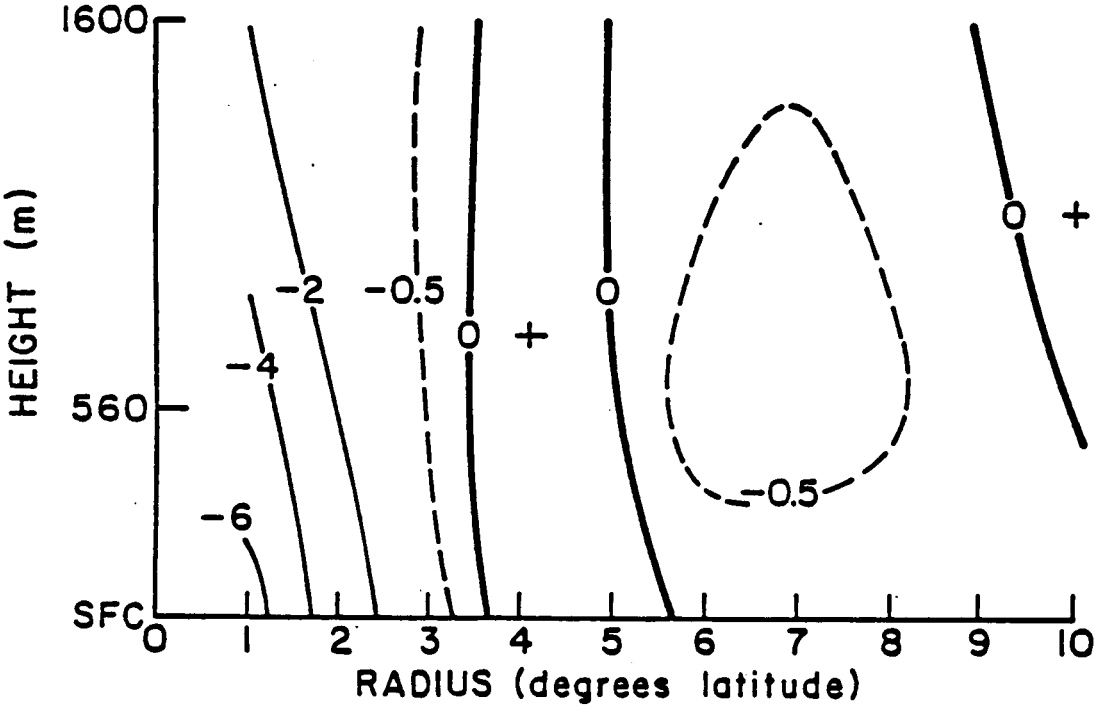

Figure 3.26 Two-dimensional cross-section of divergence (x 10^{-5} s^{-1}).

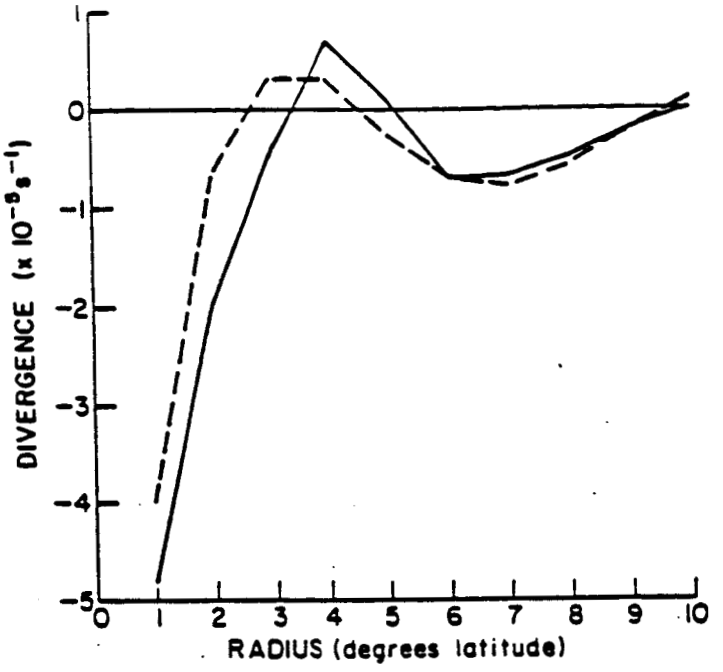

Figure 3.27 Axisymmetric values of divergence (x 10^{-5} s^{-1}) at 560 m obtained using corrected wind sets (———) and raw wind sets (– – – –).

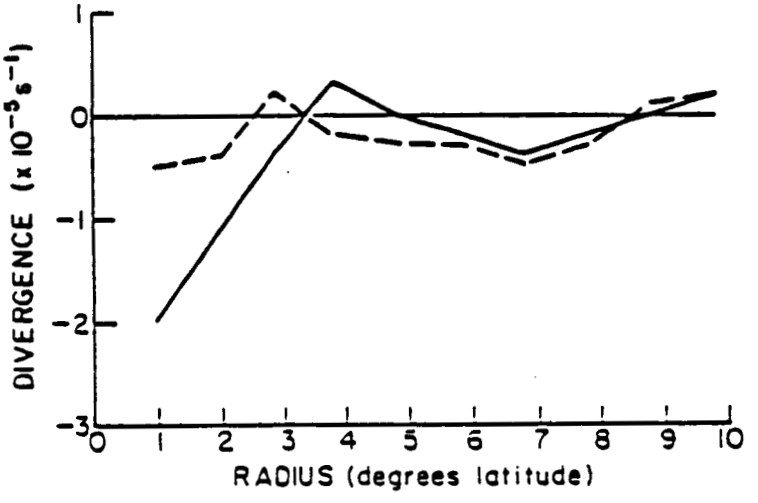

Figure 3.28 Same as Fig. 3.27, but at 1600 m.

3.4 Vorticity

Relative vorticity (ζ) is computed at each grid point using the equation:

$$\text{Vorticity} = \frac{V_t}{r} + \frac{\partial V_t}{\partial r} - \frac{\partial V_r}{r\partial\theta} \qquad (3.5)$$

Plan view analyses of ζ at the surface, 560 and 1600 m are presented in Figs. 3.29-3.31. Cyclonic ($\zeta > 0$) relative vorticity is observed inside roughly 2 deg. radius and also over a large area west of the storm center at each analysis level. The region of cyclonic relative vorticity west of the storm center is associated with the previously discussed low pressure system located in the western Gulf of Mexico. Cyclonic relative vorticity is also observed over an appreciable area at radii > 7 deg. east of the storm center. Relatively weak areas of cyclonic vorticity are scattered over the remainder of the storm domain. Principal vorticity maxima are observed about 1 deg. radius south of the storm center at the surface and 560 m and roughly 1 deg. radius north and south of the storm center at 1600 m.

Anticyclonic ($\zeta < 0$) relative vorticity is observed over a broad area north of the storm center at all levels. Randomly spaced vorticity minima are observed between 2 and 6 deg. at each level with the most pronounced minimum observed about 3 deg. radius north of the storm center at each analysis level. No well-defined areas of anticyclonic vorticity are observed beyond 6 deg. radius.

A two-dimensional cross-section of relative vorticity is presented in Fig. 3.32. Cyclonic relative vorticity is observed between the

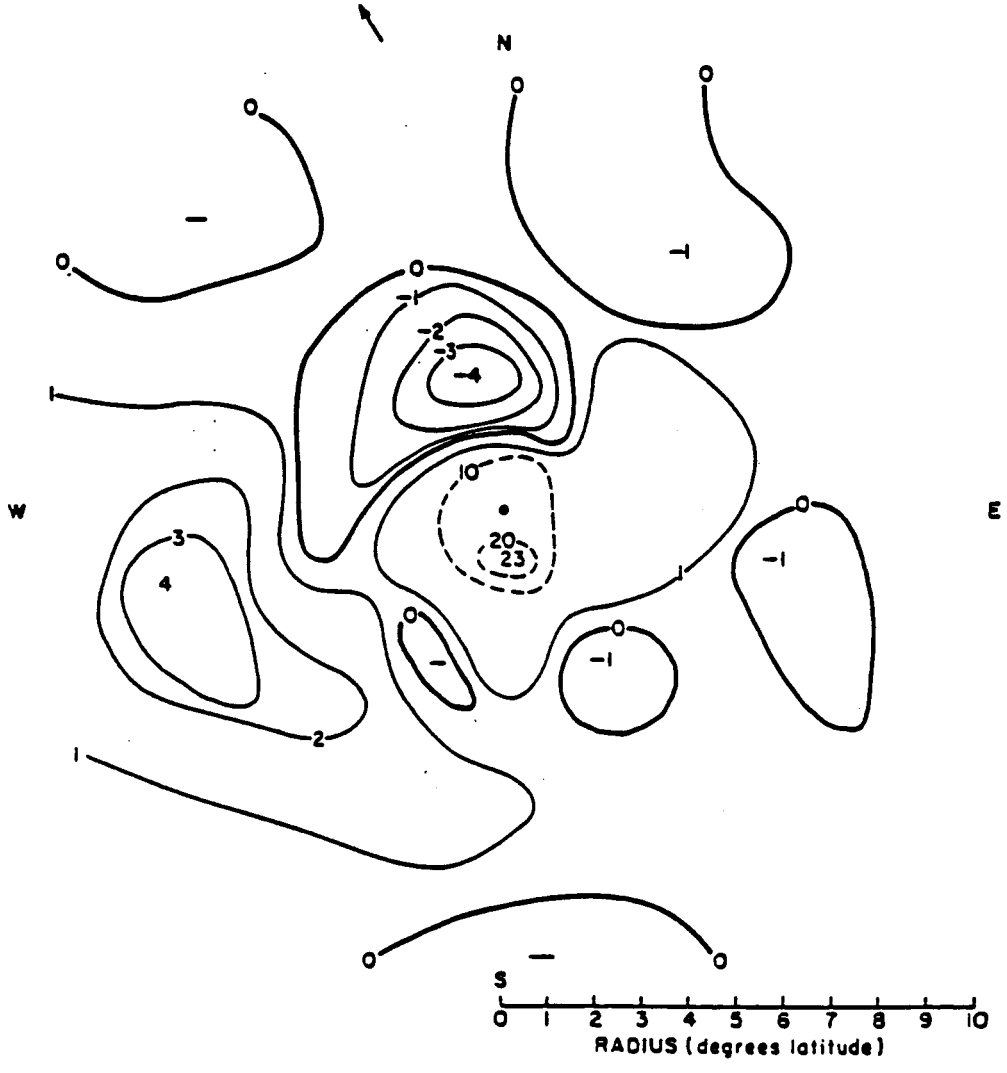

Figure 3.29 Plan view of relative vorticity (x 10^{-5} s^{-1}) at the surface.

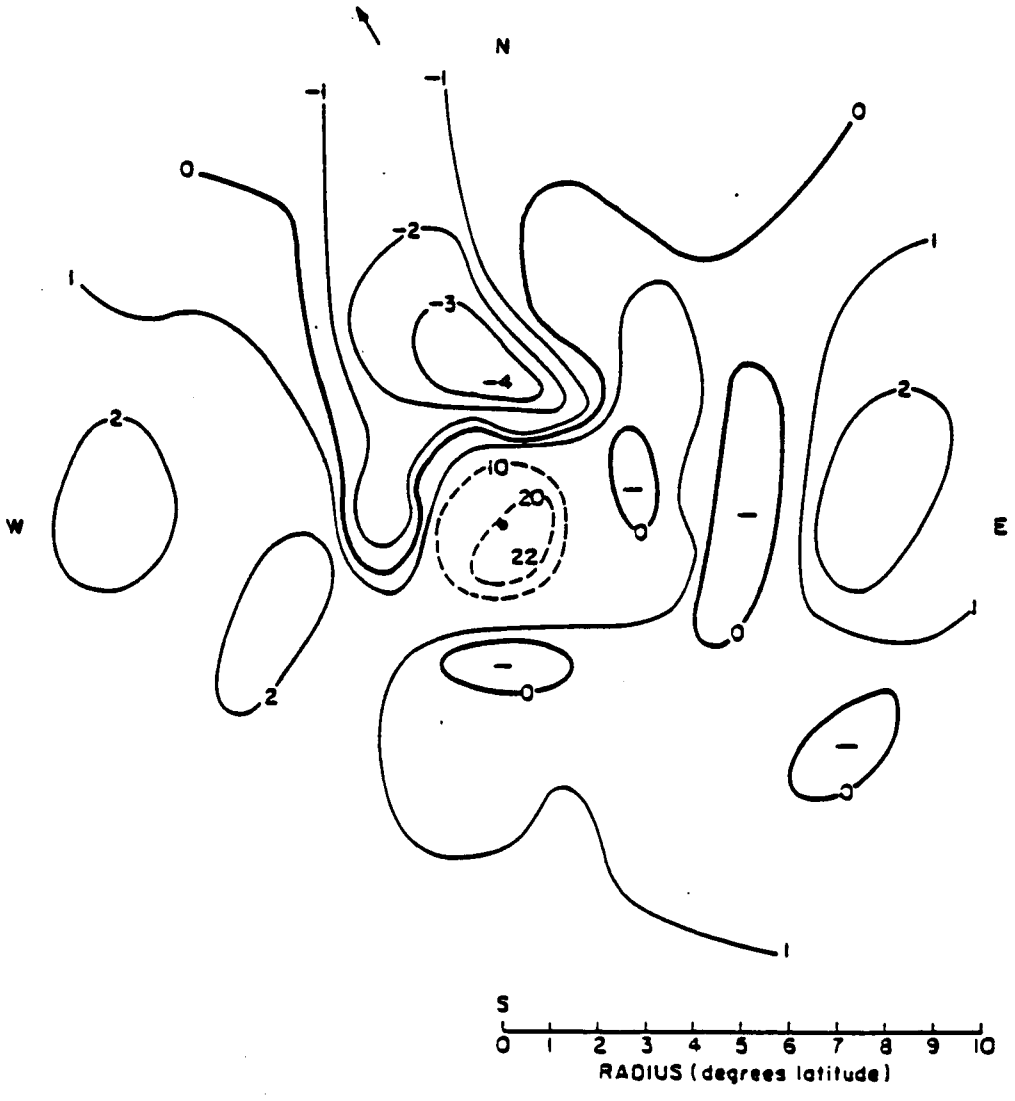

Figure 3.30 Same as Fig. 3.29, but at 560 m.

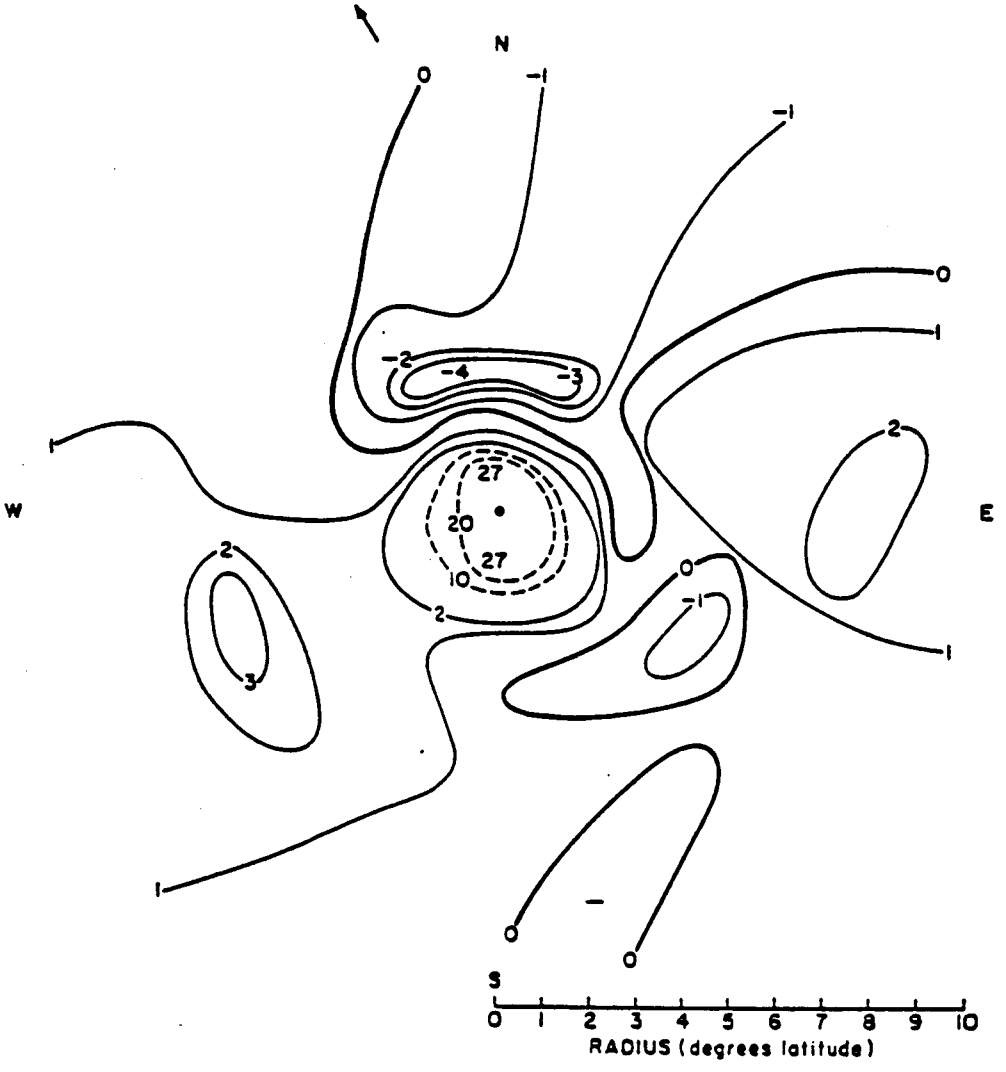

Figure 3.31 Same as Fig. 3.29, but at 1600 m.

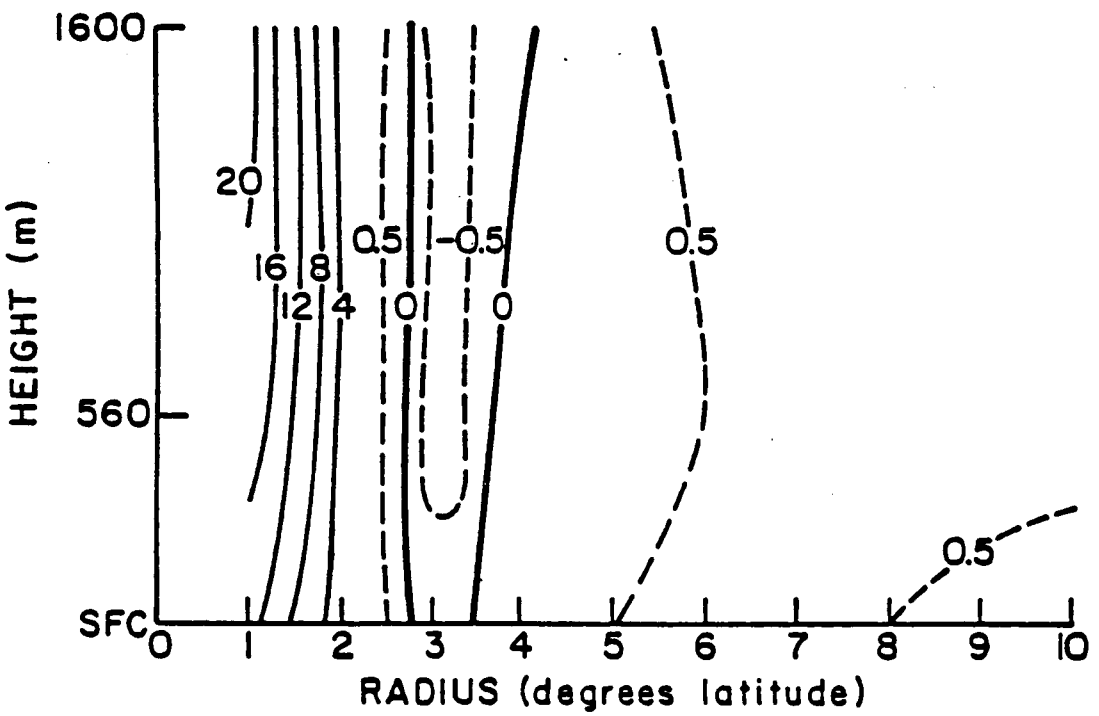

Figure 3.32 Two-dimensional cross-section of relative vorticity ($x10^{-5}$ s^{-1}).

surface and 1600 m at all radii except between roughly 3 and 3.5 deg. A principal vorticity maximum is observed near 1 deg. radius, while a secondary vorticity maximum is located at roughly 7 deg. radius. Anticyclonic relative vorticity is observed between roughly 3 and 3.5 deg. with a vorticity minimum observed at about 3.5 deg. radius near 560 m.

Axisymmetric 560 and 1600 m values of ζ obtained using raw and corrected wind sets are presented in Figs. 3.33 and 3.34 respectively. Both figures indicate that the differences between the axisymmetric values of ζ obtained using corrected and raw wind sets are relatively small at all radii. This is consistent with Figs. 3.21 and 3.22 which show that the differences between tangential wind values obtained using corrected and raw wind sets are relatively small at all radii.

3.5 Vertical Motion

The kinematic vertical velocity (w) is computed at each grid point at 560 and 1600 m assuming incompressibility. Plan view analyses of w at 560 and 1600 m are presented in Figs. 3.35 and 3.36, respectively. A broad area of upward motion is observed inside about 2 deg. radius at both 560 and 1600 m with vertical motion maxima observed roughly 1 deg. and 7 deg. radius northeast of the storm center. This secondary vertical motion maximum appears to be associated with the previously discussed stationary front positioned off of the southeast coast of the United States. Sinking motion is most visible between radii of 3 and 6 deg. with the strongest sinking motion observed approximately 4 deg. radius northeast of the storm center at 1600 m. Although the

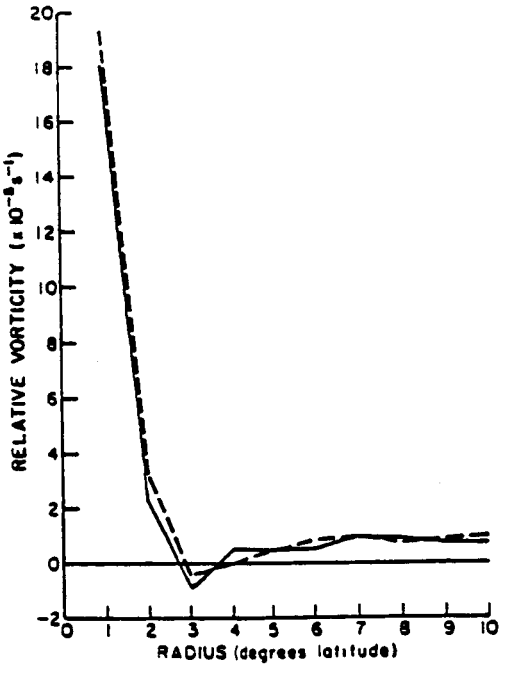

Figure 3.33 Axisymmetric values of relative vorticity ($\times 10^{-5}$ s^{-1}) at 560 m obtained using corrected wind sets (———) and raw wind sets (– – – –).

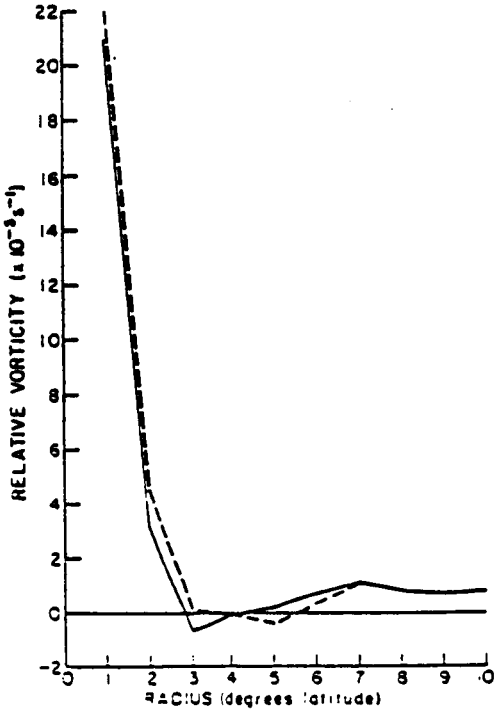

Figure 3.34 Same as Fig. 3.33, but at 1600 m.

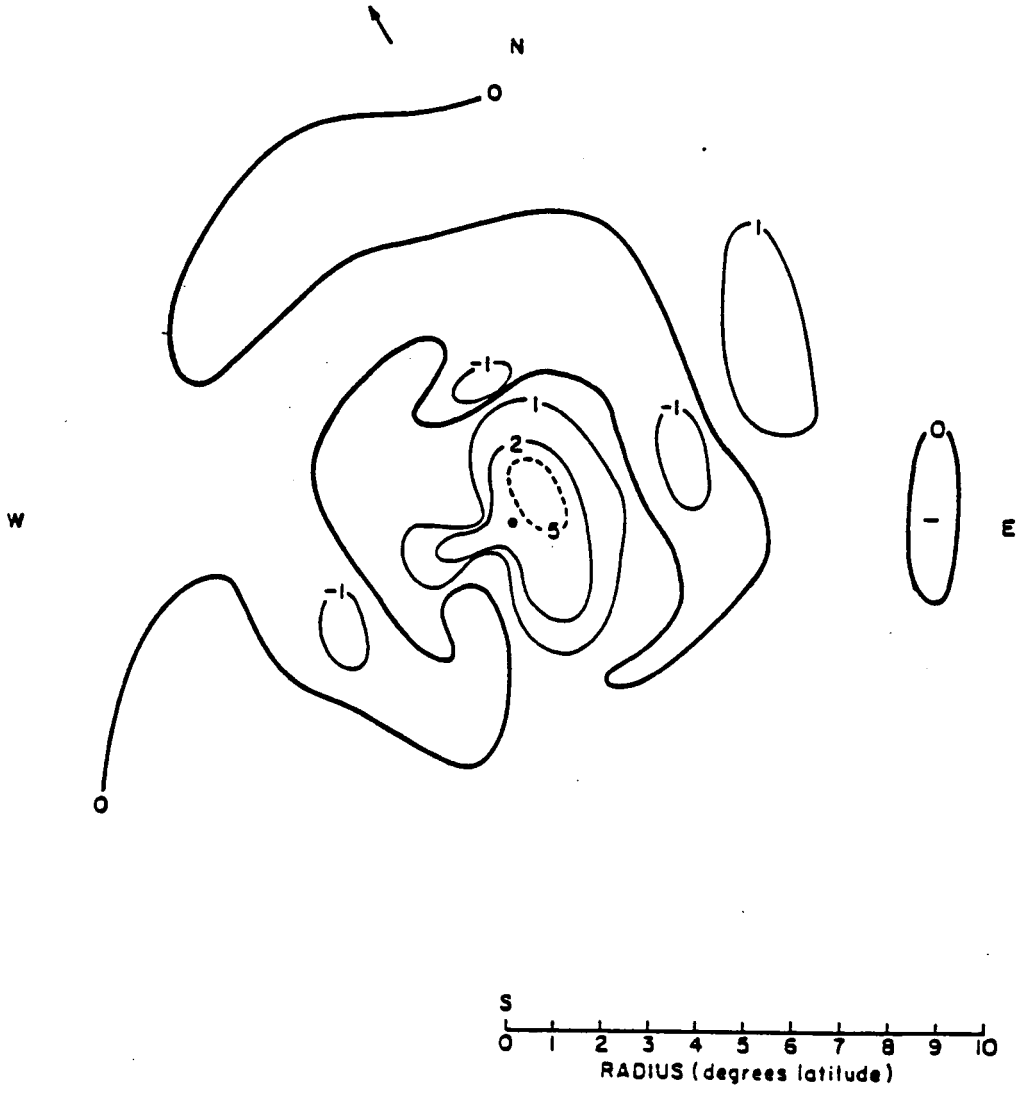

Figure 3.35 Plan view of vertical velocities (x 10^{-2} ms^{-1}) at 560 m.

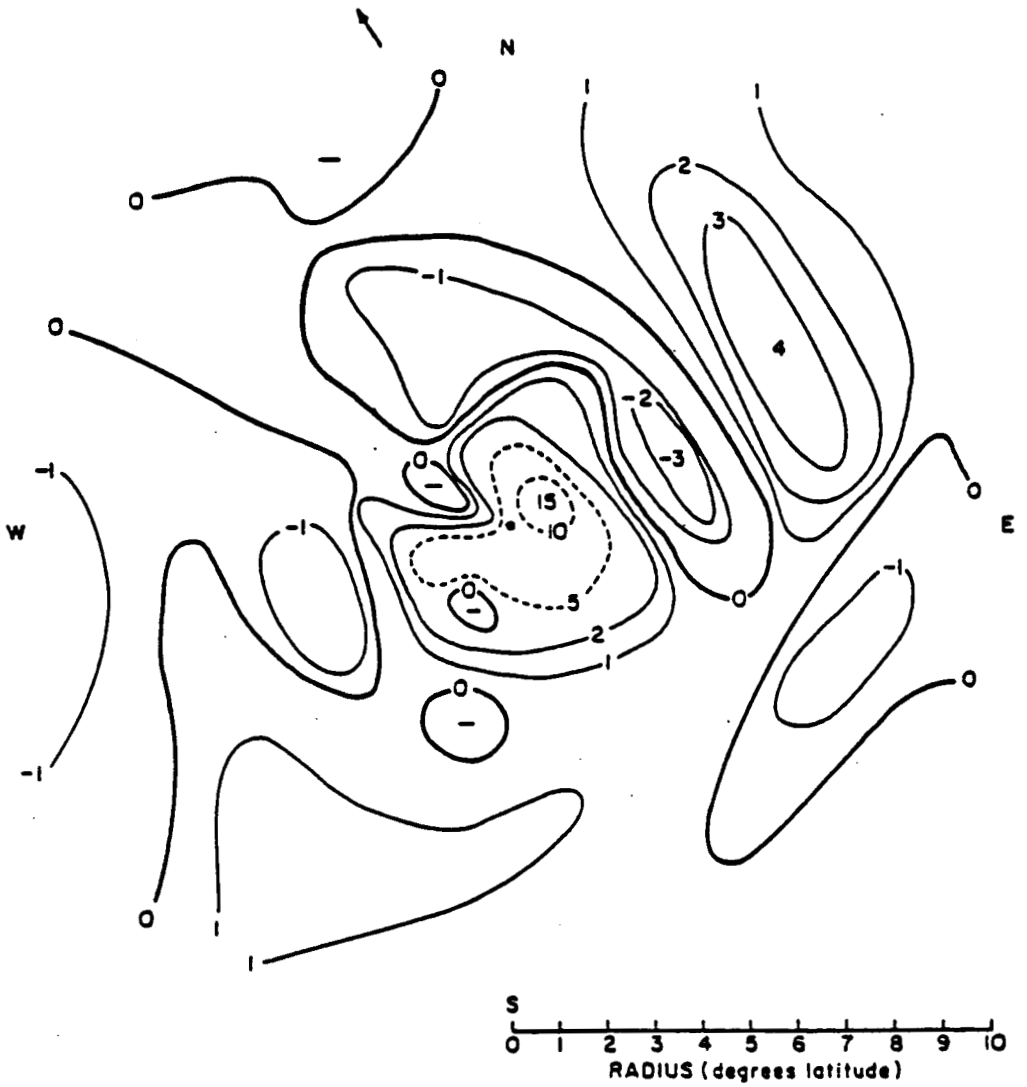

Figure 3.36 Same as Fig. 3.35, but at 1600 m.

subsidence between 3 and 6 deg. is relatively weak, it appears certain that a well-defined area of downward motion exists outside the core.

A two-dimensional vertical motion profile is shown in Fig. 3.37. Upward motion is observed at virtually all radii. A principal vertical motion maximum is observed at a radius of about 1 deg., while a secondary maximum is observed at 7 deg. radius. Sinking motion is observed between approximately 3.5 and 4.5 deg. and also beyond 9.5 deg. radius. A vertical motion minimum is observed at about 4 deg. radius. It is worth noting that the regions of upward (downward) vertical motion depicted in Fig. 3.37 agree reasonably well with the regions of positive (negative) relative vorticity depicted in Fig. 3.32 suggesting "Ekman pumping" in the boundary layer (e.g., Charney and Eliassen, 1964).

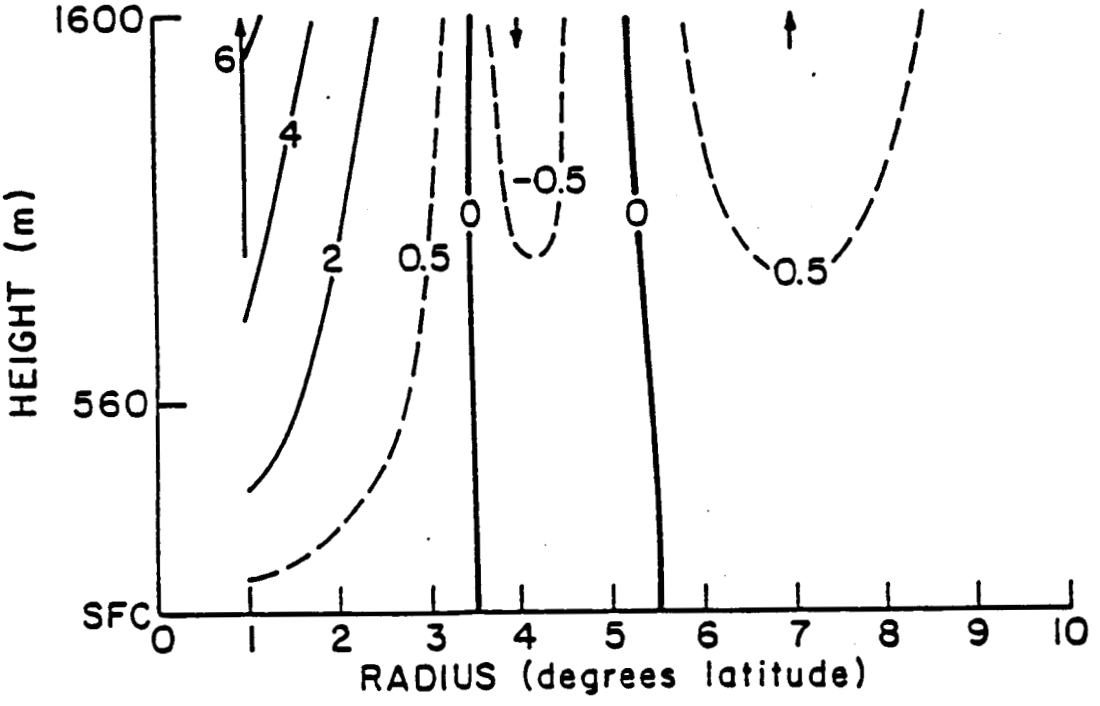

Figure 3.37 Two-dimensional cross-section of vertical velocity (x 10^{-2} ms^{-1}).

Chapter 4

ANGULAR MOMENTUM BUDGET

By analyzing the angular momentum budget of a tropical cyclone, researchers such as Holland (1983a), McBride (1981b), Frank (1977b) and others have obtained considerable information concerning the factors which contribute to tropical cyclone initiation, intensification and decay. Although these authors were reasonably successful in performing an integrated angular momentum budget for the entire layer between the surface and 100 mb, insufficient low-level wind resolution limited the quantity of information that they could obtain concerning the angular momentum budget of a storm's lowest 2 km. Consequently, uncertainties remain concerning the dissipation of momentum at the sea surface in a tropical cyclone environment.

In this chapter, composite wind data at the surface, 560 and 1600 m are employed to analyze the angular momentum budget of Frederic's lowest 1600 m at radii between 3 and 10 deg. Angular momentum budgets are calculated for the surface to 560 m layer and the 560 to 1600 m layer, with the former employed to obtain estimates of the frictional dissipation at the sea surface and hence the surface drag coefficient (C_D). No angular momentum budget is calculated from the center to 2 deg. radius because of the limited resolution in that region afforded by the grid used in this study. The momentum budget of the core was explored by Frank (1984).

4.1 The Angular Momentum Budget Equation

The absolute angular momentum (M) is defined by:

$$M = V_t r + fr/2 \tag{4.1}$$

where $m = V_t r$ is the relative angular momentum and f is the coriolis parameter. In this thesis, angular momentum is computed in Lagrangian coordinates (relative to the moving storm) using the equation:

$$\frac{h\partial(\rho m)}{\partial t} + h\underline{V} \cdot \rho m\underline{V} + h\rho f r V_r + (\rho m w_T - \rho m w_B) = -\text{Dissipation} \tag{4.2}$$

where h is the layer depth, $\underline{V}$ is the total horizontal wind component, w_T and w_B are the vertical velocities at the top and bottom of the layer respectively, and ρ is the layer mean density. From left to right, the terms on the left side of Eq. 4.2 are the local time rate of change of m, the horizontal and vertical flux divergence of m and the coriolis torque. The sum of these terms plus the dissipation due to sub-grid scale processes equals zero.

Equation 4.2 is evaluated for both the asymmetric and axisymmetric storm between the surface and 560 m and for the axisymmetric storm between 560 and 1600 m. The methodology employed to solve Eq. 4.2 for both the asymmetric and axisymmetric storm is given below.

4.2 The Asymmetric Budget

Since Frederic is assumed to be in steady-state, the local time rate of change of m is zero. The horizontal flux divergence of m is

evaluated at each of the 160 grid points at the surface and 560 m and then averaged vertically to obtain a layer-mean value for the horizontal flux divergence of m at every grid point. The vertical flux divergence of m is computed at each grid point for the surface to 560 m layer from the vertical flux at 560 m, since w and hence the vertical flux is 0 at the surface. The integrated surface to 560 m coriolis torque is computed at each grid point by averaging the surface and 560 m values. It is important to note that since the storm latitude changes continuously during the composite period, f is computed based on the north-south deviation of the grid point from the mean composite latitude of 27.3°N.

After the above terms have been evaluated at each grid point, they are added to solve for the surface to 560 m residual, which is assumed to be due to frictional dissipation. The grid point residuals are then averaged in each 1 deg. radial band between 3 and 10 deg. to obtain an azimuthally averaged residual for the surface to 560 m layer at each radius. These azimuthally averaged residuals are then employed to solve for C_D at each radius between 3 and 10 deg. using the equation:

$$\text{Frictional Dissipation} = \rho_o C_D r V_{t_o} |V_o| \qquad (4.3)$$

where ρ_o is the surface density and V_{t_o} and V_o are the axisymmetric tangential and total surface winds respectively.

The surface drag coefficient is also calculated at each grid point using the grid point residual and wind values. The resultant grid point values of C_D are then averaged at each radius to obtain

azimuthally averaged values of C_D at each radius between 3 and 10 deg. Inspection of the azimuthally averaged values of C_D obtained in this latter manner indicates that averaging grid point values of C_D yields unrealistically large values of C_D at large radii. Examination of the individual grid point values of C_D suggests that anomalous grid point surface drag coefficients are due to sensitivity to the grid point surface wind values. Since C_D is inversely proportional to the square of the surface wind speed, especially low (high) wind speeds can result in anomalously high (low) values of C_D. Although one might expect that the noise in the grid point values of C_D would be smoothed out when an azimuthally averaged value of C_D is obtained, the results of this study indicate that if the grid point residual and surface wind value are correlated, a bias in the magnitude of the azimuthally averaged C_D can result. For this storm, large negative residuals are observed to coincide with low wind speeds at large (> 5 deg.) radii east of the storm center resulting in anomalously large grid point and azimuthally averaged values of C_D at radii greater than 5 deg. Therefore, the drag coefficients computed by this method are considered unreliable and are not discussed further.

4.3 The Axisymmetric Budget

The local time rate of change of m is zero since Frederic is assumed to be in steady state. The horizontal flux divergence of m is computed at each radius at the top and bottom of the layer using the appropriate axisymmetric wind and density values. These values are then averaged to obtain the layer-mean horizontal flux divergence at each radius. The vertical flux divergence is obtained at each radius

by subtracting the vertical flux at the bottom of the layer from the vertical flux at the top of the layer using the appropriate axisymmetric values. The coriolis torque is not assumed to integrate to 0 for the axisymmetric storm and instead is evaluated at each radius using the same procedure employed for the asymmetric storm. Many previous studies (Palmen and Riehl, 1957; Pfeffer, 1958 and Hawkins and Rubsam, 1968) found that the coriolis torque integrates to 0 over the total volume for a steady-state storm since the net radial mass flux is 0. However, as noted by Frank (1977a) and Anthes (1974), while this is a good approximation at small radii where f is relatively constant, a prevailing northerly (southerly) flow can result in a net spin-up (spin-down) of a storm at large radii.

The above terms are summed at each radius between 3 and 10 deg. to obtain mean residuals for both the surface to 560 and 560 to 1600 m layers. For the surface to 560 m layer, the residuals are used to compute C_D at radii between 3 and 10 deg. using Eq. 4.3.

4.4 Momentum Budget Results

The results of the surface to 560 m angular momentum budget for both the asymmetric and axisymmetric storm are depicted in Table 4.1, while the results of the 560 to 1600 m budget are presented in Table 4.2. The surface drag coefficients computed for each of the aforementioned analyses are presented in Table 4.3.

Table 4.1 indicates that a net convergence of m (negative residual) is observed for the surface to 560 m layer at all radii between 3 and 10 deg. for both the asymmetric and axisymmetric storm, with the net convergence being an average of about 13% larger for the

Table 4.1 Surface-560 m angular momentum budgets for the asymmetric and axisymmetric storms. Time rate of change of m per unit area (x 10^3 kg s^{-2}).

	Radius (Degrees Latitude)							
	3	4	5	6	7	8	9	10
				Asymmetric Storm				
$h\frac{\partial(\rho m)}{\partial t}$	0	0	0	0	0	0	0	0
$h\underline{\nabla} \cdot \rho m\underline{V}$	- 7	8	10	- 2	- 5	- 2	1	4
$\rho m\ w_T$	16	-10	-10	2	11	10	4	0
$h\rho rfV_r$	-73	-66	-53	-55	-73	- 92	-106	-109
Residual	-64	-68	-53	-55	-67	- 84	-101	-105
				Axisymmetric Storm				
$h\frac{\partial(\rho m)}{\partial t}$	0	0	0	0	0	0	0	0
$h\underline{\nabla} \cdot \rho m\underline{V}$	-21	7	- 1	-15	-21	- 22	- 16	- 15
$\rho m\ w_T$	16	-13	- 8	8	16	14	8	4
$h\rho rfV_r$	-73	-66	-53	-55	-73	- 92	-106	-109
Residual	-78	-72	-62	-62	-78	-100	-114	-120

C-2

Table 4.2 560-1600 m angular momentum budget for the axisymmetric storm. Time rate of change of m per unit area ($\times 10^3$ kg s^{-2}).

	Radius (Degrees Latitude)							
	3	4	5	6	7	8	9	10
$\frac{h\partial(\rho m)}{\partial t}$	0	0	0	0	0	0	0	0
$h\underline{V} \cdot \rho m\underline{V}$	-22	3	- 9	-28	- 37	- 38	- 28	- 17
$(\rho m\ w_T - \rho m\ w_B)$	31	- 8	2	20	28	23	9	2
$h\rho rfV_r$	-75	-70	-62	-72	-101	-131	-152	-146
Residual	-66	-75	-69	-80	-110	-146	-171	-161

Table 4.3 Surface drag coefficient estimates derived from the surface-560 m angular momentum budgets of the asymmetric and axisymmetric storms ($C_D \times 10^{-3}$).

Radius (Degrees Latitude)	Axisymmetric Storm	Asymmetric Storm
3	1.5	1.5
4	1.9	2.0
5	1.9	1.7
6	1.9	1.7
7	2.1	1.6
8	2.3	1.9
9	2.4	2.1
10	2.6	2.1

axisymmetric storm. It is worth noting that the convergence of m increases with increasing radius for both the asymmetric and axisymmetric storm. Table 4.1 indicates that this is due primarily to the convergence of m by the coriolis torque, since the horizontal convergence (divergence) of m is nearly balanced by the upward (downward) transport of m at all radii.

Inspection of each of the terms in Table 4.1 indicates they are generally consistent with the composite wind fields discussed in Chapter 3 and the results of Frank's (1977b) angular momentum budget. Horizontal convergence of m is observed at virtually all radii for both the asymmetric and axisymmetric storm. The exceptions are at 4 and 5 deg. radius for the asymmetric storm and at 4 deg. radius for the axisymmetric storm where horizontal divergence of m is observed. This is consistent with the mean storm divergence visible in Fig. 3.26. It is also in good agreement with the Frank's composite m budget which showed horizontal divergence of m for the surface to 900 mb layer at radii between 4 and 6 deg.

Upward transport of m is observed at all radii for the axisymmetric and asymmetric storm except at 4 and 5 deg. radius where downward transport of m is observed. This is consistent with Fig. 3.37, which indicates that mean subsidence exists at these radii.

The coriolis torque is identical for the asymmetric and axisymmetric storm since the same technique is employed to evaluate the coriolis torque term for both storms as noted previously. Table 4.1 indicates that the convergence of m by the coriolis torque increases with increasing radius, except from 4 to 5 deg. radius

where a decrease in coriolis torque is observed. While the pattern of increased convergence by the coriolis torque with radius is in agreement with Frank's (1977b) study, the magnitude of the increase at radii > 6 deg. is substantially larger than that which Frank observed. The strong radial inflow characteristic of this storm at radii > 6 deg. is responsible for the significant increase in m by the coriolis torque beyond 6 deg. radius.

The surface drag coefficients obtained for the asymmetric and axisymmetric storm (Table 4.3) are in fairly good agreement, although C_D values for the asymmetric storm average about 11% larger. For the most part, C_D is observed to increase with increasing radius for both the asymmetric and axisymmetric storms. Although the observed increase is small and could be attributed to errors in surface wind speed, there is no evidence that C_D decreases with radius or wind speed in a tropical cyclone environment, as is currently believed. However, no previous study has employed observed surface winds to derive C_D outside about 2 deg. radius in a mature tropical cyclone environment. Consequently, while the estimates of C_D presented here are by no means perfect, they should not be discounted. Further research is needed to either confirm or refute these results.

Table 4.2 indicates that a net convergence of m is observed between 3 and 10 deg. for the 560 to 1600 m layer. The magnitude of the residual at each radius is roughly equal to those found for the surface to 560 m layer (Table 4.1). It is not clear why the 560 to 1600 m residual is so large. Frank (1984) showed that the convergence of m between 560 m and the top of the inflow layer (roughly 1600 m)

in Frederic's core was too large to be explained by the observed downward turbulent flux of momentum through the 560 m surface. Nevertheless, it is possible that the downward momentum flux through the 560 m surface is of sufficient magnitude to account for the observed 560 to 1600 m residual but is on a scale which is too large to be resolved by aircraft and too small to be resolved using the composite grid employed here.

Chapter 5

MOISTURE BUDGET

The moist unstable environment in which tropical cyclones are commonly observed is highly conducive to the production of copious rainfall. Passage of a tropical cyclone of even modest intensity produces rainfall averaging about 10 cm, and substantially higher amounts are common. Hawkins and Imbembo (1976) estimated that the average rainfall near the center of a particularly small but intense hurricane (Inez) was approximately 4.8 cm h^{-1}. Although such intense rainfall is unusual, Inez serves as an example of the abundant rainfall which a single tropical cyclone can produce.

In this chapter, moisture budgets are performed using both corrected and raw wind data. For both budgets, thermodynamic data for the composite typhoon (Frank, 1977a) are employed to obtain estimates of temperature (T) and specific humidity (q) needed for moisture budget computations. As noted in Chapter 3, the absence of sufficiently dense thermodynamic measurements for this storm necessitates the use of Frank's (1977a) composite thermodynamic data. Although the use of composite thermodynamic data somewhat reduces the accuracy of the moisture budgets presented in this chapter, these quantities are generally less variable than are the winds in a tropical cyclone environment. Thus, it is believed that the primary objective of assessing the differences between precipitation values obtained using corrected and raw wind sets is satisfied.

5.1 The Moisture Budget Equation

Assuming the horizontal transport of liquid water and vertical flux of specific humidity at the top of the inflow layer are negligible, the moisture budget evaluated for a cylindrical volume between the surface and the top of the inflow layer is given by:

$$- \int_{Vol} \frac{\partial(\rho q)}{\partial t} - \int_{Vol} \underset{\sim}{\nabla} \cdot \rho q \underset{\sim}{V} + E_o = P \qquad (5.1)$$

where q is the specific humidity, E_o is the evaporation from the sea surface and P is the precipitation. Storage and horizontal fluxes of liquid water are neglected, a reasonable assumption for the large-scale domain of this study.

Equation 5.1 is evaluated separately using both corrected and raw wind sets. Each of the terms on the left side of Eq. 5.1 is evaluated for each of ten, 1 deg. radial bands between the storm center and 10 deg. radius to obtain precipitation as a residual. Since Frederic is assumed to be in steady-state, the local time rate of change of moisture (the first term on the left side of Eq. 5.1) is zero. The second term on the left side of Eq. 5.1 is the horizontal moisture convergence into a volume. This term is computed by obtaining the layer mean transport of moisture ($\rho q V_r$) between the surface and the top of the inflow layer at radii between 1 and 10 deg. The third term on the left side of Eq. 5.1 is the sea-surface evaporation. This term is evaluated at each radius between 1 and 10 deg. and the resultant

values are then employed to obtain area weighted values of E_o. The sea-surface evaporation is evaluated using the bulk aerodynamic formula:

$$E_o = \rho C_E V_o (q_s - q_o) \tag{5.2}$$

where C_E is the evaporation coefficient, V_o is the total wind speed at the surface, q_s is the saturation specific humidity of the sea surface and q_o is the specific humidity of the air at the surface.

The evaporation coefficient is computed based on Rosenthal's (1971) formulation:

$$C_E = 1.1 \times 10^{-3} + 4 \times 10^{-5} |V_o| \tag{5.3}$$

where V_o is the surface wind speed in meters per second. Estimates of $(q_s - q_o)$ are obtained from Frank (1977a). Frank estimated the quantity $(q_s - q_o)$ from analysis of climatological sea-surface temperature data (Robinson and Bauer, 1971) and composite surface temperature data. Although the estimates of E_o obtained using Eq. 5.2 are by no means perfect, they agree well with the values Frank (1977a) obtained as residuals in his water budget analysis and are adequate for the comparisons described below.

5.2 Moisture Budget Results

Rainfall estimates obtained using corrected and raw wind sets are depicted in Fig. 5.1. No difference is observed in the 0-1 deg. rainfall because the wind sets are identical at 1 deg. radius. Figure 5.1 indicates that the raw wind sets substantially underestimate

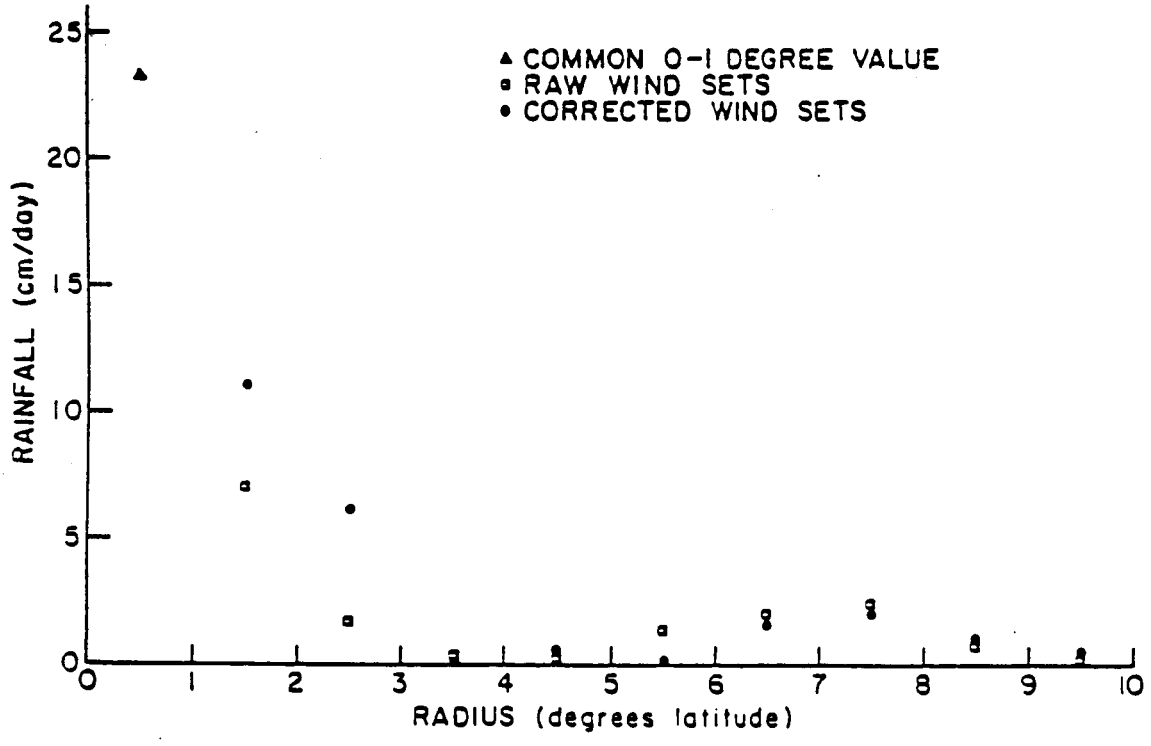

Figure 5.1 Rainfall estimates (cm/day) obtained using raw wind sets and corrected wind sets. The 0-1 deg. radius rainfall values obtained using raw and corrected wind sets are equal for reasons discussed in the text.

the rainfall between 1 and 3 deg. The greatest underestimation of rainfall is observed between 2 and 3 deg., where rainfall obtained using corrected wind sets is roughly three times the rainfall obtained using raw wind sets. Outside 3 deg. radius, no systematic or appreciable differences between rainfall estimates obtained using raw and corrected wind sets are observed.

The differences in rainfall between 1 and 3 deg. are especially significant considering that composite studies of observed tropical cyclone rainfall performed by Miller (1958a), Gray, Frank and George (1975) and Frank (1977a) indicate that most tropical cyclone rainfall falls inside about 4 deg. radius. Table 5.1 illustrates the area-averaged rainfall from 0-3 and 1-4 deg. radius computed using both raw and corrected wind sets. The table suggests that raw wind sets underestimate the 0-3 deg. area-averaged rainfall by greater than 50% and the 1-4 deg. area-averaged rainfall by almost 100%. Since the estimated rainfall from 0-1 deg. radius is identical for both corrected and raw wind sets, the difference in area-averaged rainfall between 1 and 4 deg. is thought to be a more revealing measure of the rainfall differences between raw and corrected wind sets for this storm. Although it would be presumptuous to claim that rainfall differences of comparable magnitude are found in all storms, it seems clear that substantial errors in estimated rainfall can occur when spatial CMWH variations are not accounted for.

Table 5.2 indicates that rainfall estimates obtained using corrected wind sets are in reasonably good agreement with previous estimates of tropical cyclone rainfall obtained by Miller (1958a) and

Table 5.1 Area-averaged storm rainfall (cm/day) obtained using corrected wind sets and raw wind sets.

Radius (Degrees Latitude)	0-3	1-4
Corrected Wind Sets	9.1	3.9
Raw Wind Sets	5.9	2.0

Table 5.2 Observed rainfall data for the mean tropical cyclone based on studies by Miller (1958a) and an unpublished report by Gray, Frank and George (1975) and rainfall estimates for Hurricane Frederic obtained using corrected wind sets (cm/day).

Radial Band (Degrees Latitude)	0-2	2-4	4-6	6-8	8-10
Mean Tropical Cyclone	9.0	2.3	0.7	0.7	0.7
Hurricane Frederic	14.0	2.1	0.5	1.9	0.8

Gray, Frank and George (1975). It is encouraging that the rainfall estimates obtained using corrected wind sets are consistent with the composite wind fields presented in Chapter 3. Comparison of the storm's azimuthally-averaged vertical motion field (Fig. 3.37) and the estimated rainfall obtained using corrected wind sets (Fig. 5.1) show there to be good agreement between the locations of precipitation maxima (minima) and vertical motion maxima (minima). This is reasonable since the convergence of q is the dominant term in the moisture budget equation. It is especially comforting that a precipitation minimum is observed between roughly 3 and 6 deg., since mean divergence is observed from the surface and 1600 m at roughly the same radii (Fig. 3.26).

Chapter 6

CONCLUSIONS

Aircraft, rawinsonde, satellite, ship and buoy data collected over a 40 hr period were combined with Frank's (1984) analysis of Frederic's core and Powell's (1982) surface wind analysis inside roughly 5 deg. radius to obtain a good low-level wind analysis between Frederic's center and 10 deg. radius. The availability of good low-level wind coverage made it possible to perform a detailed multiple-scale analysis of Frederic's low-level wind structure and to perform budgets of momentum and moisture. The quality of the low-level wind analysis was improved considerably by determining the most appropriate levels to which low-level cloud motion winds (CMW's) should be assigned. In the past, researchers assumed that all low-level CMW's tracked in a tropical cyclone environment approximated the wind at a level near cloud base (usually 900-950 mb). However, the results of this study suggest that low-level CMW's do not approximate the wind at cloud base or any other single level. Analysis of Frederic's low-level cloud motion wind heights (CMWH's) indicated that the heights varied systematically over Frederic's domain, with CMWH's generally decreasing with increasing radius. A CMWH maximum in excess of 4000 m was observed roughly 3 deg. radius east of the storm center while a CMWH minimum (< 500 m) was observed beyond about 5 deg. radius southeast of the storm center.

A concerted effort was made to determine the impact of assigning all low-level CMW's to a single analysis level of 560 m (raw winds)

rather than to their correct levels. Comparison of the axisymmetric radial wind fields obtained using raw and corrected wind sets showed that raw wind sets underestimated the radial inflow at all radii at 560 and 1600 m for the axisymmetric storm, with the greatest underestimation observed inside about 5 deg. radius. Moreover, it has been shown that these errors result in substantial underestimation of the radial mass flux through the storm by raw wind sets. Analysis of the storm's asymmetric radial wind field showed that employing raw wind sets also resulted in appreciable errors in the radial inflow and outflow patterns at the 560 and 1600 m analysis levels.

Comparison of axisymmetric tangential winds obtained using raw and corrected wind sets showed that raw wind sets overestimated the tangential wind at virtually all radii at 560 and 1600 m. However, the overestimates were only about 6% at 560 and 15% at 1600 m because of the small low-level tangential wind shear in this storm. Despite the small errors in the axisymmetric tangential wind values, employing raw wind sets resulted in significant errors in the asymmetric tangential wind field at 560 and 1600 m.

The errors in the radial and tangential winds which resulted from the use of raw wind sets caused errors in the axisymmetric values of divergence and relative vorticity. The errors in relative vorticity were observed to be fairly small at all radii due to the small errors in the tangential wind. Errors in divergence were found to be largest inside roughly 6 deg. radius, which is consistent with the large errors in radial wind found inside roughly 5 deg. radius.

Analysis of Frederic's low-level wind structure showed marked asymmetries in the wind fields at all analysis levels. Relative to the moving storm, strong radial inflow was observed northeast of the storm at all radii, and the strongest outflow was observed inside roughly 3 deg. radius southwest of the storm center. Consequently, a strong northeast to southwest flow of air through the storm was observed. Tangential winds exhibited a pronounced northwest to southeast asymmetry in the cyclonic wind fields at all levels, with the strongest winds observed northwest of the storm. The latter feature is in good agreement with Powell's (1982) analysis of Frederic's surface winds inside 5 deg. radius.

Frederic's divergence fields were generally consistent between levels. Convergence was observed over the vast majority of the storm domain inside 2 deg. radius, with the strongest convergence observed northeast of the storm center. Weak divergence covered much of the area between about 3 and 6 deg. radius, which is consistent with Frank's (1977a) study. Outside 6 deg. radius divergence was weak, except about 7 deg. radius northeast of the storm center, where a pronounced area of convergence was observed. Frederic's vertical motion fields at 560 and 1600 m showed upward motion inside 2 deg. radius, with the strongest upward motion observed northeast of the storm center. Sinking motion was observed over much of the storm domain between 3 and 6 deg. radius. Vertical motion was weak outside 6 deg. radius, except roughly 7 deg. radius northeast of the storm center, where a well-defined region of upward motion was observed. Analysis of Frederic's vorticity fields indicated positive relative

vorticity existed inside about 3 deg. radius. Between 3 and 6 deg. radius areas of negative relative vorticity were interspersed among areas of weakly positive relative vorticity. A well-defined region of positive relative vorticity associated with a small low pressure system in the Western Gulf of Mexico was observed 7 deg. radius west of the storm center; otherwise no strong vorticity features were observed outside 6 deg. radius.

Analysis of Frederic's surface to 560 m angular momentum budget showed that net convergence of angular momentum was observed at all radii between 3 and 10 deg. The horizontal convergence of angular momentum was nearly balanced by the vertical transport of angular momentum, so the net convergence of angular momentum was nearly equal to the coriolis torque. Estimates of the surface drag coefficient (C_D) showed that C_D generally increased with increasing radius and decreasing wind speed. While this contradicts previous estimates of C_D, it is important to note that past estimates of C_D outside the core have been rather crude since they were obtained using estimated surface winds and composite data sets. In this study, a detailed surface wind analysis and a dense data set from a single storm were used to compute C_D in the region outside of the core of a mature tropical cyclone. Thus, the estimates of C_D obtained here are expected to represent an improvement over past estimates.

By performing a moisture budget between the surface and the top of the inflow layer, estimates of storm rainfall were obtained. These were in good agreement with past estimates of observed tropical cyclone rainfall (Miller, 1958a; Gray, Frank and George, 1975). The rainfall

rates obtained here showed that most rainfall fell inside 4 deg. radius, which is consistent with the studies cited previously. A clear minimum in rainfall was observed between 3 and 6 deg. radius, which is the region of mean divergence observed earlier. Moreover, it was found that corrected wind sets substantially underestimated storm rainfall inside roughly 4 deg. radius. This indicates that accounting for low-level CMWH variations is important when estimating storm rainfall from divergence estimates based on cloud motion winds.

By analyzing Frederic's wind fields between the surface and 1600 m, a great deal of information has been obtained concerning the multiple-scale low-level wind structure of a mature tropical cyclone. Nevertheless, since the analyses presented in this thesis were performed using data from a single storm, they may not be representative of tropical cyclones with differing sizes, intensities, etc. Thus, it is believed that similar studies of tropical cyclones with different characteristics would prove quite useful, especially in obtaining additional information concerning the distribution of low-level CMWH's and the dependence of C_D on surface wind speed.

REFERENCES

Anthes, R.A., 1974: The dynamics and energetics of mature tropical cyclones. Rev. of Geoph. and Space Phys., Vol. 12, No. 3, 495-522.

Billingsley, J.B., 1976: Interactive images for meteorological application at NASA/Goddard Space Flight Center. Preprints, 7th Conf. on Aerospace and Aeronautical Meteorology and Symposium on Remote Sensing from Satellites, AMS, Melbourne, Australia, 268-275.

Black, P.G., 1983: Ocean Temperature Changes Induced by Tropical Cyclones. Ph.D. Thesis, Department of Meteorology, The Pennsylvania State University, 278 pp.

Charney, J. and A. Eliassen, 1964: On the growth of the hurricane depression. J. Atmos. Sci., 21, 68-75.

Computer Sciences Corporation, 1977: Atmospheric and Oceanographic Information Processing System Meteorology Package (Metpak) Users Guide, Task Assignment 619, 1-1 to 1-6.

Cressman, G.P., 1959: An operational objective analysis system. Mon. Wea. Rev., 87, 367-374.

Frank, W.M., 1977a: The structure and energetics of the tropical cyclone, Paper I: Storm Structure. Mon. Wea. Rev., 105, 1119-1135.

Frank, W.M., 1977b: The structure and energetics of the tropical cyclone, Paper II: Dynamics and energetics. Mon. Wea. Rev., 105, 1136-1150.

Frank, W.M., 1977c: The structure and energetics of the tropical cyclone, Paper III: Convective fluxes in tropical cyclones. J. Atmos. Sci., 34, 1554-1568.

Frank, W.M., 1984: A composite analysis of the core of a mature hurricane. Mon. Wea. Rev., 112, 2401-2420.

Glahn, H.R., G.W. Hollenbaugh and D.A. Lowry, 1969: An operationally oriented objective analysis program, ESSA. Tech. Memo. WBTM TDL-22, ESSA, U.S. Department of Commerce, 20 pp.

Gray, W.M. and D.J. Shea, 1973: The hurricane's inner core region, Part II: Thermal stability and dynamic characteristics. J. Atmos. Sci., 130, 1565-1576.

Gray, W.M., W.M. Frank and J.E. George, 1975: Typhoon studies in support of Project Stormfury, Unpublished report to NOAA, available from Colorado State University, Department of Atmos. Sci., Ft. Collins Co.

Hasler, F.A. and E.B. Rodgers, 1977: An error analysis of tropical cyclone divergence and vorticity fields derived from satellite cloud winds on the Atmospheric and Oceanographic Image Processing Systems (AOIPS). Preprints, 11th Tech. Conf. on Hurricanes and Tropical Meteorology, AMS, Miami, FL, 670-675.

Hasler, F.A., W.E. Shenk and W.C. SKillman, 1977: Wind estimation from cloud motions: Results from Phases I, II and III of an in situ aircraft verification experiment. J. Appl. Meteor., 16, 812-815.

Hasler, F.A., W.C. Skillman, W.E. Shenk and J. Steranka, 1979: In situ aircraft verification of the quality of satellite cloud winds over oceanic regions. J. Appl. Meteor., 18, 1481-1489.

Hasler, F.A. and R.K. Morris, 1986: Hurricane structure and wind fields from steroscopic infrared satellite observations and radar data. J. Climate Appl. Meteor., 25, 707-727.

Hawkins, H.F. and D.T. Rubsam, 1968: Hurricane Hilda, 1964: Structure and budgets of the hurricane on October 1, 1964. Mon. Wea. Rev., 99, 427-434.

Hawkins, H.F. and S.M. Imbembo, 1976: The structure of a small, intense hurricane-Inez 1966. Mon. Wea. Rev., 104, 418-422.

Hebert, P.J., 1980: The Atlantic hurricane season of 1979. Mon. Wea. Rev., 108, 973-979.

Holland, G.J., 1983a: Angular momentum transports in tropical cyclones. Quart. J. Roy. Meteor. Soc., 109, 187-209.

Holland, G.J., 1983b: Tropical Cyclones in the Australian/Southwest Pacific Region. Department of Atmos. Sci., Paper No. 363, Colorado State University, Fort Collins, CO, 275 pp.

Hubert, L.F. and L.F. Whitney, Jr., 1971: Wind estimation from geostationary satellite pictures. Mon. Wea. Rev., 99, 665-672.

Laseur, N.E. and H.F. Hawkins, 1963: An analysis of Hurricane Cleo (1958) based on data from research reconnaissance aircraft. Mon. Wea. Rev., 91, 694-709.

Malkus, J.S., 1949: Effects of wind shear on some aspects of convection. Trans. Amer. Geophys. Union, 30, 19-25.

McBride, J.L., 1981a: Observational analysis of tropical cyclone formation. Part I: Basic description of data sets. J. Atmos. Sci., 38, 1117-1131.

McBride, J.L., 1981b: Observational analysis of tropical cyclone formation. Part II: Budget analysis. J. Atmos. Sci., 38, 1152-1166.

Miller, B.I., 1958a; Rainfall rates in Florida hurricanes. Mon. Wea. Rev., 86(7), 258-264.

Nunez, E. and W.M. Gray, 1977: A comparison between West Indies hurricanes and Pacific typhoons. Proceedings, 11th Tech. Conf. on Hurricanes and Tropical Meteorology, AMS, Miami, FL, 528-534.

Palmén, E.H. and H. Riehl, 1957: Budget of angular momentum and energy in tropical storms. J. Meteor., 14, 150-159.

Panofsky, H.A. and J.A. Dutton, 1984: Atmospheric Turbulence, John Wiley and Sons, Inc., New York, 392 pp.

Pfeffer, R.L., 1958: Concerning the mechanics of hurricanes. J. Meteor., 15, 113-120.

Powell, M.D., 1982: The transition of the Hurricane Frederic boundary-layer wind field from the open Gulf of Mexico to landfall. Mon. Wea. Rev., 110, 1912-1932.

Riehl, H. and J.S. Malkus, 1961: Some aspects of Hurricane Daisy, 1958. Tellus, 13, 181-213.

Robinson, M.K. and R.A. Bauer, 1971: Atlas of monthly mean sea surface and subsurface temperature and depth of the top of the thermocline North Pacific Ocean. Fleet Numerical Weather Central Rept., 96 pp. Monterey, CA.

Rodgers, E.B., R.C. Gentry, W.E. Shenk and V. Oliver, 1979: The benefits of using short-interval satellite images to derive winds for tropical cyclones. Mon. Wea. Rev., 107, 577-584.

Rodgers, E.B. and R.C. Gentry, 1983: Monitoring tropical-cyclone intensity using environmental wind fields derived from short interval satellite images. Mon. Wea. Rev., 111, 979-996.

Rosenthal, S.L., 1971: The response of a tropical cyclone model to variations in boundary-layer parameters, initial conditions, lateral boundary conditions and domain size. Mon. Wea. Rev., 99(10), 767-777.

Shea, D.J. and W.M. Gray, 1973: The hurricane's inner core region. Part I: Symmetric and asymmetric structure. J. Atmos. Sci., 30, 1544-1576.

Weatherford, C. and W.M. Gray, 1984: Relating typhoon intensity to outer 1-3° radius circulation as measured by reconnaissance aircraft. Postprints, 15th Conf. on Hurricanes and Tropical Meteorology, AMS, Miami, FL, 238-242.